The CAMS interim Reanalysis of Carbon Monoxide, Ozone and Aerosol for 2003–2015

J. Flemming[1], A. Benedetti[1], A. Inness[1], R. Engelen[1], L. Jones[1], V. Huijnen[2], S. Remy[3], M. Parrington[1], M. Suttie[1], A. Bozzo[1], V.-H. Peuch[1], D. Akritidis[4] and E. Katragkou[4]

[1] European Centre for Medium-Range Weather Forecasts, Reading, UK

[2] Royal Netherlands Meteorological Institute, De Bilt, The Netherlands

[3] Laboratoire de météorologie dynamique, UPMC/CNRS, Paris, France

[4] Department of Meteorology and Climatology, Aristotle University of Thessaloniki, School of Geology, Thessaloniki, Greece

Correspondence to: J. Flemming (Johannes.Flemming@ecmwf.int)

Abstract

A new global reanalysis data set of atmospheric composition (AC) for the period 2003–2015 has been produced by the Copernicus Atmosphere Monitoring Service (CAMS). Satellite observations of total column (TC) carbon monoxide (CO) and aerosol optical depth (AOD) as well as several TC and profile observation of ozone have been assimilated with the Integrated Forecasting System for Composition (C-IFS) of the European Centre for Medium-Range Weather Forecasting. Compared to the previous MACC reanalysis (MACCRA), the new CAMS interim reanalysis (CAMSiRA) is of a coarser horizontal resolution of about 110 km compared to 80 km but covers a longer period with the intent to be continued to present day. This paper compares CAMSiRA against MACCRA and a control experiment (CR) without assimilation of AC retrievals. CAMSiRA has smaller biases than CR with respect to independent observations of CO, AOD and stratospheric ozone. However, ozone at the surface could not be improved by the assimilation because of the strong impact of surface processes such as dry deposition and titration with nitrogen monoxide (NO), which were both not changed by the assimilation. The assimilation of AOD led to a global reduction of sea salt and desert dust as well as an exaggerated increase in sulphate. Compared to MACCRA, CAMSiRA had smaller biases for AOD, surface CO and TC ozone as well as for upper stratospheric and tropospheric ozone. Finally, the temporal consistency of CAMSiRA was better than the one of MACCRA. This was achieved by using a revised emission data set as well as by applying a careful selection and bias-correction of the assimilated retrievals. CAMSiRA is therefore better suited than MACCRA for the study of inter-annual variability than MACCRA as demonstrated for trends in surface CO.

1 Introduction

Exploiting the multitude of satellite observations of atmospheric composition (AC) is a key objective of the Copernicus Atmosphere Monitoring Service (CAMS). For its global component CAMS uses the four-dimensional variational (4D-VAR) data assimilation technique to combine satellite observations with chemistry-aerosol modelling to obtain a gridded continuous representation (analysis) of the mass mixing ratios of atmospheric trace gases and aerosols.

The global CAMS system is built on the heritage of the EU-funded GEMS (Hollingsworth et al., 2008) and series of MACC projects at the European Centre for Medium-Range Weather Forecasts (ECMWF). During these projects the Integrated Forecasting System (IFS) of ECMWF was extended by modules for atmospheric chemistry, aerosols and greenhouse gases in such a way that the 4D-VAR data assimilation system, which had been developed for the analysis of the meteorological fields, could be used for the assimilation of AC retrievals.

Assimilating satellite AC retrievals into an AC model has advantages to the sole use of the AC retrievals because of their specific limitations. First, only a small subset of the trace gases or only total aerosol is directly observable with an accuracy sufficient to have an impact during the assimilation. Second, AC satellite retrievals have incomplete horizontal coverage because of the orbital cycle, viewing geometry, the presence of clouds and other factors such as surface albedo. Third, the vertical distribution of the trace species can often not or only rather coarsely be retrieved from the satellite observations, while the measurement sensitivity towards the surface is generally low.

The AC analyses are used to (i) initialise AC model forecasts and (ii) for the retrospective analysis (reanalysis) of AC for air quality and climate studies. The reanalysis of the meteorological fields has been an important activity at ECMWF (ERA-40, Uppala et al., 2005, ERA interim Dee et al., 2011) and other meteorological centres such as NCEP (CFSR, Saha et al., 2010, JMA (JRA-55, JRA-25, Onogi et al., 2007) and NASA/DAO (MERRA, Rienecker, et al., 2011). An important application of these reanalysis data sets is the estimation of the inter-annual variability and the trends of climate variables over the last decades up to the present day. The complete spatial and temporal coverage makes the trend analysis of reanalyses more robust and universal than the trend analysis of individual observing systems. However, constructing a data set which is suited for this purpose is a complex task because of the developing and changing observing system, which can introduce

spurious trends and sudden shifts in the reanalysis data record. Careful quality control of the assimilated observations and techniques (e.g. Dee et al., 2004) to address inter-instrument biases are applied to mitigate this problem.

Most meteorological reanalyses contain stratospheric ozone but other traces gases, apart from water vapour, are not included. In the last decade chemical and aerosol data assimilation has matured (Bocquet et al., 2015) and dedicated reanalysis data sets for AC have emerged. The Multi-Sensor-Reanalysis of total ozone (van der A et al., 2015) for 1970–2012 used ground based Brewer observations to inter-calibrate satellite retrievals. The MERRAero reanalysis (2002–present, http://gmao.gsfc.nasa.gov/reanalysis/merra/MERRAero/) assimilated AOD retrievals from the two Moderate Resolution Imaging Spectroradiometer (MODIS) instruments in the GOCART aerosol module of the GEOS-5 model system using the meteorological variables of the MERRA meteorological analysis. Its next version, the MERRA2 reanalysis, is a joint meteorological and aerosol reanalysis covering the period from 1979 to present. Miyazaki et al. (2015) put together a tropospheric chemistry reanalysis using a Kalman filter approach for the years 2005–2012. They use the CHASER Chemical transport model (CTM) to assimilate retrievals of tropospheric ozone and CO profiles, NO_2 tropospheric columns and HNO_3 stratospheric columns. Their approach tackles two specific challenges of AC data assimilation. First, they not only correct atmospheric concentrations but also alter the surface emissions which control the tracer distributions to a large extent. Second, the Kalman filter develops co-variances of the errors between observed and un-observed species, which are used to correct un-observed species based on the observations increments.

The MACC reanalysis (MACCRA) of reactive gases (Inness et al., 2013) and aerosols for the period 2003–2012 is an AC reanalysis that covers tropospheric and stratospheric reactive gases and aerosols as well as the meteorological fields in one consistent data set. MACCRA has proved to be a realistic data set as shown in several evaluation studies for reactive gases (Elguindi et al., 2010, Inness et al., 2013, Katragkou et al., 2015 and Gaudel et al., 2015) and aerosols (Cesnulyte et al., 2014 and Cuevas et al., 2015,). MACCRA is widely used, for example, as boundary condition for regional models (Schere et al., 2012, Im et al., 2014, Giordano et al., 2015), to construct trace gas climatologies for the IFS radiation schemes (Bechtold et al., 2009), to estimate aerosol radiative forcing (Bellouin et al., 2013), as input to

106 solar radiation schemes for solar energy applications and to report the current state of aerosol
107 and CO as part of the climate system (Benedetti et al., 2014., Flemming and Inness, 2014).

108 CAMS is committed to produce a comprehensive high-resolution AC reanalysis in the next
109 years. The CAMS interim Reanalysis (CAMSiRA) presented here has an interim status
110 between MACCRA and this planned analysis data set. It was produced at a lower horizontal
111 resolution (110 km) than the resolution of MACCRA (80 km), and the number of archived
112 AC fields was limited to the aerosol variables and selected chemical species such as ozone,
113 HNO_3, N_2O_5, NO, NO_2, PAN and SO_2.

114 The reasons for producing CAMSiRA before the more comprehensive reanalysis are as
115 follows: The MACCRA for reactive gases was produced using a coupled system consisting of
116 the IFS and the MOZART-3 (Kinnison et al., 2007) chemical transport model (CTM) as
117 described in Flemming et al. (2009). This coupled system was replaced by the much more
118 computationally efficient on-line coupled model C-IFS (Flemming et al., 2015), which uses
119 the chemical mechanism CB05 of the TM5 CTM (Huijnen et al., 2010). With the
120 discontinuation of the coupled system it was not possible to extend the MACC reanalysis to
121 the present day. For the AC monitoring service of CAMS it is however important to be able to
122 compare the present conditions with previous years in a consistent way. Another motivation
123 for producing CAMSiRA was that the aerosol module used for the MACCRA had undergone
124 upgrades (Morcrette et al., 2011) in recent years. Finally, MACCRA suffered from small but
125 noticeable shifts because of changes in the assimilated observations, the emission data and the
126 bias correction approach. These spurious shifts undermine the usefulness of the MACCRA for
127 the reliable estimation of trends. The lessons learnt from the evaluation of CAMSiRA will
128 feed into the setup of the planned CAMS reanalysis.

129 Reanalyses of AC are generally less well-constrained by observations than meteorological
130 reanalyses because of the aforementioned limitations of the AC observations and because of
131 the strong impact of the emission, which are in many cases not constrained by observations. It
132 is therefore good scientific practice to investigate the impact of the AC assimilation by
133 comparing the AC reanalysis to a control experiment that did not assimilate AC observations.
134 The control run (CR) to CAMSiRA was carried out using the same emission data as well as
135 the meteorological fields produced by CAMSiRA.

136 The purpose of this paper is firstly to document the model system, the emissions and the
137 assimilated observations used to produce CAMSiRA, and to highlight the differences to the

setup of the MACCRA. As the emissions are an important driver for variability of AC, a presentation of the totals and the inter-annual variability of the emission data used in CAMSiRA and CR is given in a supplement to the paper.

In the remainder of the paper, CO, aerosol as well as tropospheric and stratospheric ozone of CAMSiRA, CR and MACCRA are inter-compared and evaluated with independent observations in a separate section for each species. The comparison of CAMSiRA with MACCRA has the purpose to report progress and issues of CAMSiRA for potential users of the data sets. The comparison of CAMSiRA with CR shows the impact of the data assimilation and is helpful to better understand deficiencies of the C-IFS model and its input data.

Each section starts with a discussion of the spatial differences of CAMSiRA, CR and MACCRA of the considered species. Next, the temporal variability is investigated using time series of monthly mean values averaged over selected regions. We present global burdens and discuss changes in the speciation of the aerosol fields introduced by the assimilation. Finally, the three data sets are compared against independent observations, which were not used in the assimilation. A summary and recommendations for future AC reanalysis will be given in the last section.

2 Description of CAMSiRA setup

2.1 Overview

CAMSiRA is a data set of 6 hourly reanalyses of AC for the period 2003–2015. A 3 hourly data set consistent with the AC analysis is available from forecasts linking the analyses. The horizontal resolution is about 110 km on a reduced Gaussian grid (T159) and the vertical discretisation uses 60 levels from the surface to a model top of 0.1 hPa. Total columns of CO (TC CO) of the Measurements Of Pollution In The Troposphere (MOPITT) instrument, MODIS AOD and several ozone TC and stratospheric profile retrievals (see Table 2) were assimilated together with meteorological in-situ and satellite observations.

The description of MACCRA for reactive gases can be found in Inness et al. (2013). Important commonalities and differences between the two AC reanalyses are given in Table 1.

The control run is a forward simulation of C-IFS in monthly segments. The meteorological simulation is relaxed using the approach by Jung et al. (2008) to the meteorological reanalysis produced by the CAMSiRA. The emission input fields are the same as used for CAMSiRA.

2.2 C-IFS model

The model C-IFS is documented and evaluated in Flemming et al. (2015). C-IFS applies the chemical mechanism CB05, which describes tropospheric chemistry with 55 species and 126 reactions. Stratospheric ozone chemistry in C-IFS is parameterized by the “Cariolle-scheme” (Cariolle and Dèquè, 1986 and Cariolle and Teyssèdre, 2007). Chemical tendencies for stratospheric and tropospheric ozone are merged at an empirical interface of the diagnosed tropopause height in C- IFS. C-IFS benefits from the detailed cloud and precipitation physics of the IFS for the calculation of wet deposition and lightning NO emission. Wet deposition modelling for the chemical species is based on Jacob (2000) and accounts for the sub-grid scale distribution of clouds and precipitation. Dry deposition is modelled using pre-calculated monthly-mean dry deposition velocities following Wesely (1989) with a superimposed diurnal cycle. Surface emissions and dry deposition fluxes are applied as surface boundary conditions of the diffusion scheme. Lightning emissions of NO were calculated based on convective precipitation (Meijer et al., 2001).

The aerosol module (Morcrette et al., 2009) is a bulk/bin scheme simulating desert dust, sea salt at 80% relative humidity (RH), hydrophilic and hydrophobic organic carbon and black carbon as well as sulphate aerosol based on the LMDZ aerosol model (Reddy et al., 2005). Sea salt and desert dust are represented in 3 size-bins. The radii ranges of the dust bins are 0.030–0.55, 0.55–0.9 and 0.9–20 µm (DD1, DD2, and DD3) and of the sea salt at 80% RH bins 0.03–0.5, 0.5–5 and 5–20 µm (SS1, SS2, and SS3). There is no consideration of the aerosol growth, which would transfer aerosol mass from one size bin to another. Hygroscopic growth of hydrophilic species is taken into account in the computation of the aerosol optical properties only. Following the emission release, the aerosol species are subject to wet and dry deposition and the largest size bins of sea salt and dust also to sedimentation. The chemical source of sulphate is modelled by climatological conversion rates using a SO_2 tracer, which is independent of the SO_2 simulated in CB05. The SO_2 tracer is driven by prescribed SO_2 and DMS emissions. Its loss is simulated by wet and dry deposition as well as the climatological chemical conversion to SO_4.

The aerosol and chemistry modules used to simulate source and sink terms are not coupled. Also, wet and dry deposition are modelled with different parameterisations but with the same meteorological input such as precipitations fields. Aerosol and chemistry have in common that they are advected and vertically distributed by diffusion and convection in the same way. A proportional mass fixer as described in Diamantakis and Flemming (2014) is applied for all tracers in C-IFS.

2.3 Emission data sets

This section only references the origin of the emission data. The emitted totals and the linear trends of the anthropogenic, biomass burning and natural emissions as well as the modelled desert dust and sea salt emissions used in CAMSiRA and CR are presented in a supplement.

The anthropogenic surface emissions for the chemical species were taken from the MACCity inventory (Granier et al., 2011), which covers the period 1960–2010. MACCity emissions are based on the ACCMIP (Lamarque et al., 2013) inventory but have improved seasonal variability. The changes from 2000–2005 and for 2010 are obtained in the MACCity data using the representative concentration pathways (RCP) scenarios version 8.5. For the production of CAMSiRA the MACCity data set was extended to 2015 by also applying the RCP 8.5 scenario. The anthropogenic CO emissions were increased following Stein et al.

(2014). Time series of the anthropogenic CO emissions for Europe, North America, East Asia (see Table 3) and the globe are shown in Figure S2 of the supplement.

The anthropogenic emissions of organic matter, black carbon and aerosol precursor SO_2 are retrieved from AEROCOM data base, which is compiled using EDGAR and SPEW data (Dentener et al., 2006). In contrast to the anthropogenic gas emissions, the aerosol anthropogenic emissions did not account for trends but only for the seasonal cycle.

The biogenic emissions for the chemical species were simulated off-line by the MEGAN2.1 model (Guenther et al., 2006) for the 2000–2010 period (MEGAN-MACC, Sindelarova et al., 2014). For the remaining years 2011–2015 a climatology of the MEGAN-MACC data was put together. Natural emissions from soils and oceans for NO_2, DMS and SO_2 were taken from Precursors of ozone and their Effects in the Troposphere (POET) database for 2000 (Granier et al., 2005; Olivier et al., 2003).

Daily biomass burning emissions for reactive gases and aerosols were produced by the Global Fire Assimilation System (GFAS) version 1.2, which is based on satellite retrievals of fire radiative power (Kaiser et al., 2012). This is an important difference with respect to the MACCRA, which used an early version of the GFED 3.1 data from 2003 until the end 2008 and daily GFAS v1.0 data from 2009 to 2012. The GFED 3.1 is on average 20% lower than GFAS v1.2 (Inness et al., 2013). Time series of the biomass burning CO emissions for Tropical Africa, South America and Maritime South East Asia (see Table 3) and the globe are shown in Figure S3 of the supplement.

2.4 C-IFS data assimilation

C-IFS uses an incremental 4D-VAR algorithm (Courtier et al., 1994), which minimizes a cost function for selected control variables to combine the model and the observations in order to obtain the best possible representations of the atmospheric fields. The mass mixing ratios of O_3, CO and total aerosol are incorporated into the ECMWF variational analysis as additional control variables and are minimized together with the meteorological control variables. The assimilation of satellite retrieval of the chemical species and total aerosol optical depth is documented in Inness et al. (2015) and Benedetti et al. (2009). The assimilation of aerosol differs from the assimilation of CO and ozone because only the total aerosol mass can be constrained by the observations and information about the speciation must be obtained from the model.

The assimilation of AOD retrievals uses an observation operator that translates the aerosol mass mixing ratios and humidity fields of C-IFS to the respective AOD (550 nm) values using pre-computed optical properties. Total aerosol mass mixing ratio is included in the 4D-VAR cost function and the analysis increments are repartitioned into the individual aerosol components according to their fractional contribution to the total aerosol mass. This is an approximation which is assumed to be only valid over the 12 hour of the assimilation window. In reality, the relative fraction of the aerosol components is not conserved during the whole assimilation procedure because of differences in the efficiency of the removal processes. Aerosol components with a longer atmospheric lifetime will retain relatively longer the change imposed by the increments and may thereby change the relative contributions.

In the ECMWF data assimilation system the background error covariance matrix is given in a wavelet formulation (Fisher, 2004, 2006). This allows both spatial and spectral variations of the horizontal and vertical background error covariances. The background errors for AC are constant in time.

The background errors for ozone are the same as the ones used for MACCRA (Inness et al., 2013). Only the vertical correlations of the ozone background errors have been modified and restricted to ± 5 levels around a model level, to avoid correlations between the lower troposphere and upper tropospheric and stratospheric levels that affected near-surface ozone adversely. The background errors of total aerosol for both MACCRA and CAMSiRA were calculated using the method described in Benedetti and Fisher (2008). The aerosol background errors for CAMSiRA were updated using a more recent C-IFS model version. The background errors for CO are newly calculated for the CAMSiRA from an ensemble of C-IFS forecast runs (Inness et al., 2015). However, the ensemble did not account for the uncertainty of the emissions, which leads to an underestimation of the background error. This may limit the correcting impact of the observations in the assimilation process.

The background error statistics for the chemical species and for total aerosol are univariate in order to minimize the feedback effects of the chemical fields on the meteorological variables. Correlations between the background errors of different chemical species are also not accounted for (Inness et al., 2015).

A further potential interaction between the assimilated species could be introduced by the adjoint and tangent linear representations of the chemical mechanism and the aerosol module as part of the 4D-VAR approach. The applied tangent linear and adjoin formulation of C-IFS

accounts only for transport processes and not the sources and sinks of atmospheric composition in this study. Because of this limitation and the lack of aerosol-chemistry-meteorology feedbacks in C-IFS, interaction among species and with the meteorology as part of the assimilation procedure are not represented in CAMSiRA.

2.5 Assimilated observations

Table 2 shows the AC composition data sets for CO, ozone and AOD that were assimilated in CAMSiRA. The time line of the assimilation for the different retrievals is shown in Figure 1. CO is assimilated from MOPITT V5 TIR only whereas the MACCRA assimilated the V4 TIR product and additionally IASI TC CO retrievals after April 2008. The biases between the retrievals (George et al., 2015) of the two instruments in mid and higher latitudes could not be reconciled with the variational bias correction and led to a discontinuity in the time series of CO in MACCRA, which consequently could not be used for trend analyses (see Figure 4 below). It was therefore decided to only use the MOPITT V5 CO data set in CAMSiRA because it covers the whole period from 2003–2015. The MOPITT V5 product has better long term stability and a smaller SH bias than V4 (Deeter et al., 2013). V4 suffered from a positive temporal bias drift and a positive bias in SH.

An additional ozone data set in CAMSiRA were the Michelson Interferometer for Passive Atmospheric Sounding (MIPAS) ozone profiles, which were assimilated from 2005 until the end of the ENVISAT mission in April 2012. After the end of 2012 the version of the assimilated Microwave Limb Sounder (MLS) data set changed from V2 to V3.4. Information about the differences between the two versions can be found in https://mls.jpl.nasa.gov/data/v3_data_quality_document.pdf

Averaging kernels were used for the calculation of the model's first-guess fields in the observation operators for the MOPITT data. For the ozone retrieval averaging kernels were not used because they were not provided or did not improve the analysis. For example, the high vertical resolution of the MLS ozone retrievals in the stratosphere made the use of AK not necessary.

309 The AC satellite retrievals were thinned to a horizontal resolution of 1° x 1° by randomly
310 selecting an observation in the grid box to avoid oversampling and correlated observation
311 errors. Variational quality control (Andersson and Järvinen, 1999) and background quality
312 checks were applied. Only 'good' data were used in the analysis and data flagged as 'bad' by
313 the data providers were discarded.

314 Variational bias correction (Dee, 2004, McNally et al., 2006, Auligné et al., 2007, Dee and
315 Uppala, 2009) was applied to the MODIS AOD data, as well as to ozone column data from
316 the Ozone Monitoring Instrument (OMI), the SCanning Imaging Absorption spectroMeter for
317 Atmospheric CHartographY (SCIAMACHY) and the Global Ozone Monitoring Experiment 2
318 (GOME-2). The partial column of the Solar Backscatter Ultraviolet Radiometer 2 (SBUV/2),
319 MLS and MIPAS were used to anchor the bias correction. Experience from the MACC
320 reanalysis had shown that it was important to have an anchor for the bias correction to avoid
321 drifts in the fields (Inness et al., 2013).
322

3 Carbon monoxide

Global CTMs tend to underestimate the observed CO values (Shindell et al., 2006) but data assimilation (Inness et al., 2013 and 2015, Miyazaki et al., 2015, Gaubert et al., 2016) of satellite retrieval is able to successfully reduce the biases of the simulated CO fields. The correct representation of vertical CO profiles by the assimilation remains a challenge (Gaudel et al., 2015). An important next step will be the correct representation of the global CO trends by means of CO reanalyses such as CAMSiRA.

3.1 Spatial patterns of total column CO

Figure 2 shows the seasonal mean of TC CO over the period 2003–2015 of CAMSiRA and the differences with CR and MACCRA (2003–2012). Overall, the assimilation of TC CO in CAMSiRA led to an increase in the northern hemisphere (NH) and a decrease in the Southern hemisphere (SH) and most of the tropics. CAMSiRA was about 2–5% higher than CR in NH and up to 20% lower in the SH. The reduction was especially large in the tropical and sub-tropical outflow regions of the biomass burning regions in South America, Central Africa and Maritime South East Asia. The largest reduction in these regions occurred in DJF. The largest negative bias of CR with respect to CAMSiRA occurred over NH in December–February (DJF) and March–May (MAM). Overall the zonal patterns of the biases throughout all seasons were rather uniform indicating an underestimation of the hemispheric CO gradient in CR and could point to deficiencies in the simulation of the global chemical loss and production of CO as well as problems with the large scale transport. Biases in the amount of the emissions seem to play a smaller role for the problem with the hemispheric gradient.

However, more CO emission related differences occurred in September–November (SON) and to a smaller extent in June–August (JJA), when CR had (i) higher values in the biomass burning regions and the respective outflow regions in Central Africa, Maritime South East Asia and South America and (ii) lower values in the outflow regions of the emissions in North America and East Asia in the Eastern and Western Northern Pacific. This suggests that GFAS biomass burning emissions were too high whereas the anthropogenic emissions in North America and East Asia were too low. On the other hand, CR had higher values than CAMSiRA in South Asia, which indicates that the anthropogenic emissions are too high in India.

353 Compared to MACCRA, CAMSiRA was up to 10% higher in the Northern high latitudes and
354 up to 20% higher above the tropical biomass burning regions and above the parts of East
355 Asia. The differences over the biomass burning regions can be attributed to the different
356 biomass burning emissions data sets (see section 2.3). Over the oceans in NH and the tropics,
357 apart from biomass burning outflow regions, CAMSiRA CO is slightly lower (3%) than
358 MACCRA. The differences in the NH high latitudes are mainly caused by the reduction in
359 MACCRA CO in this region introduced by the assimilation of IASI CO retrieval after 2008
360 (see also Figure 4 below).

361 Figure 3 shows the average zonal mean cross section of the average CO mass mixing ratio of
362 CAMSiRA and the relative difference to CR and MACCRA. The overestimation of CR in the
363 tropics and SH extratropics was found throughout the troposphere. It was most pronounced in
364 relative terms at about 500 hPa. Stratospheric CO in CAMSiRA was much lower than in
365 MACCRA. This might be an improvement as Gaudel et al. (2015) report an overestimation in
366 the MACCRA over this region. In the upper troposphere CAMSiRA had higher CO than
367 MACCRA most notably in the tropics and SH where values are up to 40% higher. CO was
368 lower in the mid and lower troposphere in SH and higher in NH. These differences in the
369 vertical distribution might be caused by (i) a more consistent modelling approach of the
370 stratosphere-troposphere exchange with the on-line coupled C-IFS, (ii) the fact that C-IFS
371 CB05 has a very different chemistry treatment compared to MOZART and (iii) updated
372 background error statistics for CO (see Table 1).

373 ### 3.2 Inter-annual variability of CO burden

374 Figure 4 shows time series of the monthly mean CO burden from CAMSiRA, MACCRA and
375 CR for selected areas (see Table 3). Then modelled global CO burden (CR) was reduced by
376 the assimilation by about 3% at the start and by about 7% at the end of the period. CAMSiRA
377 showed a stepwise decrease of the global CO burden from 2008 and 2009 which corresponds
378 to a significant (95% confidence level) negative linear trend of -0.86%/yr over the whole
379 period. The linear trend is as expressed as percentage with respect to the mean of the burden
380 over the whole period. This figure is in good agreement with the results of Worden et al.
381 (2013) who estimates trends of -1% per year for both the globe and NH over the last decade
382 by studying different satellite-based instruments. CR also showed the largest decrease in the

period from 2007–2009 but the CO burden increased slightly after that period. The resulting linear trend of CR was still negative (-0.36%/yr) but less strong than the trend of CAMSiRA.

The higher global CO burdens of CR with respect to CAMSiRA originated mainly from the tropics and the SH mid-latitudes, which are strongly influenced by biomass burning emissions in tropical Africa and South America. CO was reduced by the assimilation in CAMSiRA especially after the start of the biomass burning season. The reduction of the biomass burning emissions of -7.4%/yr (see supplement Table S1) over South America led to a significant negative trend of the CO burden of -1.23%/yr in CAMSiRA and -0.83%/yr in CR over that region. The overestimation of CR with respect to CAMSiRA increased slightly during the period.

2015 was an exceptional year because the global CO burden reached the highest values in the whole period for both CAMSiRA and CR despite the overall decadal negative trend. The increase was caused by exceptionally high biomass burning emissions in Indonesia because of El Niño related dry conditions. The El Niño controlled inter-annual variability of CO over Maritime South East Asia was reproduced in a very similar way in CAMSiRA and CR but the assimilation reduced the burden by about 1 Tg (10%).

In the regions of high anthropogenic emissions the temporal variability at a monthly scale was very similar between CR and CAMSiRA. Both in North America and Europe CR underestimated the CO maximum of CAMSiRA in early spring by less than 5% up to the year 2010 but the biases almost disappeared in later years. This means that the negative total CO trend in these regions was larger in CAMSiRA, which contains the MOPITT observations, than in CR. It could indicate that the anthropogenic emissions were biased low at the beginning of the period but less so towards the end. Over East Asia the difference between CR and CAMSiRA was generally very small indicating a high degree of realism of the emissions in the area. A further explanation for this agreement is the fact that this area covers both the underestimation of CAMSiRA by CR in NH mid-latitudes and the overestimation in the tropics. Both CAMSiRA and CR had a negative but not a significant trend over East Asia.

Stroden et al. (2016) also find good agreement between MOPITT-based and modelled negative trends for the 2000-2010 period of total column CO over Europe and North America but disagreement in the sign of the trend over Eastern China, where their model, using MACCity emissions, simulates a positive trend but MOPITT has a negative trend. Over Eastern China also CR (2003-2015) had a small positive linear trends whereas CAMSiRA had

a negative trend but both trends were not statistically significant. The positive trend over Eastern China in CR was mainly driven by directly emitted CO at the surface. Because of the hemispheric influence, i.e. the hemispheric reduction in CO, the CO trend in CR over Eastern China became negative in the middle troposphere.

In the Arctic, which is influenced by the long-range transport from North America, Europe and Asia (Emmons et al., 2015), no MOPITT observations were assimilated (see Table 2) because of the higher biases of the MOPITT data in this region. Also in this region the variability of the CR and CAMSiRA CO burden matched well but the bias was much reduced after 2012.

The time series of the global CO burden of CAMSiRA and MACCRA agree better than CAMSiRA and CR. The global burden of MACCRA is slightly lower than in CAMSiRA (1%) until 2010 but starts to exceed CAMSiRA in 2011 and 2012. Hence, larger differences occur at the beginning and end of the MACCRA period.

The CO burden of MACCRA above the biomass burning regions of South America and Tropical Africa was lower than CAMSiRA for the period 2003–2010. This is most likely because of the use of the GFED biomass burning emissions until 2008, which are on average 20% lower than GFAS, which was used for CAMSiRA . In the years 2011–2012 MACCRA had higher values, which even led to a reversal in the sign of the trend over the two regions in MACCRA in comparison to CAMSiRA. MACCRA and CAMSiRA agreed well above the anthropogenic source regions. Only from 2008 onwards MACCRA was slightly lower which led to enhanced negative trends.

Over the Arctic, CAMSiRA is higher from 2008 whereas MACCRA was higher at the start. This is consistent with the respective trends over Europe and North America. All data sets showed a step-like reduction the CO burden at mid-2008 but it was most pronounced in MACCRA.

3.3 Evaluation with MOZAIC/IAGOS aircraft CO observations

Measurements of OZone, water vapour, carbon monoxide and nitrogen oxides by in-service AIrbus aircraft (MOZAIC) and In-service Aircraft for a Global Observing System (IAGOS) are subsequent programmes of AC observations mounted on commercial aircraft. The

MOZAIC CO data have an accuracy of ± 5 ppbv, a precision of ± 5%, and a detection limit of 10 ppbv (Nédélec et al., 2003). De Laat et al. (2014) compare MOZAIC/IAGOS profile with the MOPITT v5 NIR retrievals, which were assimilated in CAMSiRA. They find good agreement and no drift of the biases of the two data sets in their study period 2002–2010.

We use the CO profiles obtained during take-off and landing to evaluate the CO fields averaged over airports in different regions from 2003–2012. The number of MOZAIC/IAGOS CO profiles fluctuated considerably over the years. They have decreased from 2003–2014 by about 50% and certain airports had many more observations than others. Since the aircraft used in MOZAIC were based in Frankfurt, the majority of the CO profiles were observed at this airport. Therefore the observations from Frankfurt dominate the European mean values. Observations from Tokyo and other Japanese cities were the largest contribution to the mean over East Asia. Atlanta, Toronto and Vancouver had the largest number of observation in the North American domain. Windhoek had by far the largest number of observations in Tropical Africa and Caracas in South America. The mean of Maritime South East Asia sea salt is mainly calculated from observations over Jakarta and Kuala Lumpur in 2005, 2006, and 2012 with an unbalanced coverage of the difference months.

Profiles of the mean relative bias of CAMSiRA, MACCRA and CR against MOZAIC/IAGOS CO observations for different regions (see Table 3) averaged over the period 2003–2012 are shown in Figure 5. We discuss here only the annual biases since the seasonal relative biases did not differ to a large extent from the annual relative biases.

All three data sets underestimated the observed CO values throughout the troposphere in Europe, North America and East-Asia. At the surface and the lower PBL up to 900 hPa, i.e. where the highest CO concentrations are observed, CAMSiRA and CR had a relative biases of about -10% in Europe and North America and up to -20% in East Asia, whereas MACCRA had larger relative biases of -20 –-30% at this level and the largest biases occurred in DJF. On the other hand, MACCRA had smaller biases than CAMSiRA and CR in the middle and upper troposphere. The smaller biases of MACCRA may be caused by the more realistic simulation of the chemical CO production by the MOZART chemical mechanism as well as by the change in the CO background error statistic. The assimilation of MOPITT in CAMSiRA reduced the biases relative to CR in the troposphere over Europe and North America but had only little effect at the surface. Over East Asia the assimilation did not lead to changes between CR and CAMSiRA.

Whereas CR had the largest underestimation in NH it was generally higher than CAMSiRA and MACCRA in the tropics. This led to better agreement with the MOZAIC observation in South America and Tropical Africa but also to an overestimation of 20–30% in Maritime South East Asia. The limited number of observations in that region makes this result less robust. MACCRA and CAMSiRA showed little differences over South America and Tropical Africa. The 10% negative bias of MACCRA and CAMSiRA in Tropical Africa is consistent with the 10% underestimation of MOPITT v5 against MOZAIC/IAGOS over Windhoek reported by de Laat et al. (2014, their Figure 3). Over MSEA below 700hPa CAMSiRA and MACCRA overestimated CO whereas MACCRA underestimated the observations. This could be the consequence of the different fire emissions and the different chemistry schemes but the limited number of available profiles makes this result less representative.

3.4 Evaluation with NOAA GMD surface observations

NOAA Global Monitoring Division (GMD) network of flask CO surface observations (Novelli and Masarie, 2010) has a good global coverage, which also includes the high latitudes of SH and NH, to observe the background concentrations. The tropical stations represent the maritime background because they are mainly located on islands in the tropical oceans. The station density is higher in North America and Europe. The uncertainty of the NOAA/GMD CO observations is estimated to be 1–3 ppm (Novelli et al., 2003).

We calculated the mean and, for reasons of simplicity, only the linear trend at each station for the period 2003–2014 or 2003-2012 (MACCRA). The overall bias averaged over all stations of CAMSiRA and CR was 3.0 ppb for the whole period but CAMSiRA had a slighter lower RMSE (13 ppb) than CR (15 ppb). For the 2003–2012 period MACCRA had a bias of 6 ppb whereas CAMSiRA and CR had a bias of 3.1 and 3.9 ppb respectively.

Figure 6 shows the zonal means of the observed averages and the corresponding model values at station location as well as the median of the estimated linear trend from the observations and the model results. The graphs were constructed by calculating the mean concentrations and median trends of all stations in 15° wide latitude bins. The errors bars indicate the range of the observed values in the latitude bin.

In the SH high and mid-latitudes the typical observed annual mean surface concentration was 50 ppbv. The background levels started to rise in the SH extra tropics and reached a maximum of 145 ppbv in the NH mid- latitudes. The values then decreased to about 130 ppb

in the Arctic. The general structure of the zonal variation was well represented by all data sets. CR overestimated the SH mid and high values by 15 ppb whereas CAMSiRA and MACCRA had a bias of 7 ppb. In the tropics CAMSiRA had slightly lower (3 ppb) values than the observations whereas MACCRA and CR overestimated by about 5 ppb. CAMSiRA had the highest values of all three data sets in the NH mid-latitudes but still underestimated the mean of the observations by 7 ppb. However the observed means at the station locations in this latitude band varied in a range of about 100 ppb. CR had a slightly larger underestimation than CAMSiRA. MACCRA underestimated the observations by more than 20 ppb in the mid and high latitudes. The reduction towards the NH high latitudes in CR and CAMSiRA was similar to the observations.

The observations in the SH showed essentially no linear trend in the 2003–2014 period. Starting in the tropics a negative linear trend gradually occurred which reached values of about -2.2 ppb/yr in the NH mid- and high latitudes. CAMSiRA and CR had a small but still significant negative trend in SH of -0.3 and -0.5 ppb/yr respectively. The negative trends of CAMSiRA and CR started to become more pronounced from 20°S onwards. The trend in CAMSiRA was generally stronger than the trend in CR. This meant a better fit with the observed trends in the tropics for CR and a better fit in the NH mid- and high latitudes for CAMSiRA. In this region the median of the trends was -2.1ppb/yr for CAMSiRA and -2.0 ppb/yr for CR. While the trends of CAMSiRA and CR agreed reasonably well with the observations, MACCRA suffered from unrealistically strong negative trends in the mid- and high latitudes of both hemispheres. This negative trend in MACCRA was caused by the reduction in the values related to assimilation of IASI data from 2008 onwards (Inness et al., 2013).

4 Aerosols

In contrast to the assimilation of individual chemical gases, the assimilation of AOD observations is "underdetermined" because different combinations of the aerosol components can led to the same extinction, i.e. AOD value. A further complicating factor is that each aerosol component has different optical properties, which depend on relative humidity for the hydrophilic components such as sea salt, sulphate and organic matter. The correction of the speciation of the assimilated aerosol mass mixing ratio fields is therefore a big challenge despite good success in reproducing independent AOD observations with the aerosol analysis (Eskes et al. , 2015).

4.1 Global aerosol burden, speciation and AOD

In this section the global averages of burdens and AOD are presented. Spatial patterns of AOD will be discussed in section 4.2. Global area-weighted averages of AOD at 550nm and the total global burden in Tg for the different aerosol components are shown in Figure 7. The

544 figure also shows the median of the global AOD average and burdens simulated by the
545 models of the AeroCom inter-comparison study (Kinne et al., 2006 and Textor et al., 2006).
546 CR had the highest total global average aerosol burden of 46 Tg compared to MACCRA and
547 CAMSiRA, which had both 33 Tg. This number was very similar to the AeroCom median of
548 29 Tg.

549 The global sea salt burden was about twice as high in CR (15.1 Tg) than in CAMSiRA (8.3
550 Tg), and it was 16.1 Tg for MACCRA. In comparison, the median of the sea salt burden from
551 the AeroCom models is 6.3 Tg. Another study of different emission schemes by Spada et al.
552 (2013) found sea salt burdens in the range from 5.0 to 7.2 Tg. In the light of these studies as
553 well as the applied correction by the assimilation in CAMSiRA, the simulated sea salt burden
554 of CR appears to be too high. The simulated sea salt emissions of C-IFS were within the
555 reported range in the literature (see supplement). This suggests that the loss processes of sea
556 salt were underestimated in C-IFS in comparison to other models.. On the other hand, the high
557 sea salt burden of MACCRA was likely caused by an exaggeration of the sea salt emission
558 with an earlier version of the emissions module.

559 The desert dust burden in CR was 27 Tg, which was higher than the AeroCom median of 20
560 Tg. It was strongly reduced by the assimilation in CAMSiRA to 18 Tg. MACCRA had an
561 even lower desert dust burden of 12 Tg because of the underestimation of the desert dust
562 emissions scheme used in MACCRA. As in the case of the sea salt, the underestimation of the
563 desert dust loss by deposition and sedimentation may play an important role in the
564 overestimation of dust burden in CR.

565 The strongest relative change in the global burden by the assimilation occurred for sulphate,
566 which was 1.2 Tg in CR but was 4.7 Tg in CAMSiRA and 3.3 Tg in MACCRA. The
567 respective AeroCom median value is 2 Tg. Because of the larger extinction per unit mass of
568 sulphate, this increase in sulphate had a large impact on total AOD, which will be discussed
569 further below.

570 The organic matter and black carbon burden of CR (0.2 Tg and 2.0 Tg) was increased by the
571 assimilation to 0.36 Tg and 2.4 Tg respectively. The values agreed reasonably well with the
572 AeroCom median of 0.21 Tg and 1.76 Tg.

573 In contrast to the global burden, CR had the lowest global AOD average of 0.13. CAMSiRA
574 and MACCRA had values of 0.16 and 0.18. The values for CR were close to the median of

575 the AeroCom models (0.12) but the two reanalyses had a higher value than the highest global
576 average AOD value of the AeroCom models of 0.15.

577 The largest fraction of the CAMSiRA AOD came from sulphate, which was strongly
578 increased by the assimilation. The contribution of sulphate AOD to total AOD was 13% in
579 CR and 43% in CAMSiRA. Sulphate was also the largest AOD contribution in MACCRA.
580 The global average of sulphate AOD of CR (0.018) was about half of the AeroCom median
581 (0.034), which could suggest an underestimation in the global sulphate burden and AOD in
582 CR. On the other hand, global sulphate AOD of CAMSiRA was 0.06, which was higher than
583 the highest value of the AeroCom model ensemble (0.051).

584 As already discussed for the respective burdens, global desert dust AOD and sea salt AOD
585 were strongly reduced in CAMSiRA compared to CR. In CR sea salt and desert dust AOD
586 contributed each about 30% to the total AOD, whereas in CAMSiRA the contribution was
587 reduced to 15% and 19%. The reduction of sea salt by the assimilation was reasonable as the
588 sea salt burden was above the reported range by Textor (2006) and Spada et al. (2012).
589 However, the reduction in sea salt was compensated by the increase in sulphate, which
590 became the most important contribution to total AOD over many parts of the oceans.

591 The global sea salt burden of MACCRA was higher than in CAMSiRA but similar to CR.
592 However, a different distribution of the mass within the size classes meant that the resulting
593 sea salt AOD of MACCRA was 20% higher than CR. MACCRA had the lowest desert dust
594 burden but differences in the size distribution towards smaller particles meant that the
595 resulting AOD was slightly higher than CR and 20% higher than CAMSiRA. Black carbon
596 and organic matter AOD and burden were similar among CAMSiRA, CR and MACCRA.

597

598

599 ## 4.2 Spatial patterns of AOD

600 Figure 8 shows the annual mean of total AOD and AOD for desert dust, sea salt, sulphate,
601 black carbon and organic matter for period 2003–2015 from CAMSiRA and the differences
602 with CR and MACCRA (2003–2012). The global maxima of the total AOD (>0.5) in
603 CAMSiRA were found over areas of desert dust emissions such as the Sahara, the Arabian
604 Peninsula and the deserts of Central Asia. High emissions of black carbon and organic matter

605 from biomass burning sources in tropical Africa and anthropogenic sources in Eastern China
606 and Northern India also produced to AOD maxima on the global scale.

607 The increase of the global average AOD in CAMSiRA with respect to CR by the assimilation
608 (see section 4.1) occurred in most parts of the globe, in particular over the areas of industrial
609 activity in North America, Europe and East Asia (20–30%) as well as in the polar regions (>
610 50%), where AOD is generally low. The differences between CR and CAMSiRA, although
611 varying in magnitude, exhibit similar spatial patterns in all seasons, with the largest
612 differences occurring throughout NH in MAM. As discussed in section 4.1 the increase is
613 mostly caused by a wide-spread increase in sulphate AOD. Sulphate AOD was increased in
614 relative terms more strongly over the oceans and higher latitudes. In areas of higher modelled
615 sulphate AOD such as the North America, Europe and Northern Asia and the Arctic the
616 contribution to total AOD changed from 40% to 90%, which made sulphate the by far the
617 most abundant aerosol species in these areas as well as over the Antarctic, which seems
618 unrealistic given that the global SO_2 emission were only less than 2% of the total aerosol
619 emissions (see supplement).

620 The identified reduction of global desert dust in CAMSiRA with respect to CR was mainly
621 confined to the main desert dust region, where AOD was reduced by to 0.2. As total AOD
622 was dominated by desert dust, total AOD was strongly reduced in these regions, whereas total
623 AOD of CAMSiRA was always higher than CR in the other parts of the globe. The largest
624 relative reduction of desert dust AOD occurred in the remote outflow regions from Australia,
625 Tropical Africa and Eurasia. The reduction of desert dust occurred throughout all seasons
626 with the largest reduction in JJA.

627 The strongest reduction in sea salt occurred in CAMSiRA with respect to CR occurred over
628 the oceans proportional to the sea salt AOD. Because of the increase in sulphate, the sea salt
629 reduction led only to a small reduction of total AOD over the area of the highest sea salt
630 emissions in the North Atlantic in DJF and over the Southern Ocean in JJA and MAM. The
631 contribution of sea salt AOD to total AOD over most of the ocean was changed from more
632 than 80% in CR to 50% in CAMSiRA in mid- and high latitudes of SH and to 30% over the
633 rest of the maritime area by the assimilation.

634 Black carbon and organic matter AOD were reduced in CAMSiRA over tropical Africa where
635 biomass burning is the largest source on the global scale and also the CO biomass burning
636 emissions were too high. The black carbon and organic matter AOD values were higher in

637 CAMSiRA away from the sources where values are generally low. The differences of black
638 carbon and organic matter AOD between CAMSiRA and CR showed a strong reduction
639 directly over the areas of intense fire emission in tropical Africa and boreal forest of NH and
640 an increase in the adjacent outflow regions. This could indicate that the GFAS emissions, as
641 in the case of CO (see section 3.1), were too high but the atmospheric residence times of the
642 aerosol species were too short.

643 Compared to CAMSiRA, MACCRA AOD values were up to 50% (-0.2– -0.3) lower in the
644 desert dust dominated areas over the Sahara and Central Asia. The largest differences over
645 North-Africa occurred in JJA and MAM and are an indication that MODIS AOD retrievals
646 are not available over this regions because of their bright surface (Hsu et al., 2013). The
647 higher AOD values of CAMSiRA than MACCRA in the desert dust regions might be an
648 improvement as Cuevas et al. (2015) reported a general underestimation with respect to
649 AERONET observations in the dust dominated regions of MACCRA.

650 On the other hand, sea salt AOD over all oceans was much higher in MACCRA than
651 CAMSiRA and it even exceeded the high sea salt AOD of CR. Despite the higher sea salt
652 AOD, the total AOD of MACCRA over the oceans was lower than in CAMSiRA because of
653 the overall smaller sulphate AOD in maritime regions.

654 In the regions of boreal fire emissions MACCRA was lower during the JJA fire season as well
655 as in the South American fire season in SON. For the rest of the globe the CAMSiRA, was
656 about 0.05 lower than the MACCRA, which meant a large relative reduction (>50%) in
657 particular over the oceans.

658 The differences between MACCRA and CAMSiRA can mainly be explained with the
659 changes in the underlying modelling approach and the emissions since the same MODIS
660 AOD retrievals were assimilated in both reanalyses. Differences in the back ground error
661 statistics may have contributed to the differences, particularly in the high latitudes.

662 Figure 9 shows a zonally averaged cross section of the total aerosol mixing ratio of
663 CAMSiRA and its relative differences of CR and MACCRA. The highest zonal average
664 occurred over the southern ocean because of the continuous sea salt production, and over the
665 latitudes of the regions with large desert dust and anthropogenic emissions. Despite the
666 mostly higher AOD values, CAMSiRA had lower mass mixing ratios than CR throughout the
667 troposphere with the largest relative differences occurring over the SH mid-latitudes and in

668 the region of intense convection in the tropics. This is related to a change in the speciation,
669 which was discussed in section 4.1. CAMSiRA had up to 90% higher values in the
670 stratosphere and Antarctica. The higher aerosol mixing ratios of CAMSiRA in the upper
671 troposphere were dominated by sulphate aerosol. MACCRA mixing ratios were considerably
672 higher in relative terms than CAMSiRA throughout the troposphere with the exception of NH
673 extra-tropical mid- troposphere, caused by the lower dust emissions in MACCRA, and the SH
674 and tropical stratosphere related to high sulphate concentrations in CAMSiRA.

675 ### 4.3 Inter-annual variability of AOD

676 Figure 10 shows time series of average AOD from CAMSiRA, CR and MACCRA for
677 different regions. To better distinguish the impact of sea salt, the regional AOD is averaged
678 over land points only. The global average AOD time series are shown separately for land and
679 sea points.

680 CR and CAMSiRA did not have any significant (95% confidence level) trends in AOD over
681 the whole globe or any of the considered regions. There was a good agreement between
682 CAMSiRA and CR in their inter-annual variability with respect to specific years with higher
683 maxima over South and North America as well as over Maritime South East Asia and North-
684 Africa. This demonstrates that despite biases the model was able to reproduce the variability
685 related to fire emissions and wind driven desert dust suspension. A large relative difference
686 between CR and CAMSiRA occurred in the Arctic. The CAMSiRA and MACCRA AOD
687 values were almost twice as high as CR and had a much more pronounced seasonality.

688 In contrast to the lack of significant trends in CR and CAMSiRA, MACCRA had significant
689 positive trend over all sea points leading to an increase over 10 years, which was as large as
690 the seasonal variation over all sea points. Averaged over all land points, the seasonal variation
691 is much larger than over sea. The agreement in AOD in the monthly means time series was
692 generally high but MACCRA also showed a significant increasing trend, which was not
693 present in the other two data sets. Most of this trend in MACCRA was caused by dust AOD,
694 which increased by 3.7%/yr, and by sea salt AOD, which increased by 1.7%/yr over sea
695 points. We consider this trend in MACCRA as spurious. It is likely caused by an
696 accumulation of aerosol mass, which could not be corrected by the assimilation. A reason for
697 the mass accumulation could be the fact that the MACCRA model did not apply a global mass
698 fixer.

4.4 Even if CR and CAMSiRA did not show significant trends in total AOD, sulphate AOD of CAMSiRA increased significantly by 0.55%/yr and both CR and CAMSiRA had a positive trend in sea salt AOD of 0.3%/yr. This suggests an artificial accumulation of sulphate by the assimilation because t the emissions for the aerosol sulphate precursor (SO_2) were constant. The increase in sulphate was likely caused by underestimated loss processes for sulphate and SO_2 in the free and upper troposphere away from the emissions sources. The relative increase in sulphate with respect to the other aerosol species could not be corrected by the assimilation of AOD.Evaluation with AERONET AOD observations

The AOD at 550 nm was evaluated with observations of the AErosol RObotic NETwork (AERONET) network. The AERONET is a network of about 400 stations measuring spectral AOD aerosol with ground based sun-photometers (Holben et al., 1998). The stations are mostly located over land with a high number of stations situated in North America and Europe. The global number of stations contributing observations for the evaluation increased from about 60 in 2003 to about 250 in 2014 before it reduced strongly to only a couple of stations at the end of 2015.

Figure 11 shows time series of the monthly biases of CAMSiRA, MACCRA and CR for the globe and different regions. Over North America, an area with a high density of AERONET stations, CR underestimated AOD in general by 0.05 on average. On the other hand, the two analyses overestimated AOD by about 0.02 but CAMSiRA has marginally smaller biases than MACCRA. In South America a similar pattern was found only that the average underestimation of CR and overestimation of CAMSiRA and MACCRA was -0.05 and 0.05 respectively. The overestimation of CAMSiRA and MACCRA and the underestimation of CR over America leads to the conclusion that the assimilated MODIS retrievals were biased high against the AERONET observations in this region as also pointed out in Levy et al. (2010). The underlying model does not seem to be the cause of the overestimation in CAMSiRA.

Over Europe CAMSiRA had the smallest biases and MACCRA overestimated slightly whereas CR underestimated the observations. The bias of CR was -0.07 at the beginning of the period and almost zero at the end. More research is needed to understand this trend in the bias, which is also apparent in CAMSiRA and MACCRA, but it might be caused by the reduced number of available stations.

MACCRA had the lowest biases over South East Asia because of small biases in Northern India and Indochina. It was higher, as almost everywhere, than CAMSiRA and CR. CAMSiRA underestimated the observations in this region by about 0.05. The underestimation by CR was bigger and showed a pronounced seasonal cycle. The largest negative biases occurred at the time of the seasonal minimum in DJF.

The performance for desert dust and sea salt was more difficult to evaluate with AERONET stations in a robust way because only few stations are available in these regions. The average bias over Africa showed a strong reduction of the CR peak values, which occurred because of desert dust outbreaks, by the assimilation. A good example of the successful reduction of dust by the assimilations was Lake Argyle (16.11.S, 128.75E) in Australia (Figure 11, left).

The AOD AERONET observations over the oceans show generally an overestimation of all runs, in particular for MACCRA. The bias of the MODIS retrievals with respect to AERONET (Shi et al., 2011) may be a reason for this overestimation. The comparison with AOD observation at Mauna Loa Station (19.54 N, 155.58 W, not shown) in the Eastern Pacific suggests that the low AOD values of CR reproduced the observations best, although still overestimating them. At Nauru Station (0.52 º S, 166.9 º E, Figure 11, right) in the Western Pacific CAMSiRA match the observations well whereas CR underestimated and MACCRA overestimated them.

5 Stratospheric ozone

The experience from the assimilation of TC and stratospheric profiles retrievals (Inness et al., 2013, van der A et al., 2015 and Levefer et al., 2015) shows that these observations are sufficient to constrain stratospheric ozone in the reanalysis. Because almost the same ozone retrievals were assimilated in CAMSiRA as in MACCRA (see Table 2) most of the differences in the ozone analyses can be attributed to differences in the ozone simulation of the assimilating model. For CAMSiRA the Cariolle parameterization (Cariolle and Teyssèdre, 2007) of stratospheric ozone chemistry and the chemical mechanism CB05 for the troposphere were used. The tropospheric and stratospheric chemical scheme of the MOZART CTM (Kinnison et al., 2007) was used for MACCRA.

5.1 Spatial patterns of TC ozone

Figure 13 shows the seasonal average TC ozone from CAMSiRA and the difference between this data set and CR and MACCRA. The differences between CAMSiRA and CR had a

762 meridional pattern. The assimilation in CAMSiRA increased the total ozone columns in the
763 tropics and subtropics by up to 25 DU (8%) and it decreased them by 50–70 DU in the NH
764 mid and high latitudes. The largest reduction occurred in DJF and MAM. Also over
765 Antarctica the assimilation led to lower values in austral winter (JJA), when TC ozone was
766 reduced by up to 30 DU.

767 CAMSiRA was about 3–5 DU (1%) lower than MACCRA throughout the globe. Larger
768 differences of up to 10 DU (2%) were located mainly over tropical land areas. Their shape
769 suggest that they were partially caused by differences in tropospheric ozone (see section 6.1).
770 On the seasonal scale, CAMSiRA was about 10 DU lower over Antarctica and the Arctic in
771 the respective spring seasons MAM and SON.

772 Figure 14 shows the average ozone partial pressure cross section of CAMSiRA and the
773 relative differences with CR and MACCRA. The tropospheric part of the figure will be
774 discussed in section 6.1. The overestimation of CR in the high latitudes of NH and SH was
775 located predominately in the mid and upper stratosphere at around 20 hPa. The
776 underestimation in the tropics had the largest values at around 50 hPa.

777 In the lower and middle stratosphere, i.e. from 70 to 20 hPa, CAMSiRA and MACCRA
778 differed by less than 5%. Larger differences occurred above 10 hPa where MACCRA was up
779 to 30% higher than CAMSiRA.

780 ## 5.2 Inter-annual variability of TC ozone

781 Figure 15 shows area-weighted averages of the monthly TCs for the whole globe, the tropics,
782 SH and NH mid-latitudes, Antarctica and the Arctic.

783 In the tropics, CAMSiRA had a significant (95% confidence level) trend of +0.15%/yr.
784 Although the period of 13 years is too short to estimate total ozone trends with respect to
785 ozone recovery it is worth noticing that the number is in good agreement with the estimate of
786 the ozone trend for the period 1995–2013 by Coldewey-Egbers et al. (2014, see their figure
787 1), which varies in the tropics between 0.5 to 1.5%/decade. No trends could be found in CR,
788 probably because the climatological approach applied in the Cariolle scheme is not able to
789 simulate long-term trends. The tropical trend in MACCRA was 0.25%/yr, which seems too
790 high and there was also a significant trend in the SH mid-latitudes of 0.65%/yr.

The seasonal range, i.e. the difference between annual maximum and minimum, of TC ozone in CAMSiRA increased from 10 DU in the tropics to up 150 DU in the Arctic and 100 DU in Antarctica. As already mentioned in section 5.1, CR was 20% higher than CAMSiRA in NH mid-latitudes and Antarctica. However, the inter-annual variability agreed reasonably well between CAMSiRA and CR in SH and MH high and mid-latitudes. For example, the reduced Arctic ozone spring in 2011 (Manney et al., 2011) and the year-to-year differences in mid-latitudes found in CAMSiRA were well reproduced by CR.

The ozone hole in Austral spring is the most important feature of seasonal variability over Antarctica. Despite its simplicity, the Cariolle scheme in CR reproduced the ozone loss during the ozone hole periods with respect to minimum value and inter-annual variability of TC ozone very well without assimilating any observations. 2015, 2003 and 2006 were the years with the deepest ozone holes and 2011, 2013 and 2004 with the shallowest ozone hole both in CAMSiRA and CR. On the other hand, CR overestimated the average TC ozone during winter by about 30 DU.

There was generally good agreement between CAMSiRA and MACCRA over all parts of the globe but MACCRA was on average about 5–10 DU (2%) higher than CAMSiRA. The strong positive trend of MACCRA in the tropics together with a significant positive trend in the SH mid-latitudes led to increasing differences of the global average at the end of the MACC period. Larger difference between MACCRA and CAMSiRA occurred in winter (JJA) over Antarctica, when MACCRA was up to 25 DU lower than CAMSIRA. The depth of the ozone hole was slightly deeper in CAMSiRA than in MACCRA.

5.3 Evaluation with total ozone retrievals from Dobson sun-photometers

Ozone TCs are observed from the ground with Dobson, Brewer, Point Filter and FTIR spectrometers. The Dobson instruments provide the longest and best spatial coverage and we use this data set to evaluate the TC of CAMSiRA, MACCRA and CR. The Dobson instruments of the WOUDC network are well calibrated and their precision is 1% (Basher, 1982). Factors that influence the accuracy of the Dobson spectrometer are the temperature dependency of the ozone absorption coefficient and the presence of SO_2.

Figure 16 shows time series of the monthly bias against the Dobson photometer observations for different regions. Observations of about 50–60 stations were available until 2013 but the number of stations dropped steadily to about 10 Stations at the end of 2015. CAMSiRA

overestimated the observations in the tropics and the mid-latitudes of both hemisphere on average by 2 DU whereas the mean bias of MACCRA was about 5 DU larger. In Antarctica and the Arctic the biases showed a more pronounced seasonal cycle mostly between -10 and 20 DU.

The biases of MACCRA increased in the tropics and the SH-mid latitudes from 2003 to 2008 whereas CAMSiRA and CR did not show an obvious change in the biases until 2012. The variability of the bias of CAMSiRA amplified at the start of 2013 in NH. As this change in the bias is not seen at individual stations reporting until the end of 2015, we conclude that the change is caused by the reduction in the number of stations available after 2013. It is not caused by the change of the assimilated MLS data set version (from V2 to V3.4) because this took place already at the beginning of 2013 (see Table 2).

The biases of CR were much larger than the ones of CAMSiRA, and they had a strong seasonal cycle. In the tropics CR underestimated the TC by 10 DU in DJF and 0 DU in MAM. The NH biases were positive and varied between 20–50 DU and in the Arctic between 20–70 DU. Over Antarctica CR overestimated the observation by 40–60 DU in JJA but the bias was close to zero or even slightly negative during the time of the ozone hole.

5.4 Evaluation with ozone sondes in the stratosphere

The global network of ozone sondes is the most comprehensive independent data set for the evaluation of the 3D ozone fields from the surface to about 10 hPa, which is the level with the highest stratospheric ozone volume mixing ratios. The observation error of the sondes is about ±5% in the range between 200 and 10 hPa and -7–17% below 200 hPa (Beekmann et al., 1994, Komhyr et al., 1995 and Steinbrecht et al., 1996). The number of soundings varied for the different stations used here. Typically, the sondes are launched once a week but in certain periods such as during ozone hole conditions launches are more frequent. Sonde launches are carried out mostly between 9 and 12 hours local time. The global distribution of the launch sites is even enough to allow meaningful averages over larger areas such North America, Europe, the tropics, the Arctic and Antarctica.

Figure 17 shows the profiles of the relative biases of CAMSiRA, MACCRA and CR over the tropics, Antarctica, the Arctic and the NH and SH mid-latitudes for the period 2003–2012. All available observations were included in the average.

In the tropics, CAMSiRA had a relative bias of mostly below 10% in most of the stratosphere. MACCRA underestimated the ozone sondes strongly (up to 30%) in the lower stratosphere but the relative bias of MACCRA was similar or slightly smaller than the bias of CAMSiRA in most parts of the stratosphere, i.e. in the pressure range from 70 to 20 hPa. CR underestimated the ozone sondes by up to 20% in the stratosphere up to 30 hPa. The largest underestimation of CR occurred in the lower and mid stratosphere, where the maximum in ozone partial pressure is located. In the upper stratosphere above 20 hPa, where the maximum of ozone volume mixing ratio is located, the relative biases of all data sets were smaller than in the levels below. CR had almost no bias whereas MACCRA overestimated by up 10%.

Over the Arctic and NH mid-latitudes CAMSiRA and MACCRA agreed well with the sondes in the whole stratosphere with relative biases below 5%. The absolute biases of CAMSiRA were slightly smaller than the biases of MACCR in particular in the lower stratosphere and upper troposphere. CR overestimated the ozone observations by up to 25% in the stratosphere and upper troposphere over the Artic and up to 20% in the NH mid-latitudes. The relatives biases of CR tended to be slightly smaller in the mid stratosphere (50 hPa) than in the upper and lower stratosphere.

Over SH-mid latitudes and Antarctica the annual biases in the stratosphere were slightly smaller in CAMSIRA than MACCRA but for both reanalyses they were below 10%. As over the Arctic, the absolute tropospheric biases, with the exception of the surface values, were smaller in MACCRA since CAMSiRA showed an underestimation of about 10%. CR had a stronger underestimation in the lower and upper stratosphere.

As the process of the ozone-hole formation cannot easily be demonstrated with annual means, Figure 18 shows the monthly mean profile from August to November over Neumayer Station (70.7° S, 8.3° W). The two reanalysis agreed very well with the observations: vertical level and magnitude of the ozone profile at the end of the austral winter in August, the ozone depletion in September and October and the closure of the ozone hole starting in the upper stratosphere were well captured because of the assimilation of TC and limb-sounders profiles.

In contrast, CR showed a strong overestimation in August in the middle and lower stratosphere. Ozone in the upper stratosphere in September was underestimated in CR because of an exaggerated depletion whereas ozone was overestimated in the lower stratosphere. In the following months CR ozone remained too high in the lower stratosphere

and too low in the upper troposphere but the resulting TCs matched the observations in a reasonable way (see Figure 16)

5.5 Evaluation with the GOZCARDS ozone product in the upper stratosphere

Ozone sondes do not provide accurate measurements above 10 hPa. The ozone bias profiles shown in Figure 17 indicate higher values of MACCRA in the upper stratosphere and mesosphere, i.e. from above 10 hPa to the model top of 0.1 hPa. Although the ozone mass in this region is relatively small, the high values of the mixing ratios have a large impact on the radiative transfer and the associated heating rates. To investigate the biases in that region we used the Global OZone Chemistry And Related trace gas Data records for the Stratosphere (GOZCARDS) product (Froidevaux et al., 2015). It consists of merged SAGE I, SAGE II, HALOE, UARS and Aura MLS, and ACE-FTS data from late 1979 to 2012. SAGE II is used as the primary reference in the merging procedure for the instruments. For most of the CAMSiRA period, i.e. from 2004 onwards, Aura MLS and ACE-FTS are the dominating instruments in the upper stratosphere. Tegtmeier et al. (2013) showed that ozone retrievals from various instruments show a considerable spread in the upper stratosphere. ACE-FTS is biased high (5-10%) above 10 hPa and biased low (5-10%) below 10 hPa against the median of various retrievals.

Figure 19 shows cross sections of the GOZCARDS product and relative bias of CAMSiRA, MACCRA and CR in the vertical range from 50–0.3 hPa. In the region from 10–5 hPa MACCRA had a positive bias of 10–15% in the tropics and mid-latitudes, which has already been reported in Inness et al. (2013). About half of the 10 DU higher TCs in MACCRA compared to CAMSiRA were caused by this overestimation in the levels above 10 hPa. The biases of CAMSiRA in that region were smaller and vary between 2.5 and -2.5%. CAMSiRA underestimated the GOZCARDS data between 5 and 1 hPa by up to 7%, whereas MACCRA slightly overestimated. In the lower mesosphere MACCRA underestimated the ozone concentrations by up to 30%.

CR had very similar biases as CAMSiRA above 5 hPa in the tropics and mid-latitudes. This means that the assimilation of observations had already little influence in this region even if no increments were added during the CAMSiRA assimilation above 1 hPa. Below 10 hPa the cross section of the bias shows the already discussed strong overestimation of CR in the mid

913 and higher latitudes, which was largest in relative terms at around 20–15 hPa and the
914 underestimation in the tropics, which was largest at around 50 hPa.

915 # 6 Tropospheric ozone

916 Correcting tropospheric ozone by the assimilation of TC and stratospheric ozone profiles
917 remains a challenge because the observations are dominated by the high stratospheric mixing
918 ratios (Wagner et al., 2015). The modelled ozone fields as well as the specification of the
919 vertical background error correlation have therefore a large impact on the analysed
920 tropospheric ozone fields (Inness et al., 2015).

921 ## 6.1 Spatial patterns of ozone at 850 hPa

922 We focus the discussion of the seasonal spatial patterns of monthly mean tropospheric ozone
923 mole fraction to the 850 hPa pressure level values but we also discuss tropospheric ozone at
924 500 and 200 hPa in the section 6.2 and comparisons with ozone sondes for different
925 tropospheric layers in section 6.3. Figure 20 shows the seasonal means of CAMSiRA and the
926 differences with CR and MACCRA at 850 hPa. Extratropical NH ozone values of CAMSiRA
927 were mostly in the range from 35–55 ppb. The season of the maximum was MAM, when
928 values were about 20 ppb higher than in the seasonal minimum in DJF. Regional maxima of
929 over 60 ppb were situated over the East Asia and the Arabian Peninsula. JJA was the season
930 when the highest values occurred over the areas of the regional maxima. In this season an
931 additional regional maxima occurred over tropical Africa. The SH values were generally
932 below 35 ppb. The seasonal maximum was in Austral spring (SON) and the minimum in
933 Austral summer and late autumn (SON).

934 CR was about 2–4 ppb higher than CAMSiRA in most parts of the globe. Only in the higher
935 latitudes of SH as well as over the biomass burning regions in Africa, South America and
936 Maritime South East Asia, CAMSiRA was up to 4 ppb lower than CR. The biggest large-
937 scale reduction by the assimilation in NH occurred in DJF and the biggest increase in SH in
938 SON. The largest absolute increases of CAMSiRA of up to 10 ppb occurred over the Southern
939 end of the Arabian Peninsula at the time of the seasonal maximum in JJA. This was the only
940 local maximum in CAMSiRA that was increased by the assimilation.

941 Tropospheric ozone was the only considered species for which the differences between
942 CAMSiRA and MACCRA were larger than the difference between CAMSiRA and CR. This
943 indicates the importance of the chemistry model parameterization and the limitations of the

data assimilation in this respect. In the extra-tropics of NH and SH, CAMSiRA was 2–5 ppb lower than MACCRA with an increasing difference towards the poles. The largest difference occurred in NH summer in JJA. CAMSiRA was up to 10 ppb lower than MACCRA over the continents in the tropics. On the other hand, CAMSiRA had higher values than MACCRA over the tropical oceans, the Sahara as well as at the location of the strong maximum over the Arabian Peninsula, which was not present in MACCRA. The strong land-sea contrast in the differences could be caused by (i) a different efficiency of deposition over the oceans, (ii) the discussed differences in biomass burning emissions and (iii) differences in the chemistry treatment (e.g. the isoprene degradation scheme).

The vertical distribution (see Figure 14) of the mean ozone partial pressure in the troposphere shows that CAMSiRA was lower than CR in the whole troposphere apart from the tropical upper troposphere, where it was up to 10% higher, as well as below 500 hPa in the SH troposphere. Compared to MACCRA, CAMSiRA was up to 20% higher in the middle and upper troposphere in the tropics and subtropics but increasingly lower towards the surface.

6.2 Inter-annual variability

Estimating and understanding tropospheric ozone trends have been studied widely in the literature, as reviewed in Cooper et al. (2014) and Monks et al. (2015). Factors that influence the inter-annual variability and trends of tropospheric ozone are changes in anthropogenic and biomass burning emissions, the stratosphere-troposphere exchange and the variability of the meteorological fields. The observed trends vary strongly because these different factors are not uniform in space and time. Trends are often confined to specific seasons or levels. Positive trends are more common than negative trends and are found over Europe and North America during spring (Cooper et al., 2014).

Figure 21 shows time series of average ozone volume mixing rations over selected regions and pressure levels at 850, 500 and 200 hPa. It is beyond the scope of the paper to investigate the robustness of the trends in CAMSiRA in detail. But it is worth noting that there were only positives trends in the considered region at 850, 500 and 200 hPa in CAMSiRA. The trends varied between 0-1.1%/yr, with a global mean of 0.5%/yr. Many of these trends were significant (95% confidence level). CR also had mostly positive but much smaller trends with a global mean of 0.17%/yr. The only significant trend in CR of 0.35%/yr was found over East-Asia and the corresponding trend in CAMSiRA had the same value. Focusing over

Easter China, Verstraeten et al. (2015) find a trend of about 1.2%/yr between 2005 and 2010, which is considerably larger than the trend in CAMSiRA and CR.

The time series in Figure 21 show that the higher values in NH of CR with respect to CAMSiRA occurred in the entire troposphere. In the lower and mid troposphere CAMSiRA was lower than CR especially during the seasonal minimum. In the tropics, CR and CAMSiRA agreed well at 850 hpa, CR was slightly higher at 500 hPa and about 5 ppb lower than CAMSiRA at 200 hPa. At this level CAMSiRA had a significant trend of 0.95%/yr in the tropics, which was not present in CR. More detailed studies are needed to confirm the realness of this upper tropospheric trend in CAMSiRA.

A more detailed inspection of the time series shows that from the start of 2013 CR and CAMSiRA agree to higher degree than before in the middle and upper part of the troposphere in NH. The agreement is most likely caused by a reduced correction by the assimilation in the NH troposphere in this period. In early 2013 the assimilated MLS ozone retrieval switched from version V2 to the NRT V3.4 product (see Table 2), which had different levels and observations errors. The discontinuation of the MIPAS in spring 2012 do not seem to be the reason for this behaviour.

The year-to-year variability of tropospheric ozone from MACCRA did often not resemble that of CAMSiRA. In NH at 850 hPa (most prominently seen in the Arctic) MACCRA had increasing values until 2008 after which they dropped to the values of CAMSiRA. This drift of MACCRA and the associated negative trends are not realistic (as confirmed in section 6.3). They were caused by applying the variational bias correction scheme to MLS data in MACCRA (see Inness at al. 2013 for more details). The agreement between CAMSiRA and MACCRA increases with increasing height in the extra-tropics but in the tropics MACCRA showed a much stronger trend at 200 hPa than CAMSiRA.

6.3 *Evaluation with ozone sondes in the troposphere*

Figure 22 show time series of seasonal biases in pressure ranges representing the lower, middle and upper troposphere from 6 different ozone sonde sites. The selected stations had at least one observations for each month of the 2003-2105 period and are examples for Europe (De Bilt), North America (Huntsville), the tropics (Nairobi), the Arctic (Ny-Ålesund) and Antarctica (Neumayer Station). To present South-Asia we chose Hong Kong Observatory, which had complete cover from 2003-2012. These individual time series depend on the

specific characteristics of the individual stations and are therefore less representative than the averages over the gridded data sets shown in section 6.2.

In the lower troposphere (950-700 hPa) over DeBilt, Huntsville and Nairobi, CR and CAMSiRA had seasonal biases in the mostly in the range of -7–7 ppb. In the polar regions at Neumayer Station and Ny-Ålesund both CR and CAMSiRA underestimated the observations. At all locations CAMSiR was lower in the lower troposphere than CR, which meant that CAMSiRA had mostly a larger absolute bias than CR. At Hong Kong Observatory both CAMSiRA and CR overestimated the observations with biases in the range between 0-10 ppb.

In the middle troposphere the absolute biases of CAMSiRA and CR were of the same magnitude but of different signs. In the upper troposphere CR overestimated the observations by about 10 ppb whereas the bias of CAMSiRA remained below 5 ppb. The overestimation of CR is likely caused by the influence of the stratosphere where CR was too high (see section 5.4). Over Nairobi the biases of CR and CAMSiRA were very similar in all levels but CAMSiRA had overall lower biases in the lower troposphere. In the pressure range 400–300 hPa in the tropics the impact of stratospheric biases on CR is less strong because of the higher tropopause height in this region.

The biases for all three data sets at Ny-Ålesund, Hunstville and Hong Kong Observatory showed a pronounced seasonality in the middle and upper troposphere. At Huntsville the spring maximum was especially overestimated, i.e. it occurred 2-3 month too early. At Ny-Ålesund the overestimation was caused by too high values in summer and autumn. Over Hong Kong Observatory the pronounced observed spring maximum was not well reproduced.

As already discussed in section 6.2, the characteristics of the bias of CAMSiRA changed at the start of 2013 mainly in the upper parts of the NH troposphere but also throughout the troposphere over higher latitudes. In this period the CAMSiRA biases resembles much more the bias of CR which often mean an increase in the average values, which could cause a spurious enhancement of positive trends.

At Neumayer Station CAMSiRA increased in a step-wise manner already at the start of 2012, which changed the bias from an underestimation to a slight overestimation together with an increased seasonality. This behaviour could be caused by the discontinuation of MIPAS in spring 2012 (see Table 2). Although the MIPAS retrievals were only stratospheric profiles,

the combined assimilation with total column retrievals can trigger a correction in the troposphere (Flemming et al., 2011).

MACCRA had a less stable bias than CAMSiRA. In the lower and mid-troposphere biases from 2006–2008 were much higher than in the rest of the period, when they resembled more the biases of CAMSiRA and CR. This confirms that the discussed inter-annual variability of MACCRA seem less realistic than that of CR and CAMSiRA.

It should be noted that both MACCRA and CAMSiRA suffered from larger than typical negative biases in the NH in the first half of 2003, which can probably be explained by biases in the initial conditions and the short spin-up period of 1 month only.

6.4 *Evaluation with Airbase Ozone surface observations*

The AirBase and EMEP databases host operational air quality observations from different national European networks. All EMEP stations are located in rural areas, while Airbase stations are designed to monitor pollution at different scales. Stations of the rural regime can capture the larger scale signal in particular for O_3, which is spatially well correlated (Flemming et al., 2005). Therefore EMEP stations and only rural Airbase stations were used in the evaluation to account for the model resolution of C-IFS.

Figure 23 shows the average diurnal cycle for each season of the observed values and CAMSiRA, CR and MACCRA. CR and CAMSiRA were very similar and matched well the shape of the observed diurnal cycle. However there was a constant bias of about 5 ppb in MAM and DJF. CR had slightly smaller biases than CAMSiRA in JJA in the afternoon. MACCRA had a larger diurnal range because the day-time values were higher than the ones of CAMSiRA. This meant smaller day-time biases in MAM and DJF and hence a smaller seasonal bias for MACCRA. But it also led to a considerable (10 ppb) day time overestimation in JJA and a smaller overestimation in SON as well as a less well fit with the shape of the observed diurnal cycle in all seasons.

The winter and spring underestimation of CAMSiRA and CR has already been reported in Flemming et al. (2015). To investigate the possible causes of this seasonal bias Figure 24 shows the average seasonal cycle at the surface at the EMEP-AirBase stations and in the lower troposphere (950–750 hPa) over ozone sonde stations. The differences between CAMSiRA, CR and MACCRA were more pronounced in the lower troposphere than at the surface. This indicates again that the assimilation has little influence on the surface values.

CR matched the observations in the lower troposphere well in all seasons apart from SON, when it overestimated. MACCRA had similar biases as CR but overestimated additionally in JJA and especially over southern Europe, as shown in Katragkou et al. (2015). CAMSiRA underestimated throughout the year with the exception of SON. As the patterns of the seasonal biases were different in the lower troposphere and at the surface, we conclude that the winter and spring-time bias at the surface is not predominately caused by tropospheric biases. It is more likely that the simulation of surface processes such dry deposition and titration by freshly emitted NO are the reasons for this bias at the surface.

7 Summary and conclusions

CAMSiRA is a new reanalysis data set of aerosol, CO and ozone for the period 2003–2015. It has been produced by assimilating satellite retrievals of AOD, TC CO as well as TC and stratospheric ozone profile retrievals from various sensors in C-IFS using the ECMWF 4D-VAR approach. A similar set of observations was assimilated in MACCRA, a previous reanalysis data set for the period 2003–2012. A control run with C-IFS (CR) without the assimilation of AC observations was carried to infer the impact of the assimilated observations.

7.1 CAMSiRA compared to MACCRA

Compared to its predecessor MACCRA, CAMSiRA had smaller biases of surface and lower tropospheric CO as shown by the comparison with MOZAIC/IAGOS CO profiles and NOAA-GMD CO flask observations. However, MACCRA had lower CO biases in NH mid and upper troposphere with respect to the MOZAIC/IAGOS CO profiles. The biases of TC ozone against the WOUDC Dobson sun photometers where reduced from 5–10 DU in MACCRA to 0–5 DU in CAMSiRA. The biases of CAMSiRA against AERONET AOD observations were lower in most parts of the globe with the exception of South East Asia. A larger improvement was the elimination of the positive bias of upper stratospheric ozone in MACCRA as shown by the comparison with the GOZCARDS ozone product. CAMSiRA also had a better agreement with the shape of the mean observed diurnal cycle of AIRBASE ground-level ozone observations in Europe in all seasons but winter and spring time seasonal values were still underestimated by 5 ppb. We attribute all the aforementioned differences between CAMSiRA and MACCRA, which were mainly improvements, to the change of the

assimilating model, which was the coupled system IFS-MOZART for MACCRA and C-IFS with updated aerosol parameterizations for CAMSiRA.

Progress achieved by changes to the assimilated observations was a noteworthy improvement of the temporal consistency of the tropospheric CO and ozone fields in CAMSiRA. The assimilation of IASI CO in MACCRA from 2008 onwards had led to a decrease in the TC CO values because of the biases against the MOPITT data set, which was assimilated during the whole period. Consequently, the MACCRA CO fields in the mid- and high latitudes of both hemispheres showed strong negative trends which were not in agreement with linear trends estimated from CO flask surface observations. On the other hand, the linear trends of CAMSiRA agreed well with the observed trends, which were close to zero in SH and reached values of about 2 ppb/yr in the NH mid and high latitudes. The mid and upper tropospheric ozone fields of MACCRA suffered from an increase in the period 2004–2008 caused by a applying disproportionate application of the inter-instrument bias correction to the MLS column retrievals, which was corrected for CAMSiRA (Inness et al., 2015).

A discontinuity in the upper and middle tropospheric ozone field was noted for CAMSiRA after January of 2013 and was due to a change in version of the assimilated MLS ozone retrievals. Although this change in CAMSiRA did not mean an increase in the bias, it has to be considered when trends of tropospheric ozone fields are to be calculated from the CAMSiRA data set.

The AOD in CAMSiRA was about 0.01 lower than MACCRA in most parts of the globe, mainly because of a 50% lower burden of sea salt in CAMSiRA. CAMSiRA had higher AOD values over the desert dust emitting regions in North-Africa and the global desert dust burden was higher in CAMSiRA. CAMSiRA had 25% higher AOD contribution by sulphate than MACCRA, which is currently under scrutiny.

7.2 CAMSiRA compared to CR

The comparison with CR showed that the assimilation led to a clear improvement for CO, AOD and TC ozone as well as stratospheric and upper tropospheric ozone.

The assimilation of MOPITT CO increased the values in the NH mid-latitudes more in the beginning of the period, which could indicate a stronger underestimation of the anthropogenic emissions in this period as well as an overestimation of the trend in the emissions. The tropical and SH values were reduced by the assimilation, which may indicate an

overestimation of the biomass burning emissions in this region. However, the rather zonally homogeneous CO differences between CR and CAMSiRA suggest that not only biases in the fire emissions but also of the CO lifetime and chemical production as well as the CO transport need to be investigated further.

The Cariolle scheme for stratospheric ozone, which was used in C-IFS, suffered from a large overestimation of NH mid-and high latitude stratospheric ozone (50–100DU) and an underestimation in the tropics (-20 DU). These biases were corrected by the assimilation and the resulting biases of CAMSiRA were of 5 DU and lower. Also in the SH high-latitudes the Cariolle scheme overestimated the mean TCs especially in JJA by up to 30 DU but the depth and the year-to-year variability of the ozone hole was well reproduced by CR. Nevertheless, CAMSiRA had more realistic TCs and profiles than CR during the annual ozone hole events.

The assimilation had only little impact on the ozone values at the surface and in lower troposphere, where the biases of CAMSiRA where sometimes even slightly larger than of CR. The small influence could be explained by the fact, that dry deposition velocities and important ozone precursors such as NO_x were not constrained during the assimilation process. Also contributing was the fact that no direct tropospheric ozone observations were assimilated nor that the vertical correlations in the model background errors were strong enough to cause a correction of the surface levels based on the levels above. The assimilation was more beneficial in the upper troposphere, where the stratospheric influence is more important.

CAMSiRA had about 0.05 higher AOD values than CR apart from the desert dust emission regions, where the assimilation strongly reduced the modelled values. CAMSiRA tended to slightly overestimate the AERONET AOD observations and CR to underestimate but the overall biases of CAMSiRA were smaller.

Despite moderate differences in AOD, CR and CAMSiRA had considerable differences in the aerosol speciation. The global annual sea salt burden by C-IFS in CR of 15 Tg was considerably higher than the result of other modelling studies (Textor et al., 2006 and Spada et al., 2012). Less efficient loss processes may have played a large role in this overestimation. The assimilation strongly reduced the sea salt burden in CAMSiRA to about half of the value in CR. Also the global desert dust burden was reduced by 25% by the assimilation leading to lower total AOD values over the desert dust emissions regions of Sahara, Australia and Middle Asia. Despite the fact that CAMSiRA had a 30% smaller global aerosol burden, its average global AOD was about 10% higher than the one of CAMSiRA. This was caused by a

strong increase in sulphate in CAMSiRA. The optical properties and assumed size distribution of sulphate make extinction more efficient for the same amount of mass. Sulphate became the dominant contribution to AOD in the regions away from the main aerosol emissions. The strong contribution of sulphate may have partly compensated for the inadequate representation of other secondary aerosols in C-IFS. However its magnitude and spread over the whole globe seems excessive. It might be caused by the lack of strong loss processes in the free troposphere as well as biases in the assimilated observations over the open oceans. As the CR underestimates the assimilated AOD, the aerosol mass is increased during the assimilation, initially by the same relative amount for all components. However, a longer life-time of sulphate causes a longer lasting change compared to the other aerosol species, which made sulphate the dominating aerosol. This distortion of the speciation can not be corrected by the assimilated MODIS AOD retrievals, which do not contain information about the speciation.

7.3 Recommendations for future AC reanalysis

CAMSiRA is considerable improvement over MACCRA especially with respect to the temporal consistency. To further improve on this important aspect, one should make sure that consistent input emission data sets and assimilated observations are used. Changes in the assimilated observations, such as the version change in the MLS after 2012 should be avoided. The use of MEGAN simulated biogenic emissions for the whole period is advisable even if no related jumps were detected in this study. To ensure consistency between the aerosols and chemistry components, the same SO_2 emissions should be used.

As improvements to lower tropospheric ozone by assimilating current satellite observations are difficult to achieve, emphasis needs to be put on the improved simulation of chemistry and dry deposition. The assimilation of tropospheric ozone column retrievals as well as of tropospheric NO_2 may further help to improve the ground level ozone in the reanalysis.

A prospect is to enable the correction of emissions based on observations of atmospheric composition with the C-IFS data assimilation system. This could also improve the analysis of tropospheric ozone as ozone precursor emissions would be corrected. An intermediate step in this direction is to better account for the emission uncertainty in the model background error statistics.

The high sulphate burden introduced by the assimilation can be avoided by (i) the introduction of more intensive loss processes in the free troposphere, (ii) an increase of the organic matter to better represent non-accounted SOA components and (iii) changes to the vertical structure of the background errors to avoid the accumulation of aerosol mass away from the surface. In general, any modelling improvements for a better speciation will reflect in a more realistic aerosol analysis and a better exploitation of the available observations. If possible the latest reprocesses MODIS AOD dataset should be used (collection 6).

In CAMSiRA and MACCRA the aerosol and chemistry schemes were independent. A better coupling between the two and the meteorological simulation is desirable. For example the use of aerosol to modulate photolysis rates and heterogeneous uptake on aerosol as well as the simulating the impact on aerosols and ozone within the radiation transfer calculation of IFS will be important next steps.

Data access

The CAMSiRA data are freely available. Please contact copernicus-support@ecmwf.int

Acknowledgments

CAMS is funded by the European Union's Copernicus Programme. The GOZCARDS data were obtained from the NASA Goddard Earth Science Data and Information Services Centre. We are grateful to the World Ozone and Ultraviolet Radiation Data Centre (WOUDC) for providing ozone sonde and Dobsen-photometer observations. We thank the Global Atmospheric Watch programme for the provision of CO and ozone surface observations. We thank the European Environmental Agency for providing access to European ozone observations in the AirBase data base. We also thank the MOZAIC (Measurements of OZone, water vapour, carbon monoxide and nitrogen oxides by in-service AIrbus aircraft) and IAGOS (In-Service Aircraft for a Global Observing System) programmes for providing CO profile observations.

References

Auligne, T., McNally, A. P., and Dee, D. P.: Adaptive bias correction for satellite data in a numerical weather prediction system, Q. J. Roy. Meteor. Soc., 133, 631–642, 2007.

Basher, R. E. (1982), Review of the Dobson spectrophotometer and its accuracy, Global Ozone Res. Monit. Proj., Rep. 13, World Meteorol. Organ., Geneva, Switzerland, Dec. (Available at http://www.esrl.noaa. gov/gmd/ozwv/dobson/papers/report13/report13.html)

Bechtold, P., Orr, A. Morcrette, J.-J., Engelen, R., Flemming, J. and Janiskova, M.: Improvements in the stratosphere and mesosphere of the IFS, ECMWF Newsletter No. 120–Summer, 2009.

Beekmann M., Ancellet G., Megie G., Smit H. G. J., and Kley D.: Intercomparison campaign for vertical ozone profiles including electrochemical sondes of ECC and Brewer-Mast type and aground based UV-differential absorption radar, J. Atmos. Chem., 10, 259–288, 1994.

Bellouin, N., Quaas, J., Morcrette, J.-J., and Boucher, O.: Estimates of aerosol radiative forcing from the MACC re-analysis, Atmos. Chem. Phys., 13, 2045-2062, doi:10.5194/acp-13-2045-2013, 2013.

Benedetti, A., Morcrette, J.-J., Boucher, O., Dethof, A., Engelen, R. J., Fisher, M., Flentje, H., Huneeus, N., Jones, L.,Kaiser, J. W., Kinne, S., Mangold, A., Razinger, M.,Simmons, A. J., Suttie, M., and the GEMS-AER team: Aerosol analysis and forecast in the European Centre for Medium-Range Weather Forecasts Integrated Forecast System: 2. Data assimilation, J. Geophys. Res., 114, D13205, doi:10.1029/2008JD011115, 2009.

Benedetti, A. Jones, L., Kaiser, J. W., Morcrette, J.-J. and Rémy, S.: [Global climate] Aerosols [in “State of the Climate in 2013”]. Bull. Amer. Meteor. Soc., 95 (7), S36-37, 2014.

Bhartia, P. K. and Wellemeyer, C.: TOMS-V8 total O3 algorithm, in: OMI Ozone Product ATBD Volume II, NASA Goddard Space Flight Center, Greenbelt, MD, USA, 2002.

Bhartia, P. K., McPeters, R. D., Mateer, C. L., Flynn, L. E., and Wellemeyer, C., Algorithm for the estimation of vertical ozone profiles from the backscattered ultraviolet technique, J. Geophys. Res., 101, 18793–18806, 1996.

Bocquet, M., Elbern, H., Eskes, H., Hirtl, M., Žabkar, R., Carmichael, G. R., Flemming, J., Inness, A., Pagowski, M., Pérez Camaño, J. L., Saide, P. E., San Jose, R., Sofiev, M., Vira, J., Baklanov, A., Carnevale, C., Grell, G., and Seigneur, C.: Data assimilation in atmospheric

chemistry models: current status and future prospects for coupled chemistry meteorology models, Atmos. Chem. Phys., 15, 5325-5358, doi:10.5194/acp-15-5325-2015, 2015.

Boucher, O.: Atmospheric Aerosols, Properties and Climate Impacts, Springer Netherlands, 10.1007/978-94-017-9649-1, 311p. 2015.

Cariolle, D. and Dèquè, M.:. Southern hemisphere medium-scale waves and total ozone disturbances in a spectral general circulation model, J. Geophys. Res., 91D, 10825–10846, 1986.

Cariolle, D. and Teyssèdre, H.: A revised linear ozone photochemistry parameterization for use in transport and general circulation models: multi-annual simulations, Atmos. Chem. Phys., 7, 2183-2196, doi:10.5194/acp-7-2183-2007, 2007.

Cesnulyte, V., Lindfors, A. V., Pitkänen, M. R. A., Lehtinen, K. E. J., Morcrette, J.-J., and Arola, A.: Comparing ECMWF AOD with AERONET observations at visible and UV wavelengths, Atmos. Chem. Phys., 14, 593-608, doi:10.5194/acp-14-593-2014, 2014.

Coldewey-Egbers, M., Loyola R., D. G., Braesicke, P., Dameris, M., van Roozendael, M., Lerot, C. and Zimmer, W.: A new health check of the ozone layer at global and regional scales, Geophys. Res. Lett., 41, 4363–4372, doi:10.1002/2014GL060212, 2014.

Cooper, O. R., Parrish, D. D., Ziemke, J., Balashov, N. V., Cupeiro, M., Galbally, I. E., Gilge, S., Horowitz, L., Jensen, N. R., Lamarque, J.-F., Naik, V., Oltmans, S. J., Schwab, J., Shindell, D. T., Thompson, A. M., Thouret, V., Wang, Y., and Zbinden, R. M.: Global distribution and trends of tropospheric ozone: An observation-based review, Elementa: Science of the Anthropocene, 2, 1–28, doi:10.12952/journal.elementa.000029, 2014.

Courtier, P., Thépaut, J.-N., and Hollingsworth, A.: A strategy for operational implementation of 4D-Var, using an incremental approach, Q. J. Roy. Meteorol. Soc., 120, 1367–1388, 1994.

Cuevas, E., Camino, C., Benedetti, A., Basart, S., Terradellas, E., Baldasano, J. M., Morcrette, J. J., Marticorena, B., Goloub, P., Mortier, A., Berjón, A., Hernández, Y., Gil-Ojeda, M., and Schulz, M.: The MACC-II 2007–2008 reanalysis: atmospheric dust evaluation and characterization over northern Africa and the Middle East, Atmos. Chem. Phys., 15, 3991-4024, doi:10.5194/acp-15-3991-2015, 2015.

Dee, D. P.: Variational bias correction of radiance data in the ECMWF system, in: Proceedings of the ECMWF workshop on assimilation of high spectral resolution sounders in NWP, Reading, UK, 28 June–1 July 2004, 97–112, 2004.

Dee, D. P. and Uppala, S.: Variational bias correction of satellite radiance data in the ERA-Interim reanalysis, Q. J. Roy. Meteor. Soc., 135, 1830–1841, 2009.

Dee, D.P., Uppala, S.M., Simmons, A.J., Berrisford, P., Poli, P., Kobayashi, S., Andrae, U., Balmaseda, M.A., Balsamo, G., Bauer, P., Bechtold, P., Beljaars, A.C.M., van de Berg, L., Bidlot, J., Bormann, N., Delsol, C., Dragani, R., Fuentes, M., Geer, A.J., Haimberger, L., Healy, S.B., Hersbach, H., Hólm, E.V., Isaksen, L., Kållberg, P., Köhler, M., Matricardi, M., McNally, A.P., Monge-Sanz, B.M., Morcrette, J.-J., Park, B.-K., Peubey, C., de Rosnay, P., Tavolato, C., Thépaut, J.-N., Vitart, F.: The ERA-Interim reanalysis: Configuration and performance of the data assimilation system, Quarterly Journal of the Royal Meteorological Society, 2011.

Deeter, M.N., MOPITT Version 5 Product User's Guide, Technical Report, NCAR, Boulder, USA, www.acom.ucar.edu/mopitt/v5_users_guide_beta.pdf (last access 24.7.2016), 2011.

Deeter, M. N., S. Martínez-Alonso, D. P. Edwards, L. K. Emmons, J. C. Gille, H. M. Worden, J. V. Pittman, B. C. Daube, and S. C. Wofsy: Validation of MOPITT Version 5 thermal-infrared, near-infrared, and multispectral carbon monoxide profile retrievals for 2000–2011, J. Geophys. Res. Atmos., 118, 6710–6725, doi:10.1002/jgrd.50272, 2013.

de Laat, A. T. J., Aben, I., Deeter, M., Nédélec, P., Eskes, H., Attié, J.-L., Ricaud, P., Abida, R., El Amraoui, L., and Landgraf, J.: Validation of nine years of MOPITT V5 NIR using MOZAIC/IAGOS measurements: biases and long-term stability, Atmos. Meas. Tech., 7, 3783-3799, doi:10.5194/amt-7-3783-2014, 2014.

Dentener, F., Kinne, S., Bond, T., Boucher, O., Cofala, J., Generoso, S., Ginoux, P., Gong, S., Hoelzemann, J. J., Ito, A., Marelli, L., Penner, J. E., Putaud, J.-P., Textor, C., Schulz, M., van der Werf, G. R., and Wilson, J.: Emissions of primary aerosol and precursor gases in the years 2000 and 1750 prescribed data-sets for AeroCom, Atmos. Chem. Phys., 6, 4321-4344, doi:10.5194/acp-6-4321-2006, 2006.

Diamantakis, M. and Flemming, J.: Global mass fixer algorithms for conservative tracer transport in the ECMWF model, Geosci. Model Dev., 7, 965-979, doi:10.5194/gmd-7-965-2014, 2014.

1309 Elguindi, N., Clark, H., Ordóñez, C., Thouret, V., Flemming, J., Stein, O., Huijnen, V.,
1310 Moinat, P., Inness, A., Peuch, V.-H., Stohl, A., Turquety, S., Athier, G., Cammas, J.-P., and
1311 Schultz, M.: Current status of the ability of the GEMS/MACC models to reproduce the
1312 tropospheric CO vertical distribution as measured by MOZAIC, Geosci. Model Dev., 3, 501-
1313 518, doi:10.5194/gmd-3-501-2010, 2010.

1314 Emmons, L. K., Arnold, S. R., Monks, S. A., Huijnen, V., Tilmes, S., Law, K. S., Thomas, J.
1315 L., Raut, J.-C., Bouarar, I., Turquety, S., Long, Y., Duncan, B., Steenrod, S., Strode, S.,
1316 Flemming, J., Mao, J., Langner, J., Thompson, A. M., Tarasick, D., Apel, E. C., Blake, D. R.,
1317 Cohen, R. C., Dibb, J., Diskin, G. S., Fried, A., Hall, S. R., Huey, L. G., Weinheimer, A. J.,
1318 Wisthaler, A., Mikoviny, T., Nowak, J., Peischl, J., Roberts, J. M., Ryerson, T., Warneke, C.,
1319 and Helmig, D.: The POLARCAT Model Intercomparison Project (POLMIP): overview and
1320 evaluation with observations, Atmos. Chem. Phys., 15, 6721-6744, doi:10.5194/acp-15-6721-
1321 2015, 2015.

1322 Eskes, H., Huijnen, V., Arola, A., Benedictow, A., Blechschmidt, A.-M., Botek, E., Boucher,
1323 O., Bouarar, I., Chabrillat, S., Cuevas, E., Engelen, R., Flentje, H., Gaudel, A., Griesfeller, J.,
1324 Jones, L., Kapsomenakis, J., Katragkou, E., Kinne, S., Langerock, B., Razinger, M., Richter,
1325 A., Schultz, M., Schulz, M., Sudarchikova, N., Thouret, V., Vrekoussis, M., Wagner, A., and
1326 Zerefos, C.: Validation of reactive gases and aerosols in the MACC global analysis and
1327 forecast system, Geosci. Model Dev., 8, 3523-3543, doi:10.5194/gmd-8-3523-2015, 2015.

1328

1329 Field, R.D., G.R. van der Werf, and S.S.P. Shen, Human amplification of drought-induced
1330 biomass burning in Indonesia since 1960, Nature Geoscience, 2 (3), 185-188,
1331 doi:10.1038/ngeo443, 2009.

1332 Flemming, J., Stern, R., and Yamartino, R. J.: A new air quality regime classification scheme
1333 for O3, NO2, SO2 and PM10 observations sites, Atmos. Environ., 39, 6121–6129, 2005.

1334 Flemming, J., Inness, A., Flentje, H., Huijnen, V., Moinat, P., Schultz, M. G., and Stein, O.:
1335 Coupling global chemistry transport models to ECMWF's integrated forecast system, Geosci.
1336 Model Dev., 2, 253-265, doi:10.5194/gmd-2-253-2009, 2009.

1337 Flemming, J., Inness, A., Jones, L., Eskes, H. J., Huijnen, V., Schultz, M. G., Stein, O.,
1338 Cariolle, D., Kinnison, D., and Brasseur, G.: Forecasts and assimilation experiments of the

Antarctic ozone hole 2008, Atmos. Chem. Phys., 11, 1961–1977, doi:10.5194/acp-11-1961-2011, 2011.

Flemming J, and Inness, A.: [Global climate] Carbon Monxide [in "State of the Climate in 2013"]. Bull. Amer. Meteor. Soc., 95 (7), S43, 2014.

Flemming, J., Huijnen, V., Arteta, J., Bechtold, P., Beljaars, A., Blechschmidt, A.-M., Diamantakis, M., Engelen, R. J., Gaudel, A., Inness, A., Jones, L., Josse, B., Katragkou, E., Marecal, V., Peuch, V.-H., Richter, A., Schultz, M. G., Stein, O., and Tsikerdekis, A.: Tropospheric chemistry in the Integrated Forecasting System of ECMWF, Geosci. Model Dev., 8, 975-1003, doi:10.5194/gmd-8-975-2015, 2015.

Froidevaux, L., Anderson, J., Wang, H.-J., Fuller, R. A., Schwartz, M. J., Santee, M. L., Livesey, N. J., Pumphrey, H. C., Bernath, P. F., Russell III, J. M., and McCormick, M. P.: Global OZone Chemistry And Related trace gas Data records for the Stratosphere (GOZCARDS): methodology and sample results with a focus on HCl, H_2O, and O_3, Atmos. Chem. Phys., 15, 10471-10507, doi:10.5194/acp-15-10471-2015, 2015.

Froidevaux, L., Jiang, Y. B., Lambert, A., Livesey, N. J., Read, W. G., Waters, J. W., Browell, E. V., Hair, J. W., Avery, M. A., McGee, T. J., Twigg, L.W., Sumnicht, G. K., Jucks, K.W., Margitan, J. J., Sen, B., Stachnik, R. A., Toon, G. C., Bernath, P. F., Boone, C. D., Walker, K. A., Filipiak, M. J., Harwood, R. S., Fuller, R. A., Manney, G. L., Schwartz, M. J., Daffer, W. H., Drouin, B. J., Cofield, R. E., Cuddy, D. T., Jarnot, R. F., Knosp, B.W., Perun, V. S., Snyder, W. V., Stek, P. C., Thurstans, R. P., and Wagner, P. A.: Validation of Aura Microwave LimbSounder stratospheric ozone measurements, J. Geophys. Res., 113, D15S20, doi:10.1029/2007JD008771, 2008.

Gaubert, B., Arellano Jr. A. F., Barré, J., Worden, H. M., Emmons, L. K., Tilmes, S., Buchholz, R. R., Vitt, F., Raeder, K., Collins, N., Anderson, J. L., Wiedinmyer, C., Martinez Alonso, S., Edwards, D. P., Andreae, M. O., Hannigan, J. W., Petri, C., Strong, K. and Jones, N.: Toward a chemical reanalysis in a coupled chemistry-climate model: An evaluation of MOPITT CO assimilation and its impact on tropospheric composition, J. Geophys. Res. Atmos., 121, 7310–7343, doi:10.1002/2016JD024863, 2016.

Gaudel, A., Clark, H., Thouret, V., Jones, L., Inness, A., Flemming, J., Stein, O., Huijnen, V., Eskes, H., Nédélec, and P. Boulangerand,D.: On the use of MOZAIC-IAGOS data to assess

the ability of the MACC reanalysis to reproduce the distribution of O3 and CO in the UTLS over Europe. Tellus B. 67, 27955. DOI: http://dx.doi.org/10.3402/tellusb.v67.27955, 2015.

Giordano, L., Brunner, D., Flemming, J., Hogrefe, C., Im, U., Bianconi, R., Badia, A., Balzarini, A., Baró, R., Chemel, C., Curci, G., Forkel, R., Jiménez-Guerrero, P., Hirtl, M., Hodzic, A., Honzak, L., Jorba, O., Knote, C., Kuenen, J. J. P., Makar, P. A., Manders-Groot, A., Neal, L., Pérez, J. L., Pirovano, G., Pouliot, G., San José, R., Savage, N., Schröder,W., Sokhi, R. S., Syrakov, D., Torian,A., Tuccella, P., Werhahn, J., Wolke, R., Yahya, K., Žabkar, R., Zhang, Y., and Galmarini, S.: Assessment of the MACC reanalysis and its influence as chemical boundary conditions for regional air quality modelling in AQMEII-2, Atmos. Environ., 115, 371–388, 2015.

George, M., Clerbaux, C., Bouarar, I., Coheur, P.-F., Deeter, M. N., Edwards, D. P., Francis, G., Gille, J. C., Hadji-Lazaro, J., Hurtmans, D., Inness, A., Mao, D., and Worden, H. M.: An examination of the long-term CO records from MOPITT and IASI: comparison of retrieval methodology, Atmos. Meas. Tech., 8, 4313-4328, doi:10.5194/amt-8-4313-2015, 2015.

Granier, C., J.F. Lamarque, A. Mieville, J.F. Muller, J. Olivier, J. Orlando, J. Peters, G. Petron, G. Tyndall, S. Wallens, POET, a database of surface emissions of ozone precursors, available on internet at http://www.aero.jussieu.fr/projet/ACCENT/POET.php, 2005.

Granier, C., B. Bessagnet, T. Bond, A. D'Angiola, H.D.v.d. Gon, G.J. Frost, A. Heil, J.W. Kaiser, S. Kinne, Z. Klimont, S. Kloster, J.-F. Lamarque, C. Liousse, T. Masui, F. Meleux, A. Mieville, T. Ohara, J.-C. Raut, K. Riahi, M.G. Schultz, S.J. Smith, A. Thomson, J.v. Aardenne, G.R.v.d. Werf, and D.P.v. Vuuren, Evolution of anthropogenic and biomass burning emissions of air pollutants at global and regional scales during the 1980-2010 period, Climatic Change, 109(1-2), 163-190, doi:10.1007/s10584-011-0154-1, 2011.

Grythe, H., Ström, J., Krejci, R., Quinn, P., and Stohl, A.: A review of sea-spray aerosol source functions using a large global set of sea salt aerosol concentration measurements, Atmos. Chem. Phys., 14, 1277-1297, doi:10.5194/acp-14-1277-2014, 2014.

Guenther, A. B., Karl, T., Harley, P., Wiedinmyer, C., Palmer, P. I., and Geron, C.: Estimates of global terrestrial isoprene emissions using MEGAN (Model of Emissions of Gases and Aerosols from Nature), Atmos. Chem. Phys., 6, 3181–3210, doi:10.5194/acp-6-3181-2006, 2006.

1399 Hao, N., Koukouli, M. E., Inness, A., Valks, P., Loyola, D. G., Zimmer, W., Balis, D. S.,
1400 Zyrichidou, I., Van Roozendael, M., Lerot, C., and Spurr, R. J. D.: GOME-2 total ozone
1401 columns from MetOp-A/MetOp-B and assimilation in the MACC system, Atmos. Meas.
1402 Tech., 7, 2937-2951, doi:10.5194/amt-7-2937-2014, 2014.

1403 Holben B.N., Eck, T.F., Slutsker, I., Tanré, D., Buis, J.P., Setzer, A., Vermote, E., Reagan,
1404 J.A. . Kaufman, Y., Nakajima, T., Lavenu, F., Jankowiak, I. and Smirnov, A.: AERONET - A
1405 federated instrument network and data archive for aerosol characterization, Rem. Sens.
1406 Environ., 66, 1-16, 1998.

1407 Hollingsworth, A., Engelen, R.J., Textor, C., Benedetti, A., Boucher, O., Chevallier, F.,
1408 Dethof, A., Elbern, H., Eskes, H., Flemming, J., Granier, C., Kaiser, J.W., Morcrette, J.-J.,
1409 Rayner, P., Peuch, V.H., Rouil, L., Schultz, M.G.,. Simmons, A.J and The GEMS
1410 Consortium: Toward a Monitoring and Forecasting System For Atmospheric Composition:
1411 The GEMS Project. Bull. Amer. Meteor. Soc., 89, 1147-1164, 2008.

1412 Hsu N. C., Jeong M.-J., Bettenhausen C, Sayer A.M., Hansell R., Seftor C.S., Huang J., Tsay
1413 S.-C.: Enhanced Deep Blue aerosol retrieval algorithm: The second generation, J. Geophys.
1414 Res., VOL. 118, 120, doi:10.1002/jgrd.50712, 2013.

1415 Huneeus, N., Schulz, M., Balkanski, Y., Griesfeller, J., Prospero, J., Kinne, S., Bauer, S.,
1416 Boucher, O., Chin, M., Dentener, F., Diehl, T., Easter, R., Fillmore, D., Ghan, S., Ginoux, P.,
1417 Grini, A., Horowitz, L., Koch, D., Krol, M. C., Landing, W., Liu, X., Mahowald, N., Miller,
1418 R., Morcrette, J.-J., Myhre, G., Penner, J., Perlwitz, J., Stier, P., Takemura, T., and Zender, C.
1419 S.: Global dust model intercomparison in AeroCom phase I, Atmos. Chem. Phys., 11, 7781-
1420 7816, doi:10.5194/acp-11-7781-2011, 2011.

1421 Huijnen, V., Williams, J., van Weele, M., van Noije, T., Krol, M., Dentener, F., Segers, A.,
1422 Houweling, S., Peters, W., de Laat, J., Boersma, F., Bergamaschi, P., van Velthoven, P., Le
1423 Sager, P., Eskes, H., Alkemade, F., Scheele, R., Nédélec, P., and Pätz, H.-W.: The global
1424 chemistry transport model TM5: description and evaluation of the tropospheric chemistry
1425 version 3.0, Geosci. Model Dev., 3, 445-473, doi:10.5194/gmd-3-445-2010, 2010.

1426 Huijnen V., Wooster, M. J., Kaiser, J. W., Gaveau, D.L.A., Flemming, J., Parrington, M.
1427 Inness, A., Murdiyarso, D., Main, B.and van Weele, M.: Fire carbon emissions over maritime
1428 southeast Asia in 2015 largest since 1997, Scientific Reports, 6:26886, DOI:
1429 10.1038/srep26886, 2016.

Im, U., Bianconi, R., Solazzo, E., Kioutsioukis, I., Badia, A., Balzarini, A., Baró, R., Bellasio, R., Brunner, D., Chemel, C., Curci, G., Flemming, J., Forkel, R., Giordano, L., Jiménez-Guerrero, P., Hirtl, M., Hodzic, A., Honzak, L., Jorba, O., Knote, C., Kuenen, J.J.P., Makar, P.A., Manders-Groot, A., Neal, L., Pérez, J.L., Pirovano, G., Pouliot, G., San Jose, R., Savage, N., Schroder, W., Sokhi, R.S., Syrakov, D., Torian, A., Tuccella, P., Werhahn, J., Wolke, R., Yahya, K., Zabkar, R., Zhang, Y., Zhang, J., Hogrefe, C., Galmarini, S.: Evaluation of operational on-line-coupled regional air quality models over Europe and North America in the context of AQMEII phase 2. Part I: Ozone, Atmospheric Environment, doi: 10.1016/j.atmosenv.2014.09.042, 2014.

Inness, A., Baier, F., Benedetti, A., Bouarar, I., Chabrillat, S., Clark, H., Clerbaux, C., Coheur, P., Engelen, R. J., Errera, Q., Flemming, J., George, M., Granier, C., Hadji-Lazaro, J., Huijnen, V., Hurtmans, D., Jones, L., Kaiser, J. W., Kapsomenakis, J., Lefever, K., Leitão, J., Razinger, M., Richter, A., Schultz, M. G., Simmons, A. J., Suttie, M., Stein, O., Thépaut, J.-N., Thouret, V., Vrekoussis, M., Zerefos, C., and the MACC team: The MACC reanalysis: an 8 yr data set of atmospheric composition, Atmos. Chem. Phys., 13, 4073-4109, doi:10.5194/acp-13-4073-2013, 2013.

Inness, A., Blechschmidt, A.-M., Bouarar, I., Chabrillat, S., Crepulja, M., Engelen, R. J., Eskes, H., Flemming, J., Gaudel, A., Hendrick, F., Huijnen, V., Jones, L., Kapsomenakis, J., Katragkou, E., Keppens, A., Langerock, B., de Mazière, M., Melas, D., Parrington, M., Peuch, V. H., Razinger, M., Richter, A., Schultz, M. G., Suttie, M., Thouret, V., Vrekoussis, M., Wagner, A., and Zerefos, C.: Data assimilation of satellite retrieved ozone, carbon monoxide and nitrogen dioxide with ECMWF's Composition-IFS, Atmos. Chem. Phys., 15, 5275-5303, doi:10.5194/acp-15-5275-2015, 2015.

Jacob, D.J. H. Liu, C.Mari, and R.M. Yantosca, Harvard wet deposition scheme for GMI, Harvard University Atmospheric Chemistry Modeling Group, revised March 2000. http://acmg.seas.harvard.edu/geos/wiki_docs/deposition/wetdep.jacob_etal_2000.pdf, 2000.

Jung, T., T. N. Palmer, M. J. Rodwell, and S. Serrar: Diagnosing forecast error using relaxation experiments. ECMWF Newsletter 82, ECMWF, Shinfield Park, Reading, Berkshire RG2 9AX, UK, 2008.

Kaiser, J. W., Heil, A., Andreae, M. O., Benedetti, A., Chubarova, N., Jones, L., Morcrette, J.-J., Razinger, M., Schultz, M. G., Suttie, M., and van der Werf, G. R.: Biomass burning

emissions estimated with a global fire assimilation system based on observed fire radiative power, Biogeosciences, 9, 527-554, doi:10.5194/bg-9-527-2012, 2012.

Katragkou, E., Zanis, P., Tsikerdekis, A., Kapsomenakis, J., Melas, D., Eskes, H., Flemming, J., Huijnen, V., Inness, A., Schultz, M. G., Stein, O., and Zerefos, C. S.: Evaluation of near surface ozone over Europe from the MACC reanalysis, Geoscientific Model Development, 8, 2299-2314, 2015.

Kinne, S., Schulz, M., Textor, C., Guibert, S., Balkanski, Y., Bauer, S. E., Berntsen, T., Berglen, T. F., Boucher, O., Chin, M., Collins, W., Dentener, F., Diehl, T., Easter, R., Feichter, J., Fillmore, D., Ghan, S., Ginoux, P., Gong, S., Grini, A., Hendricks, J., Herzog, M., Horowitz, L., Isaksen, I., Iversen, T., Kirkevåg, A., Kloster, S., Koch, D., Kristjansson, J. E., Krol, M., Lauer, A., Lamarque, J. F., Lesins, G., Liu, X., Lohmann, U., Montanaro, V., Myhre, G., Penner, J., Pitari, G., Reddy, S., Seland, O., Stier, P., Takemura, T., and Tie, X.: An AeroCom initial assessment – optical properties in aerosol component modules of global models, Atmos. Chem. Phys., 6, 1815-1834, doi:10.5194/acp-6-1815-2006, 2006.

Kinnison, D. E., Brasseur, G. P., Walters, S., Garcia, R. R.,. Marsh, D. R, Sassi, F., Harvey, V. L., Randall, C. E., Emmons, L., Lamarque, J. F., Hess, P., Orlando, J. J., Tie, X. X., Randel, W., Pan, L. L., Gettelman, A., Granier, C., Diehl, T., Niemeier, U. and Simmons, A. J.: Sensitivity of Chemical Tracers to Meteorological Parameters in the MOZART-3 Chemical Transport Model. J. Geophys. Res, 112, D03303, doi:10.1029/2008JD010739, 2007.

Komhyr, W. D., Barnes, R. A., Borthers, G. B., Lathrop, J. A., Kerr, J. B., and Opperman, D. P.: Electrochemical concentration cell ozonesonde performance evaluation during STOIC 1989, J. Geophys. Res., 100, 9231–9244, 1995.

Lamarque, J.-F., Shindell, D. T., Josse, B., Young, P. J., Cionni, I., Eyring, V., Bergmann, D., Cameron-Smith, P., Collins, W. J., Doherty, R., Dalsoren, S., Faluvegi, G., Folberth, G., Ghan, S. J., Horowitz, L. W., Lee, Y. H., MacKenzie, I. A., Nagashima, T., Naik, V., Plummer, D., Righi, M., Rumbold, S. T., Schulz, M., Skeie, R. B., Stevenson, D. S., Strode, S., Sudo, K., Szopa, S., Voulgarakis, A., and Zeng, G.: The Atmospheric Chemistry and Climate Model Intercomparison Project (ACCMIP): overview and description of models, simulations and climate diagnostics, Geosci. Model Dev., 6, 179-206, doi:10.5194/gmd-6-179-2013, 2013.

1492 Lefever, K., van der A, R., Baier, F., Christophe, Y., Errera, Q., Eskes, H., Flemming, J.,
1493 Inness, A., Jones, L., Lambert, J.-C., Langerock, B., Schultz, M. G., Stein, O., Wagner, A.,
1494 and Chabrillat, S.: Copernicus stratospheric ozone service, 2009–2012: validation, system
1495 intercomparison and roles of input data sets, Atmos. Chem. Phys., 15, 2269-2293,
1496 doi:10.5194/acp-15-2269-2015, 2015.

1497 Levelt, P. F., van den Oord, G. H. J., Dobber, M. R., Malkki, A., Visser, H., de Vries, J.,
1498 Stammes, P., Lundell, J. O. V., and Saari, H.: The ozone monitoring instrument, IEEE T.
1499 Geosci. Remote, 44, 1093–1101, 2006.

1500 Levy, R. C., Remer, L. A., Kleidman, R. G., Mattoo, S., Ichoku, C., Kahn, R., and Eck, T. F.:
1501 Global evaluation of the Collection 5 MODIS dark-target aerosol products over land, Atmos.
1502 Chem. Phys., 10, 10399-10420, doi:10.5194/acp-10-10399-2010, 2010.

1503 Liu, X., Bhartia, P. K., Chance, K., Spurr, R. J. D., and Kurosu, T. P.: Ozone profile retrievals
1504 from the Ozone Monitoring Instrument, Atmos. Chem. Phys., 10, 2521–2537, 2010,
1505 http://www.atmos-chem-phys.net/10/2521/2010/.

1506 Manney, G., Santee, M. L., Rex, M., Livesey, N. J., Pitts, M. C., Veefkind, P., Nash, R. R.,
1507 Wohltmann, I., Lehmann, R., Froidevaux, L., Poole, L. R., Schoeberl, M. R., Haffner, D. P.,
1508 Davies, J., Dorokhov, V., Gernandt, H., Johnson, B., Kivi, R., Kyr o, E., Larsen, N., Levelt, P.
1509 F., Makshtas, A., McElroy, C. T., Nakajima, H., Parrondo, M. C., Tarasick, D.W., von der
1510 Gathen, P.,Walker, P. K. A., and Zinoviev, N. S.: Unprecedented Arctic ozone loss in 2011,
1511 Arctic winter 2010/2011 at the brink of an ozone hole, Nature, 478, 469–475,
1512 doi:10.1038/nature10556, 2011.

1513 McNally, A. P., Watts, P. D., Smith, J. A., Engelen, R. J., Kelly, G. A., Th´epaut, J.-N., and
1514 Matricardi, M.: The assimilation of AIRS radiance data at ECMWF, Q. J. Roy. Meteor. Soc.,
1515 132, 935–957, 2006.

1516 Marenco, A., Thouret, V., Ńeḑelec, P., Smit, H. G., Helten, M., Kley, D., Karcher, F., Simon,
1517 P., Law, K., Pyle, J., Poschmann, G., Von Wrede, R., Hume, C., and Cook, T.: Measurement
1518 of ozone and water vapour by Airbus in-service air-craft: The MOZAIC airborne programme,
1519 an overview, J. Geophys. Res., 103, 25631–25642, 1998.

1520 Meijer, E.W., P. F. J. van Velthoven, D. W. Brunner, H. Huntrieser and H. Kelder:
1521 Improvement and evaluation of the parameterization of nitrogen oxide production by

1522 lightning, Physics and Chemistry of the Earth, Part C, Volume 26, Issue 8, Pages 577-583,
1523 2001.

1524 Miyazaki, K., Eskes, H. J., and Sudo, K.: A tropospheric chemistry reanalysis for the years
1525 2005–2012 based on an assimilation of OMI, MLS, TES, and MOPITT satellite data, Atmos.
1526 Chem. Phys., 15, 8315-8348, doi:10.5194/acp-15-8315-2015, 2015.

1527 Monks, P. S., Archibald, A. T., Colette, A., Cooper, O., Coyle, M., Derwent, R., Fowler, D.,
1528 Granier, C., Law, K. S., Mills, G. E., Stevenson, D. S., Tarasova, O., Thouret, V., von
1529 Schneidemesser, E., Sommariva, R., Wild, O., and Williams, M. L.: Tropospheric ozone and
1530 its precursors from the urban to the global scale from air quality to short-lived climate forcer,
1531 Atmos. Chem. Phys., 15, 8889-8973, doi:10.5194/acp-15-8889-2015, 2015.

1532 Morcrette, J.-J., Boucher, O., Jones, L., Salmond, D., Bechtold, P., Beljaars, A., Benedetti, A.,
1533 Bonet, A., Kaiser, J. W., Razinger, M., Schulz, M., Serrar, S., Simmons, A. J., Sofiev, M.,
1534 Suttie, M., Tompkins, A. M. and Untch, A.: Aerosol analysis and forecast in the ECMWF
1535 Integrated Forecast System. Part I: Forward modelling, J. Geophys. Res., 2009.

1536 Morcrette, J. J., Benedetti, A., Jones, L., Kaiser, J. W., Razinger, M., and Suttie, M.:
1537 Prognostic Aerosols in the ECMWF IFS: MACC vs. GEMS Aerosols, ECMWF Technical
1538 Memorandum, 659, 2011.

1539 Nedelec, P., Cammas, J.-P., Thouret, V., Athier, G., Cousin, J.-M., Legrand, C., Abonnel, C.,
1540 Lecoeur, F., Cayez, G., and Marizy, C.: An improved infrared carbon monoxide analyser for
1541 routine measurements aboard commercial Airbus aircraft: technical validation and first
1542 scientific results of the MOZAIC III programme, Atmos. Chem. Phys., 3, 1551–1564,
1543 doi:10.5194/acp-3-1551-2003, 2003.

1544 Munro, R., R. Siddans, W. J. Reburn, and B. J. Kerridge, Direct measurements of
1545 tropospheric ozone distributions from space, Nature, 392, 168–171, 1998.

1546 Munro, R., Eisinger, M., Anderson, C., Callies, J., Corpaccioli, E., Lang, R., Lefebvre, A.,
1547 Livschitz, Y., and Albinana, A. P.: GOME-2 on MetOp, Proc. of The 2006 EUMETSAT
1548 Meteorological Satellite Conference, Helsinki, Finland, 2006.

1549 Novelli, P.C. and Masarie, K.A.:, Atmospheric Carbon Monoxide Dry Air Mole Fractions
1550 from the NOAA ESRL Carbon Cycle Cooperative Global Air Sampling Network, 1988-2012,
1551 Version: 2013-08-08, Path: ftp://aftp.cmdl.noaa.gov/data/trace_gases/co/flask/surface/, 2013.
1552 (last access 6.5.2016)

1553 Novelli, P. C., Masarie, K. A., Lang, P. M., Hall, B. D., Myers, R. C., and Elkins, J. W.:
1554 Reanalysis of tropospheric CO trends: effects of the 1997–1998 wildfires, J. Geophys. Res.,
1555 108, 4464, doi:10.1029/2002JD003031, 2003.

1556 Olivier J., J. Peters, C. Granier, G. Petron, J.F. Muller, and S. Wallens: Present and future
1557 surface emissions of atmospheric compounds, POET report #2, EU project EVK2-1999-
1558 00011, 2003.

1559 Onogi, K., Tsutsui, J., Koide, H., Sakamoto, M., Kobayashi, S., Hatsushika, H., Matsumoto,
1560 T., Yamazaki, N., Kamahori, H., Takahashi, K., Kadokura, S., Wada, K., Kato, K., Oyama,
1561 R., Ose, T., Mannoji, N., and Taira, R.: The JRA-25 Reanalysis, Q. J. Roy. Meteorol. Soc.,
1562 85, 369–432, 2007.

1563 Reddy M. S., Boucher O., Bellouin N., Schulz M., Balkanski Y., Dufresne J.-L., Pham M.:
1564 Estimates of global multicomponent aerosol optical depth and direct radiative perturbation in
1565 the Laboratoire de Me´te´orologie Dynamique general circulation model, J. Geophys. Res.,
1566 110, D10S16, doi:10.1029/2004JD004757, 2005.

1567 Remer, L. A., Kaufman, Y. J. M, Tanré, D., Mattoo, S., Chu, D. A. M, Martins, J. V., Li, R.-
1568 R., Ichoku, C., Levy, R. C., Kleidman, R. G., Eck, T. F., Vermote, E. and Holben, B. N.: The
1569 MODIS Aerosol Algorithm, Products, and Validation Journal of the Atmospheric Sciences
1570 2005 62:4, 947-973, 2005.

1571 Rienecker, M. M., Suarez, M. J., Gelaro, R., Todling, R., Bacmeister, J., Liu, E., Bosilovich,
1572 M. G., Schubert, S. D., Takacs, L., Kim, G.- K., Bloom, S., Chen, J., Collins, D., Conaty, A.,
1573 da Silva, A., Gu, W., Joiner, J., Koster, R. D., Lucchesi, R., Molod, A. M., Owens, T.,
1574 Pawson, S., Pegion, P., Redder, C. R., Reichle, R., Robertson, F. R., Ruddick, A. G.,
1575 Sienkiewicz, M., and Woollen, J.: MERRA – NASA's Modern- Era Retrospective, Anal. Res.
1576 Appl., J. Climate, 24, 3624–3648, doi:10.1175/JCLID-11-00015.1, 2011.

1577 Saha, S., Moorthi, S., Pan, H. L., Wu, X., Wang, J., Nadiga, S., Tripp, P., Kistler, R.,
1578 Woollen, J., Behringer, D., Liu, H., Stokes, D., Grumbine, R., Gayno, G., Hou, Y. T.,
1579 Chuang, H. Y., Juang, H. M. H., Sela, J., Iredell, M., Treadon, R., Kleist, D., Van Delst, P.,
1580 Keyser, D., Derber, J., Ek, M., Meng, J., Wei, H., Yang, R., Lord, S., Van Den Dool, H.,
1581 Kumar, A., Wang, W., Long, C., Chelliah, M., Xue, Y., Huang, B., Schemm, J. K., Ebisuzaki,
1582 W., Lin, R., Xie, P., Chen, M., Zhou, S., Higgins, W., Zou, C. Z., Liu, Q., Chen, Y., Han, Y.,

Cucurull, L., Reynolds, R. W., Rutledge, G., and Goldberg, M.: The NCEP climate forecast system reanalysis, B. Am. Meteorol. Soc., 91, 1015–1057, 2010.

Schere, K., Flemming, J., Vautard, R., Chemel, C., Colette, A., Hogrefe, C., Bessagnet, B., Meleux, F., Mathur, R., Roselle, S., Hu, R.-M., Sokhi, R. S., Rao, S. T., and Galmarini, S.: Trace gas/aerosol boundary concentrations and their impacts on continental-scale AQMEII modeling domains, Atmos. Environ., 53, 38–50, doi:10.1016/j.atmosenv.2011.09.043, 2012.

Schutgens, N. A. J., Nakata, M., and Nakajima, T.: Estimating aerosol emissions by assimilating remote sensing observations into a Global transport model, Remote Sens., 4, 3528–3543, 2012.

Sindelarova, K., Granier, C., Bouarar, I., Guenther, A., Tilmes, S., Stavrakou, T., Müller, J.-F., Kuhn, U., Stefani, P., and Knorr, W.: Global data set of biogenic VOC emissions calculated by the MEGAN model over the last 30 years, Atmos. Chem. Phys., 14, 9317-9341, doi:10.5194/acp-14-9317-2014, 2014.

Shi, Y., Zhang, J., Reid, J. S., Holben, B., Hyer, E. J., and Curtis, C.: An analysis of the collection 5 MODIS over-ocean aerosol optical depth product for its implication in aerosol assimilation, Atmos. Chem. Phys., 11, 557-565, doi:10.5194/acp-11-557-2011, 2011.

Shindell, D.T., G. Faluvegi, D.S. Stevenson, M.C. Krol, L.K. Emmons, J.-F. Lamarque, G. Pétron, F.J. Dentener, K. Ellingsen, M.G. Schultz, O. Wild, M. Amann, C.S. Atherton, D.J. Bergmann, I. Bey, T. Butler, J. Cofala, W.J. Collins, R.G. Derwent, R.M. Doherty, J. Drevet, H.J. Eskes, A.M. Fiore, M. Gauss, D.A. Hauglustaine, L.W. Horowitz, I.S.A. Isaksen, M.G. Lawrence, V. Montanaro, J.-F. Müller, G. Pitari, M.J. Prather, J.A. Pyle, S. Rast, J.M. Rodriguez, M.G. Sanderson, N.H. Savage, S.E. Strahan, K. Sudo, S. Szopa, N. Unger, T.P.C. van Noije, and G. Zeng: Multi-model simulations of carbon monoxide: Comparison with observations and projected near-future changes. J. Geophys. Res., 111, D19306, doi:10.1029/2006JD007100, 2006.

Spada, M., Jorba, O., Pérez García-Pando, C., Janjic, Z., and Baldasano, J. M.: Modeling and evaluation of the global sea-salt aerosol distribution: sensitivity to size-resolved and sea-surface temperature dependent emission schemes, Atmos. Chem. Phys., 13, 11735-11755, doi:10.5194/acp-13-11735-2013, 2013.

1612 Stein, O., Schultz, M. G., Bouarar, I., Clark, H., Huijnen, V., Gaudel, A., George, M., and
1613 Clerbaux, C.: On the wintertime low bias of Northern Hemisphere carbon monoxide in global
1614 model studies, Atmos. Chem. Phys., 14, 9295–9316, doi:10.5194/acp-14-9295-2014, 2014

1615 Steinbrecht, W., Shwartz, R., and Claude, H.: New pump correction for the Brewer-Mast
1616 ozonesonde: Determination from experiment and instrument intercomparisons, J. Atmos.
1617 Ocean. Tech.15, 144–156, 1998.

1618 Tegtmeier, S., Hegglin, M. I., Anderson, J., Bourassa, A., Brohede, S., Degenstein, D.,
1619 Froide- vaux, L., Fuller, R., Funke, B., Gille, J., Jones, A., Kasai, Y., Krüger, K., Kyrölä, E.,
1620 Lingen- felser, G., Lumpe, J., Nardi, B., Neu, J., Pendlebury, D., Remsberg, E., Rozanov, A.,
1621 Smith, L., Toohey, M., Urban, J., von Clarmann, T., Walker, K. A., and Wang, R. H. J.:
1622 SPARC Data Initiative: a comparison of ozone climatologies from international satellite limb
1623 sounders, J. Geophys. Res., 118, 12229–12247, doi:10.1002/2013JD019877, 2013.

1624 Textor, C., Schulz, M., Guibert, S., Kinne, S., Balkanski, Y., Bauer, S., Berntsen, T., Berglen,
1625 T., Boucher, O., Chin, M., Dentener, F., Diehl, T., Easter, R., Feichter, H., Fillmore, D.,
1626 Ghan, S., Ginoux, P., Gong, S., Grini, A., Hendricks, J., Horowitz, L., Huang, P., Isaksen, I.,
1627 Iversen, I., Kloster, S., Koch, D., Kirkevåg, A., Kristjansson, J. E., Krol, M., Lauer, A.,
1628 Lamarque, J. F., Liu, X., Montanaro, V., Myhre, G., Penner, J., Pitari, G., Reddy, S., Seland,
1629 Ø., Stier, P., Takemura, T., and Tie, X.: Analysis and quantification of the diversities of
1630 aerosol life cycles within AeroCom, Atmos. Chem. Phys., 6, 1777-1813, doi:10.5194/acp-6-
1631 1777-2006, 2006.

1632 Uppala, S., Kallberg, P., Simmons, A. J., Andrae, U., Bechtold, V. D. C., Fiorino, M., Gibson,
1633 J. K., Haseler, J., Hernandez, A., Kelly, G. A., Li, X., Onogi, K., Saarinen, S., Sokka, N.,
1634 Allan, R. P., Andersson, E., Arpe, K., Balmaseda, M. A., Beljaars, A. C. M., van de Berg, L.,
1635 Bidlot, J., Bormann, N., Caires, S., Chevallier, F., Dethof, A., Dragosavac, M., Fisher, M.,
1636 Fuentes, M., Hagemann, S., Holm, E., Hoskins, B. J., Isaksen, L., Janssen, P. A. E. M., Jenne,
1637 R., McNally, A. P., Mahfouf, J. F., Morcrette, J. J., Rayner, N. A., Saunders, R. W., Simon,
1638 P., Sterl, A., Trenberth, K. E., Untch, A., Vasiljevic, D., Viterbo, P., and Woollen, J.: The
1639 ERA-40 re-analysis, Q. J. R. Meteorol. Soc., 131, 2961–3012, 2005.

1640 Wagner, A., Blechschmidt, A.-M., Bouarar, I., Brunke, E.-G., Clerbaux, C., Cupeiro, M.,
1641 Cristofanelli, P., Eskes, H., Flemming, J., Flentje, H., George, M., Gilge, S., Hilboll, A.,
1642 Inness, A., Kapsomenakis, J., Richter, A., Ries, L., Spangl, W., Stein, O., Weller, R., and

1643 Zerefos, C.: Evaluation of the MACC operational forecast system – potential and challenges
1644 of global near-real-time modelling with respect to reactive gases in the troposphere, Atmos.
1645 Chem. Phys., 15, 14005-14030, doi:10.5194/acp-15-14005-2015, 2015.

1646 Wesely, M.L.: Parameterization of Surface Resistances to Gaseous Dry Deposition in
1647 Regional-Scale Numerical Models. Atmos. Environ., 23, 1293-1304, 1989.

1648 Worden, H. M., Deeter, M. N., Frankenberg, C., George, M., Nichitiu, F., Worden, J., Aben,
1649 I., Bowman, K. W., Clerbaux, C., Coheur, P. F., de Laat, A. T. J., Detweiler, R., Drummond,
1650 J. R., Edwards, D. P., Gille, J. C., Hurtmans, D., Luo, M., Martínez-Alonso, S., Massie, S.,
1651 Pfister, G., and Warner, J. X.: Decadal record of satellite carbon monoxide observations,
1652 Atmos. Chem. Phys., 13, 837-850, doi:10.5194/acp-13-837-2013, 2013.

1653 Van der A, R.J.; Allaart, M.A.F.; Eskes, H.J. Multi sensor reanalysis of total ozone. Atmos.
1654 Chem.Phys. 2010, 10, 11277–11294.

1655 van der A, R. J., Allaart, M. A. F., and Eskes, H. J.: Extended and refined multi sensor
1656 reanalysis of total ozone for the period 1970-2012, Atmos. Meas. Tech., 8, 3021-3035,
1657 doi:10.5194/amt-8-3021-2015, 2015.

1658 Verstraeten, W. W., Neu, J. L., Williams, J. E., Bowman, K. W., Worden, J. R., Boersma, K.
1659 F.: Rapid increases in tropospheric ozone production and export from China, Nat. Geosci., 8,
1660 690–695, doi:10.1038/ngeo2493, 2015.

1661 von Clarmann, T., Glatthor, N., Grabowski, U., Höpfner, M., Kellmann, S., Kiefer, M.,
1662 Linden, A., Mengistu Tsidu, G., Milz, M., Steck, T., Stiller, G. P., Wang, D. Y., Fischer, H.,
1663 Funke, B., Gil-López, S., and López-Puertas, M.: Retrieval of temperature and tangent
1664 altitude pointing from limb emission spectra recorded from space by the Michelson
1665 Interferometer for Passive Atmospheric Sounding (MIPAS), J. Geophys. Res., 108, 4736,
1666 doi:10.1029/2003JD003602, 2003.

1667 Waters, J.W., Froidevaux, L., Harwood, R. S., Jarnot, R. F., Pickett, H. M., Read, W. G.,
1668 Siegel, P. H., Cofield, R. E., Filipiak, M. J., Flower, D. A., Holden, J. R., Lau, G. K., Livesey,
1669 N. J., Manney, G. L., Pumphrey, H. C., Santee, M. L., Wu, D. L., Cuddy, D. T., Lay, R. R.,
1670 Loo, M. S., Perun, V. S., Schwartz, M. J., Stek, P. C., Thurstans, R. P., Boyles, M. A.,
1671 Chandra, K. M., Chavez, M. C., Chen, G. S., Chudasama, B. V., Dodge, R., Fuller, R. A.,
1672 Girard, M. A., Jiang, J. H., Jiang, Y., Knosp, B. W., Labelle, R. C., Lam, J. C., Lee, A. K.,
1673 Miller, D., Oswald, J. E., Patel, N. C., Pukala, D. M., Quintero, O., Scaff, D. M., Vansnyder,

1674 W., Tope, M. C., Wagner, P. A., and Walch, M. J.: The Earth Observing System Microwave
1675 Limb Sounder (EOS MLS) on theAura Satellite, IEEE T. Geosci. Remote, 44, 1075–1092,
1676 2006.

1677 Yarwood, G., Rao, S., Yocke, M., and Whitten, G.: Updates to the carbon bond chemical
1678 mechanism: CB05. Final report to the US EPA, EPA Report Number: RT-0400675, available
1679 at: www.camx.com, last access: 1 July 2014, 2005.

1680

	MACCRA	**CAMSiRA**
Period	01/2003–12/2012	01/2003–12/2015
Horizontal resolution	80 km (T255)	110 km (T159)
Vertical resolution	60 layers from surface to 0.1 hPa	*as MACCRA*
Anthropogenic Emissions	MACCity (trend: ACCMIP + RCP 8.5), AEROCOM	*as MACCRA* & CO emission upgrade (Stein et al., 2014)
Chemistry module	MOZART-3	C-IFS CB05 / Cariolle ozone
Assimilated CO observations	MOPITT (V4) & IASI (from 2008 onwards)	MOPITT (V5) & updated error statistics (Inness et al., 2015)
Assimilated ozone observations	SBUV-2, OMI, MLS, GOME-2, SCIAMACHY, GOME, MIPAS (01/2003–06/2004)	*as MACCRA* & MIPAS (2003–2012)
Ozone MLS bias correction	On	Off
Assimilated AOD observations	MODIS (Aqua and Terra) + VarBC	*as MACCRA*
Fire emissions	GFED (2003–2008) and GFAS v0 (2009-2012)	GFAS v 1.2 (2003–2015)
IFS model version	CY36R2	CY40R2
Assimilation method and model	ECMWF 4D-VAR	*as MACCRA*
Meteorological observations assimilated	ECMWF RD setup (satellites, sondes, surface)	*as MACCRA*

1681 *Table 1 Important commonalities and differences between MACCRA and CAMSiRA*

1682

1683

1684

Instrument	References	Version	Period	Type	Data usage
MOPITT Terra	Deeter et al. (2011)	V5 TIR NRT	20030101–20121218 From 20121219	CO TC	65N–65S QC=0
GOME ERS-2	Munro et al. (1998)		20030101–20030531	O3 profile	80N–80S SOE>15, QC=0
GOME-2 Metop A	Hao et al. (2014)	NRT GDP4.4 NRT GDP4.7	20120901–20130714 From 20130715	O3 TC	SOE>10 QC=0
GOME-2 Metop B	Hao et al. (2014)	NRT GDP4.7	From 20140101	O3 TC	SOE>10 QC=0
MIPAS Envisat	von Clarmann et al. (2003, 2009)	NRT CCI	20030101–20040326 20050127–20120331	O3 profile	QC=0
MLS Aura	Froidevaux et al. (2008)	V2 NRT V3.4	20040808–20121231 From 20130107	O3 profile	QC=0
OMI Aura	Liu et al. (2010)	V003 NRT	20041001–20121231 From 20130101	O3 TC	SOE>10 QC=0
SBUV/2 NOAA-16	Bhartia et al. (1996)	V8	20040101–20081020	O3 PC 6 layers	SOE>6 QC=0
SBUV/2 NOAA-17	Bhartia et al. (1996)	V8	20030101–20121130	O3 PC 6 layers	SOE>6 QC=0
SBUV/2 NOAA-18	Bhartia et al. (1996)	V8	20050604–20121217	O3 PC 6 layers	SOE>6 QC=0
SBUV/2 NOAA-19	Bhartia et al. (1996)	V8	From 20090100	O3 PC 6 layers	SOE>6 QC=0
SCIAMACHY Envisat	Eskes et al. (2012)	CCI	20030101–20120408	O3 TC	SOE>6 QC=0
MODIS / Terra	Remer et al. (2005)	Col.5 NRT Col.5	20030101–20080731 From 20080801	AOD 550nm	70N-70S
MODIS / Aqua	Remer et al. (2005)	Col.5 NRT Col.5	20030101–20080731 From 20080801	AOD 550nm	70N–70S

1685 *Table 2 Assimilated satellite observations in CAMSiRA*

Area	Coordinates
North America	165°W-55°W, 25°N–75°N
Europe	10°W–45°E, 38°N–70°N
East Asia	90°E–150°E/10°N–55°N
South America	82°W–30°W/40°S–15°N
Tropical Africa	15°W–55°E/10°S–20°N
Northern Africa	15°W–55°E/20°N–35°N
Maritime South East Asia	90°E–150°E/10°S–10°N
Tropics	23°S–23°N
Arctic	60°N–90°N
Antarctica	90°S–60°S
NH mid latitudes	30°N–60°N
SH mid-latitudes	60°S–30°S

Table 3 Coordinates of regions

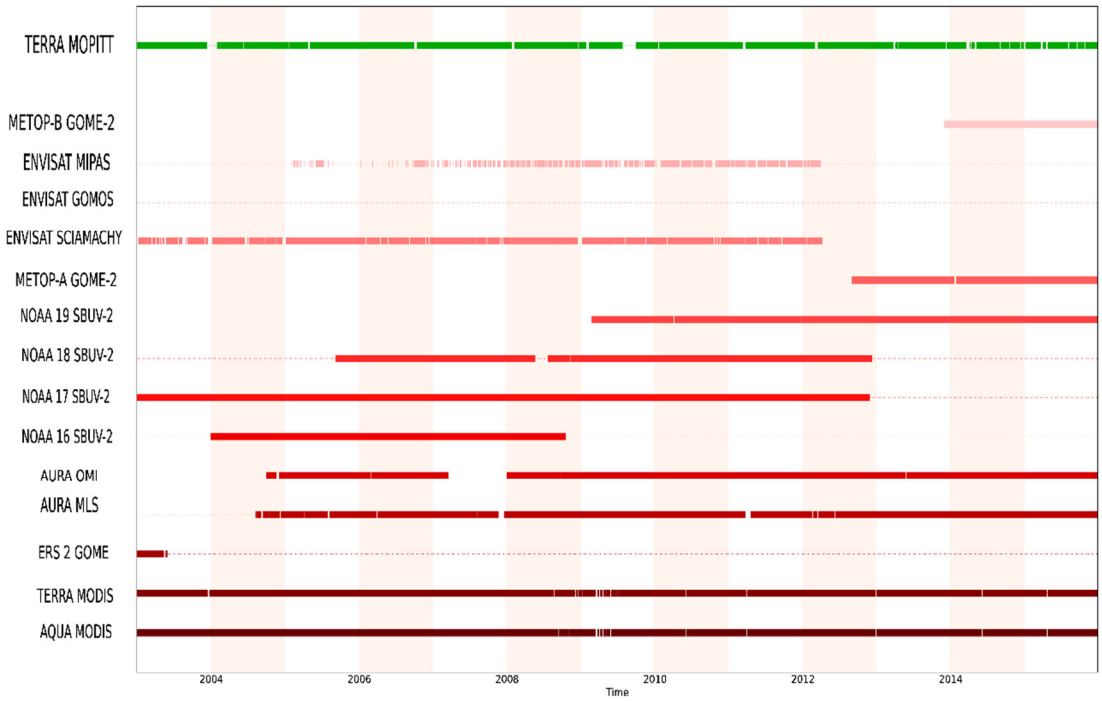

Figure 1 Time line of assimilated AC satellite retrievals from different instruments assimilated in CAMSiRA (see Table 2)

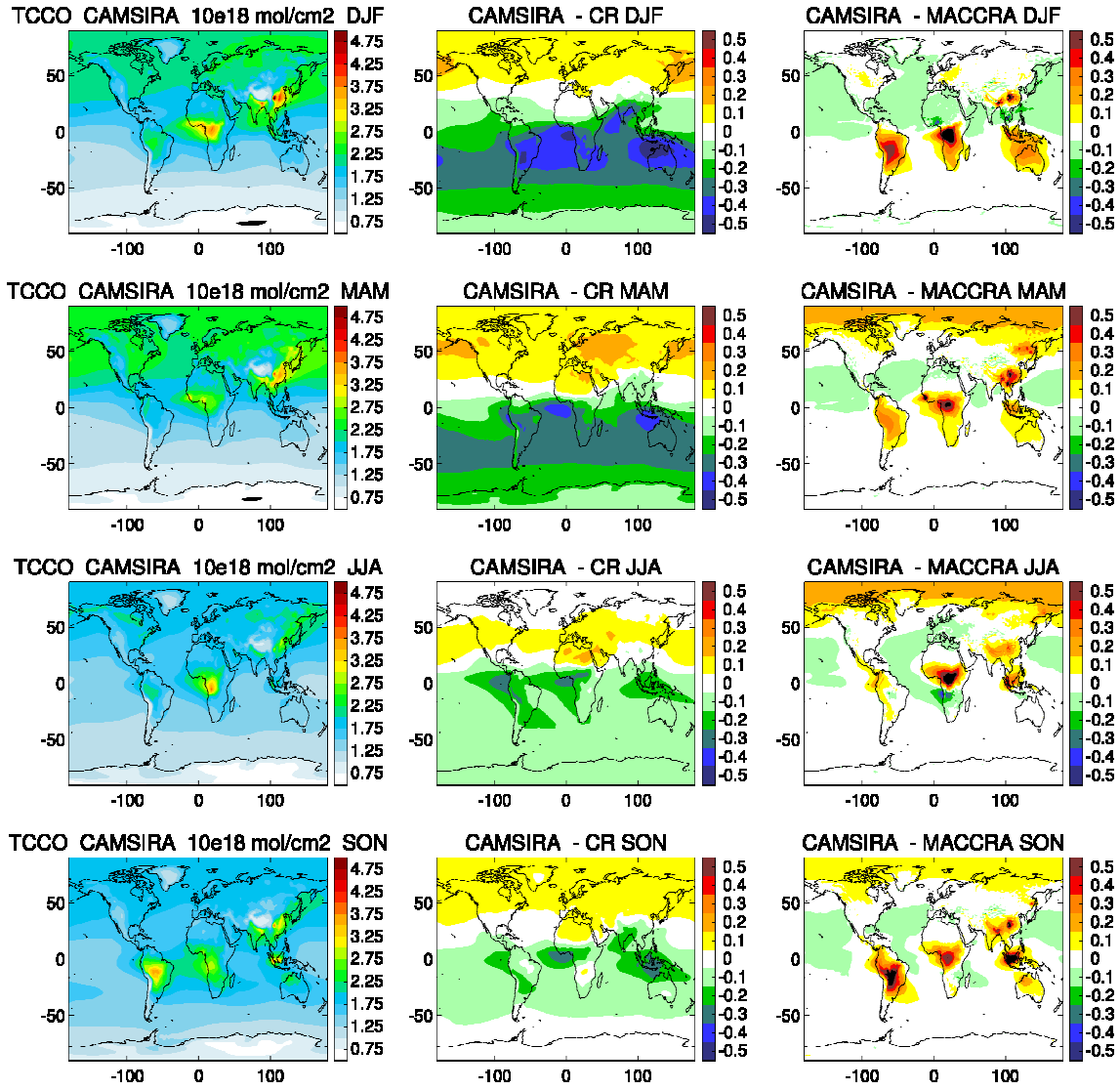

Figure 2 Average TC CO (10^{18}molecules/cm^2) of CAMSiRA (2003–2015, left) and difference against CR (2003–2015, middle) and MACCRA (2003–2012, right) for the seasons DJF (row 1), MAM (row 2), JJA (row 3) and SON (row 4).

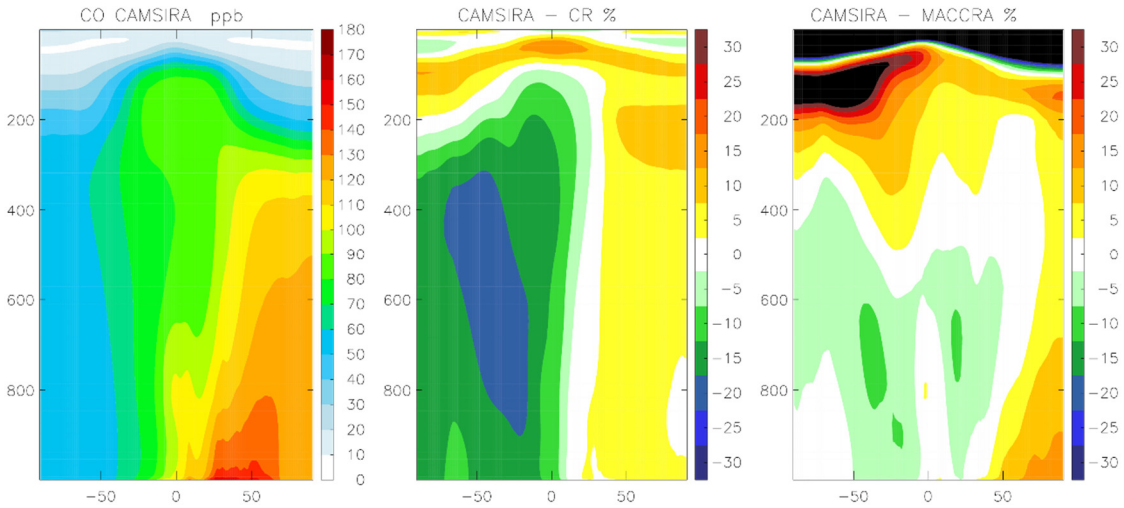

1700

1701 *Figure 3 Zonally averaged CO cross section of CAMSiRA (ppb) (2003–2015, left) and*
1702 *relative difference (%) against CR (2003–2015, middle) and MACCRA (2003–2012,*
1703 *right).*

1704

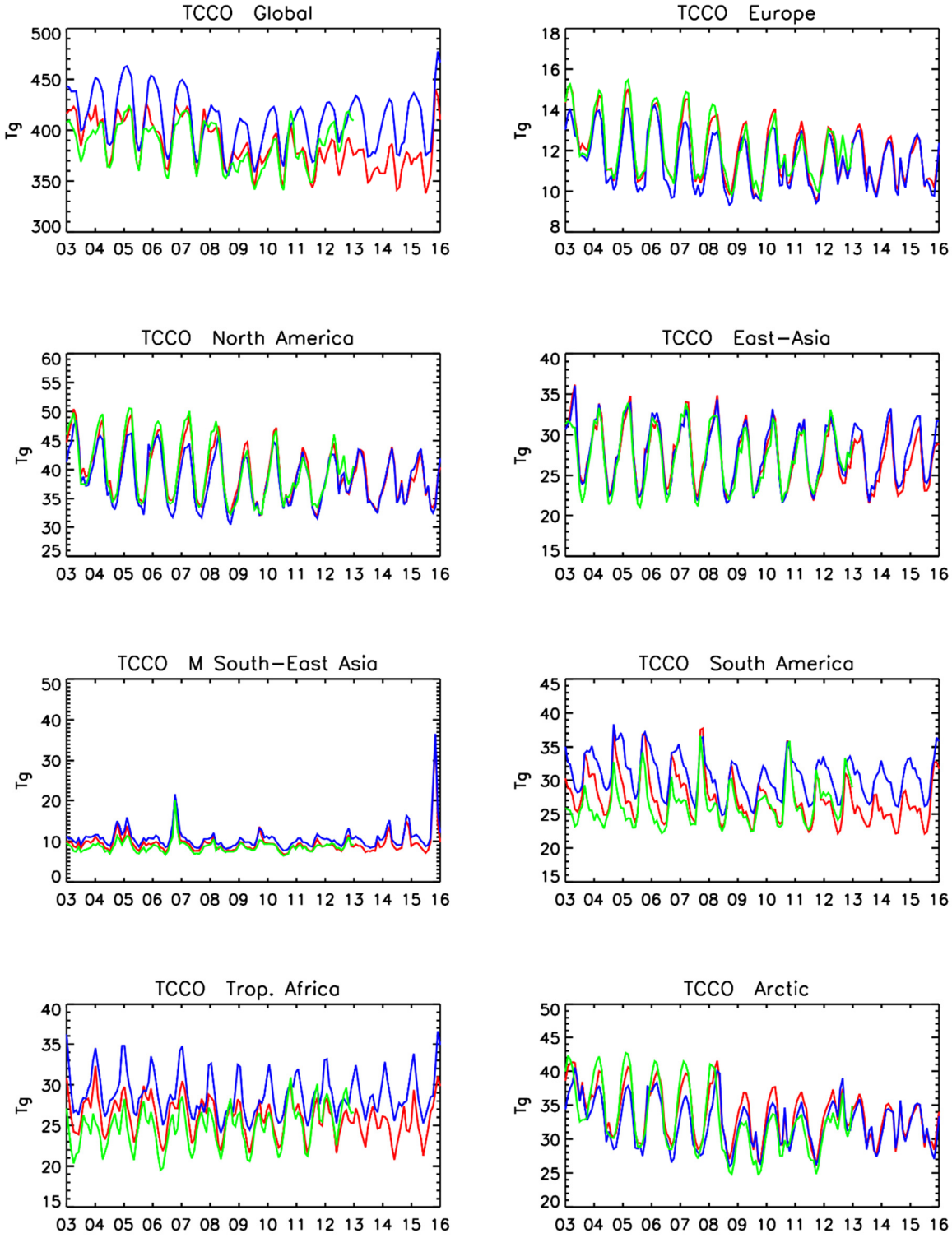

1705

1706 *Figure 4 Time series of monthly mean CO burden (Tg) over different regions (see Table*
1707 *3) for the period 2003–2015 from CAMSiRA (red), CR (blue) and MACCRA (green,*
1708 *2003–2012).*

1709

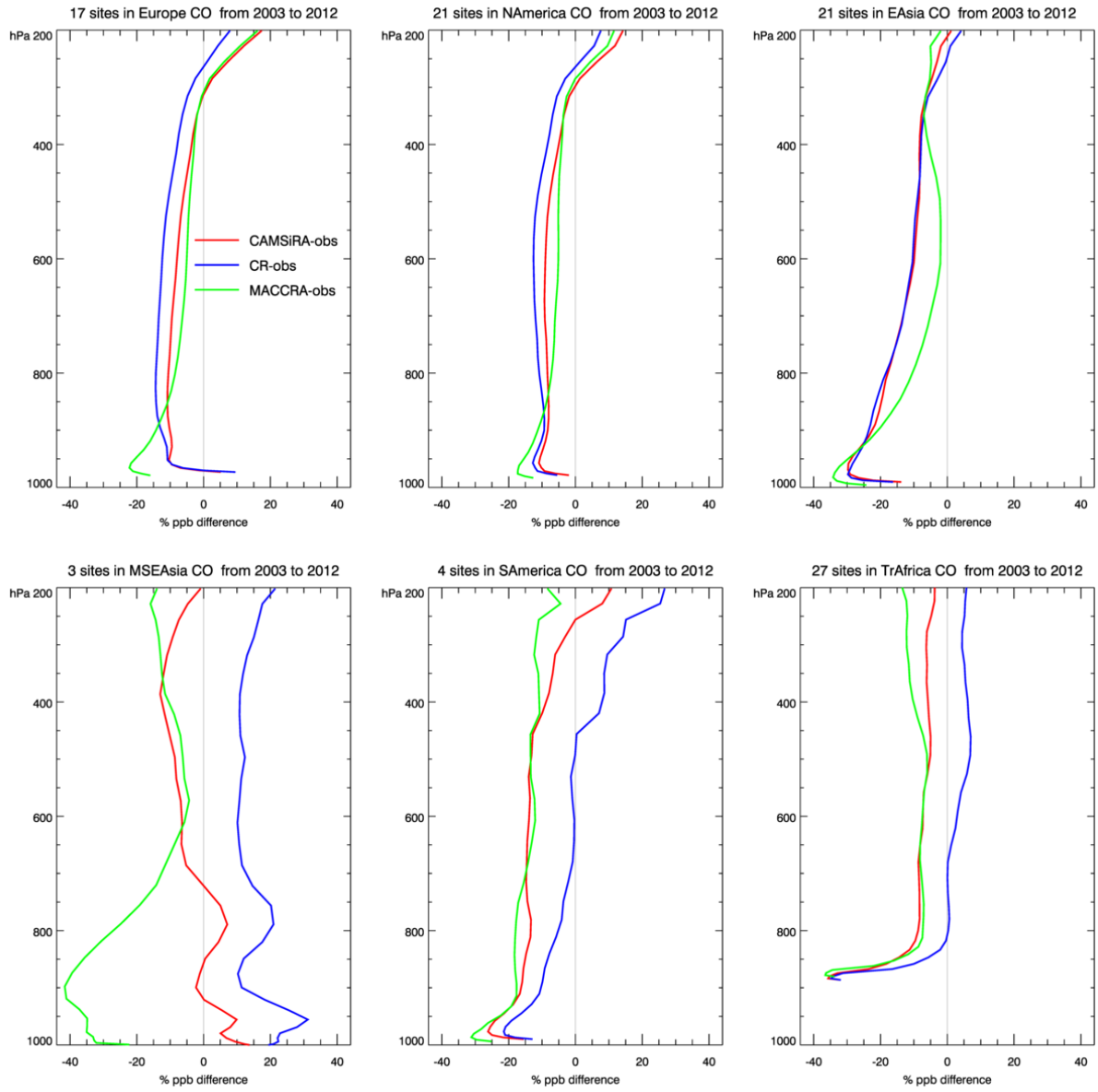

Figure 5 Average relative bias (%) in CO of CAMSiRA, MACCRA and CR against MOZAIC / IGAOS flight profiles averaged over different regions (see Table 3) for the period 2003–2012.

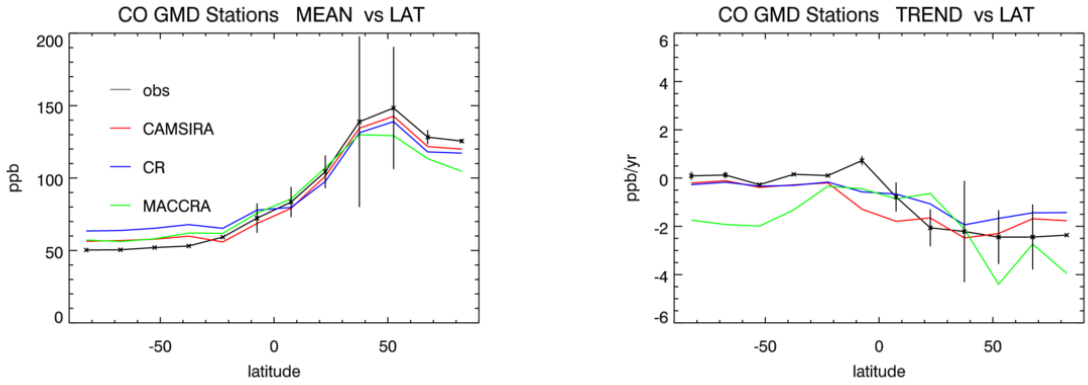

Figure 6 Zonal average of mean surface CO in ppb observed at NOAA-GMD stations (2003–2014) and values from CAMSiRA, CR and MACCRA (2003–2012) (left) and zonal median of linear trend in ppb/yr (right). The error bars indicate the range of the observed values.

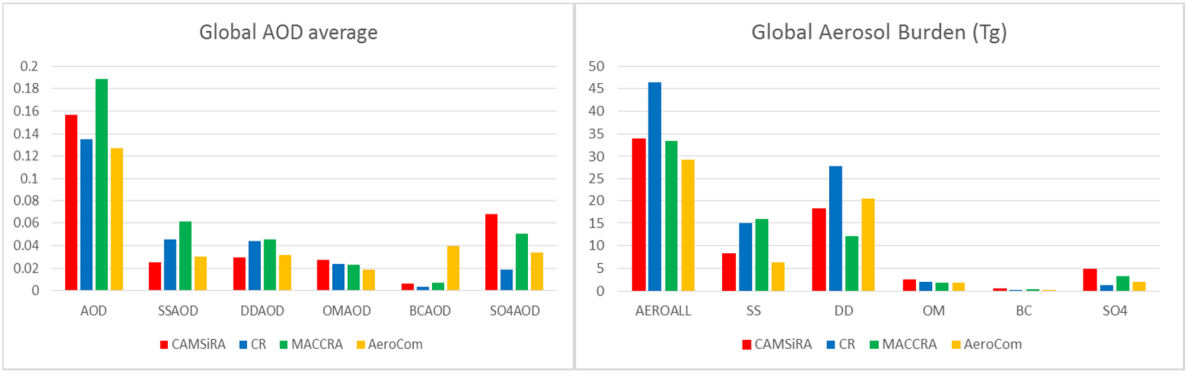

Figure 7 Globally average of total AOD (550 nm) and species AOD (left) and global total and species and burden in Tg (right) of sea salt (SS), desert dust (DD), organic matter (OM), black carbon (BC) and sulphate aerosol (SO_4) for CAMSiRA (red|), CR (blue) and MACCRA (green) and the median of the AeroCom model inter-comparison (yellow, Kinne et al., 2006 and Textor et al., 2006).

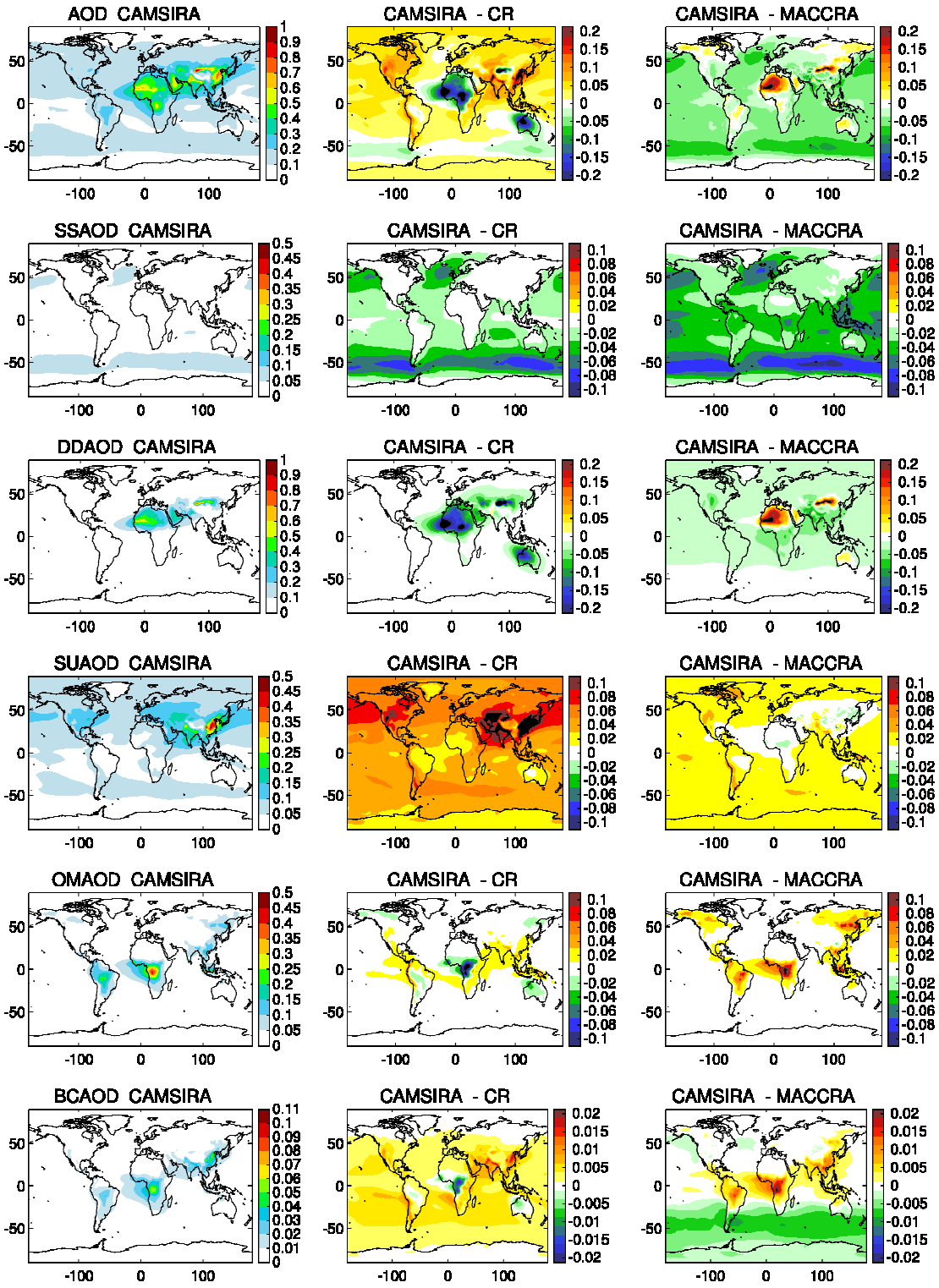

Figure 8 Total average AOD (row 1, scale max 1.0), AOD of desert dust (row 2, 1.0), sea salt (row 3, 0.5), sulphate (row 4, 0.5), organic matter (row 5, 0.5) and black carbon (row 6, 0.11) of CAMSiRA (average 2003–2015, left) and differences against CR (average 2003–2015, middle) and MACCRA (average 2003–2012, right).

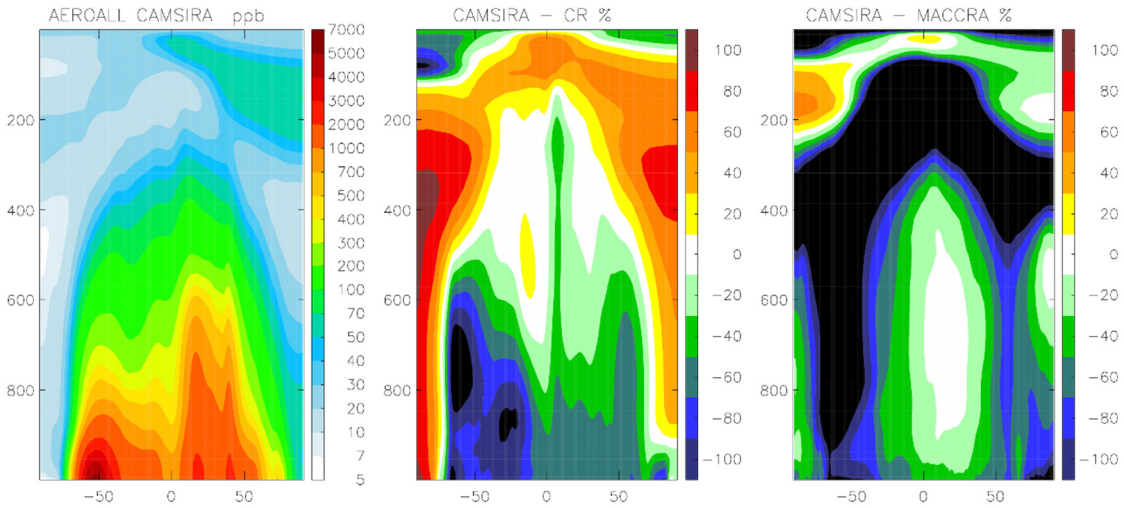

1735

1736 *Figure 9 Zonally averaged total aerosol mass mixing ratio (10^{-9}kg/kg) of CAMSiRA*
1737 *(2003–2015, left) and relative difference (%) against CR (2003–2015, middle) and*
1738 *MACCRA (2003–2012, right).*

1739

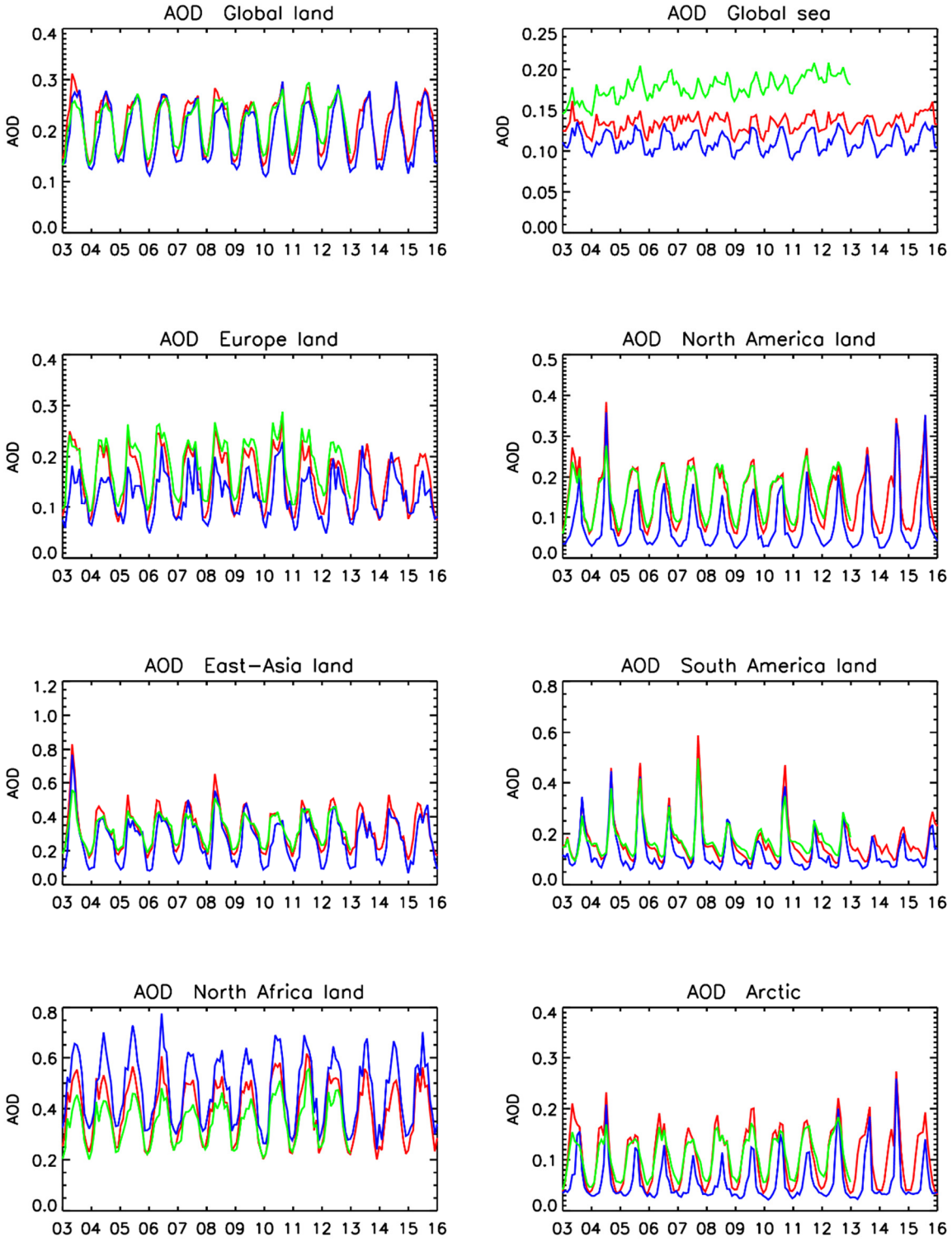

Figure 10 Time series of monthly mean AOD over the whole globe (land or seas points) and for different regions (see Table 3) for the period 2003–2015 from CAMSiRA (red), CR(blue) and MACCRA(green, 2003–2012).

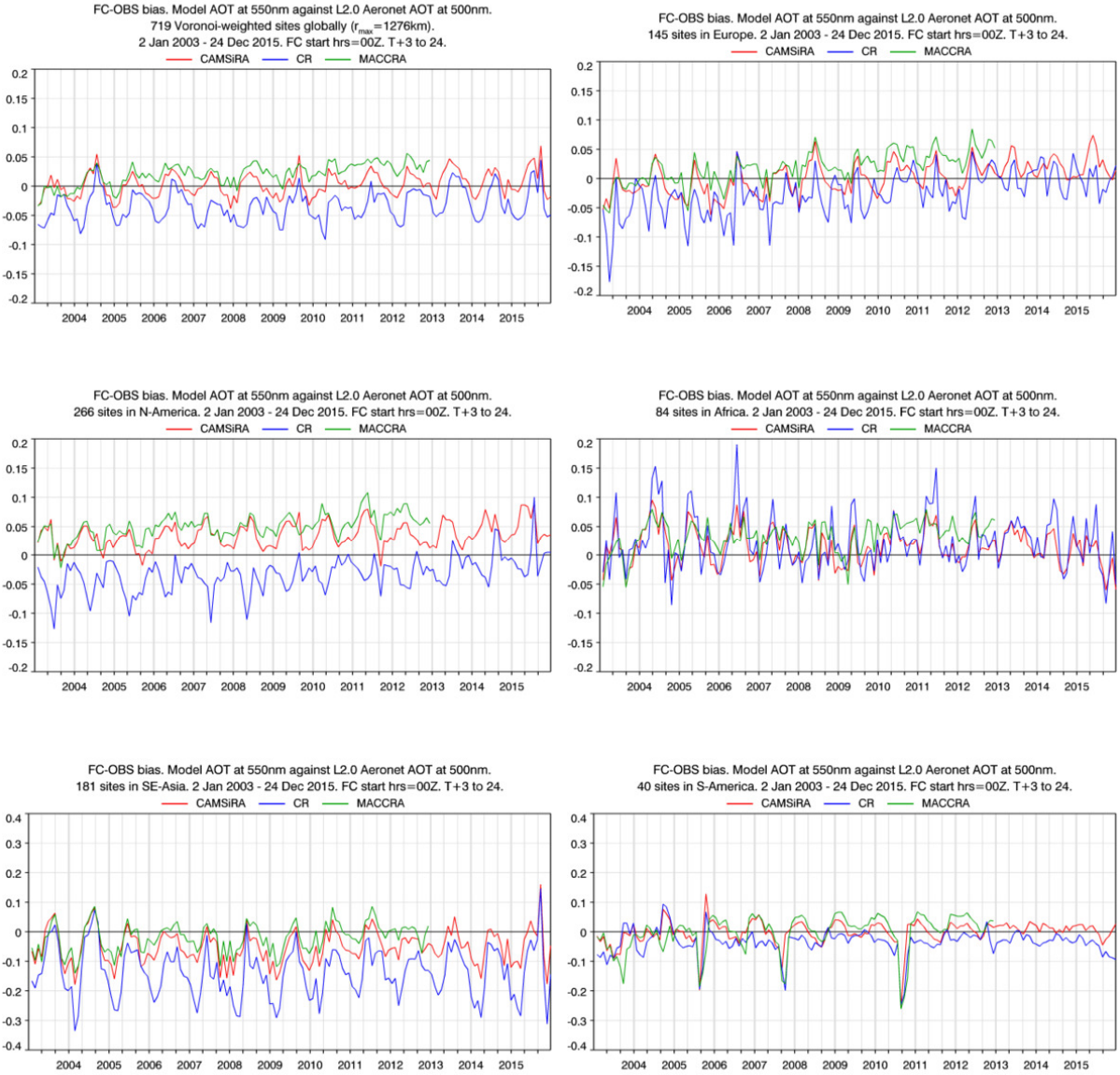

Figure 11 Time series of monthly mean bias against AERONET AOD observations averaged over the whole globe (top left), Europe (top right), North America (middle left), Africa (middle right), South East Asia (bottom left) and South America (bottom right) for CAMSiRA (red), CR (blue) and MACCRA (green).

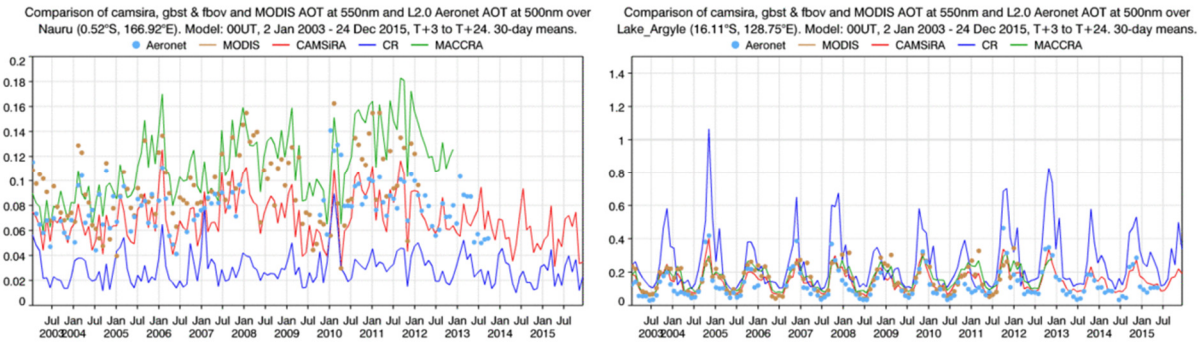

1752

1753 *Figure 12 Time series of monthly mean AOD from AERONET observations (light blue*
1754 *dots), MODIS retrievals (brown dots) and from CAMSiRA (red), CR (blue) and MACCRA*
1755 *(green) at Nauru (left) and Lake Argyle (right).*

1756

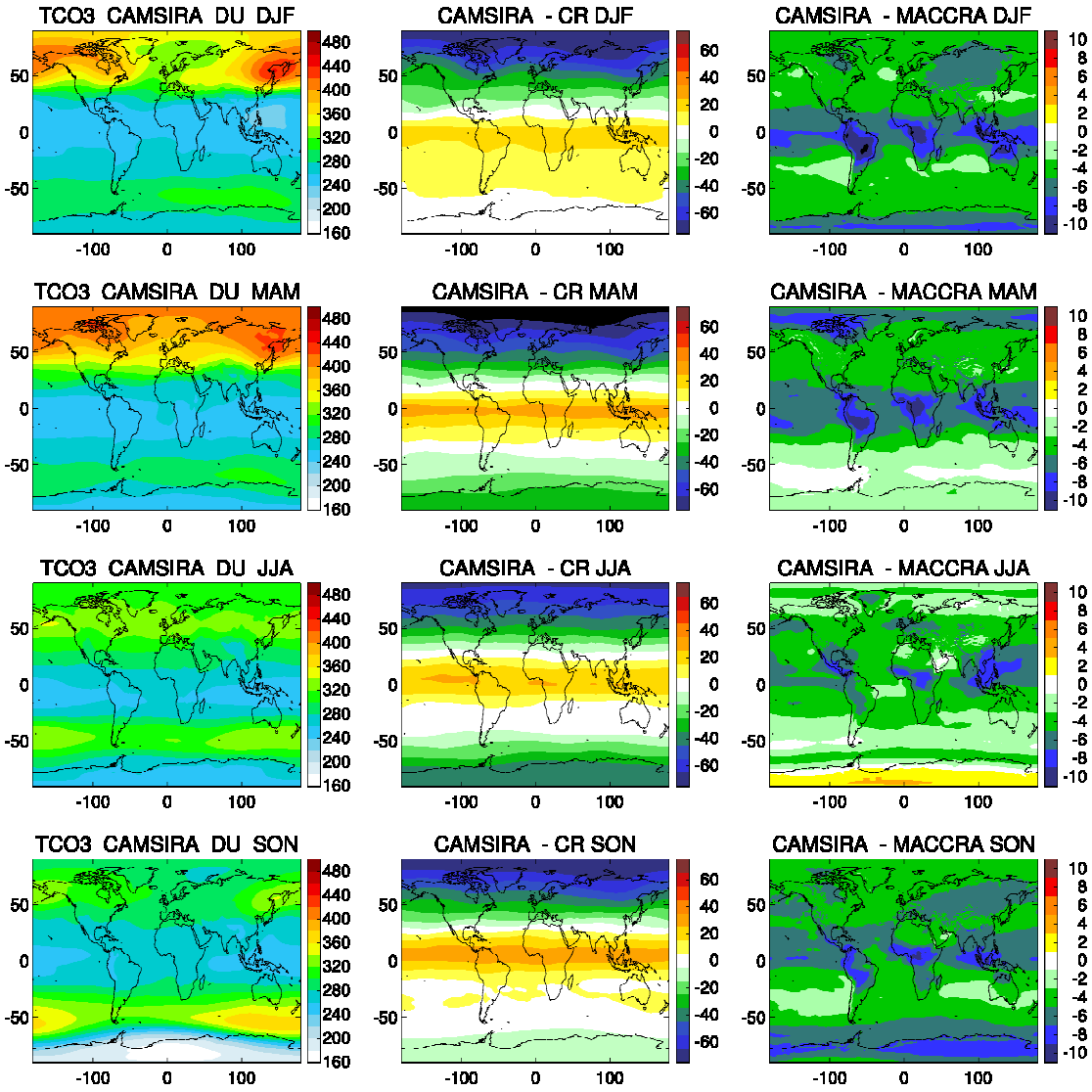

1757

1758 *Figure 13 Seasonal averaged TC ozone (DU) from CAMSiRA (left), difference between*
1759 *CAMSIRA and CR (middle) and CAMSiRA and MACCRA (right, 2003–2012, different*
1760 *scale) for the seasons DJF (row 1) MAM (row 2), JJA (row 3) and SON (row 4).*

1761

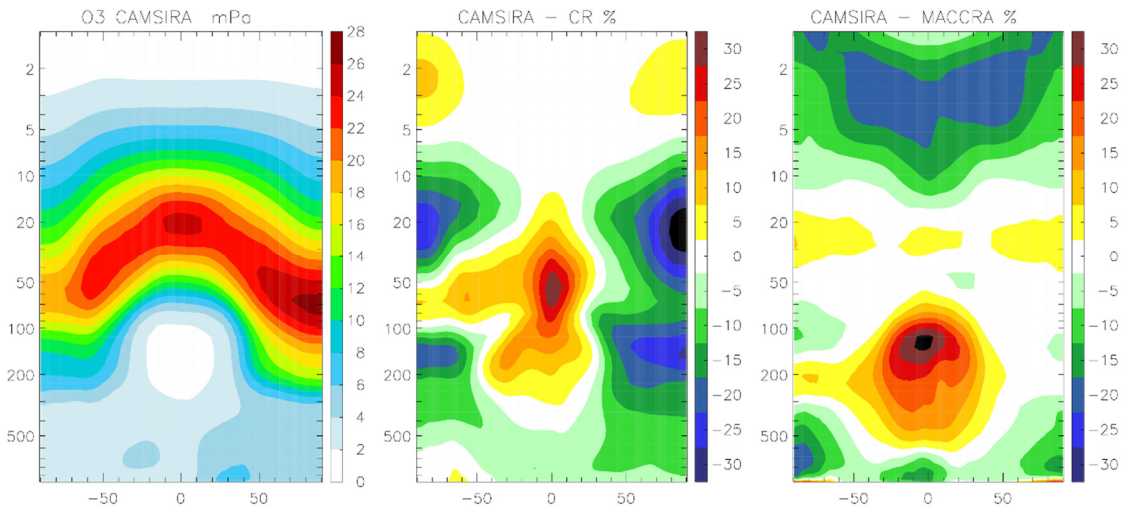

1762

1763 *Figure 14 Zonally averaged ozone partial pressure (mPa) of CAMSiRA (2003–2015, left)*
1764 *and relative difference (%) against CR (2003–2015, middle) and MACCRA (2003–2012)*

1765

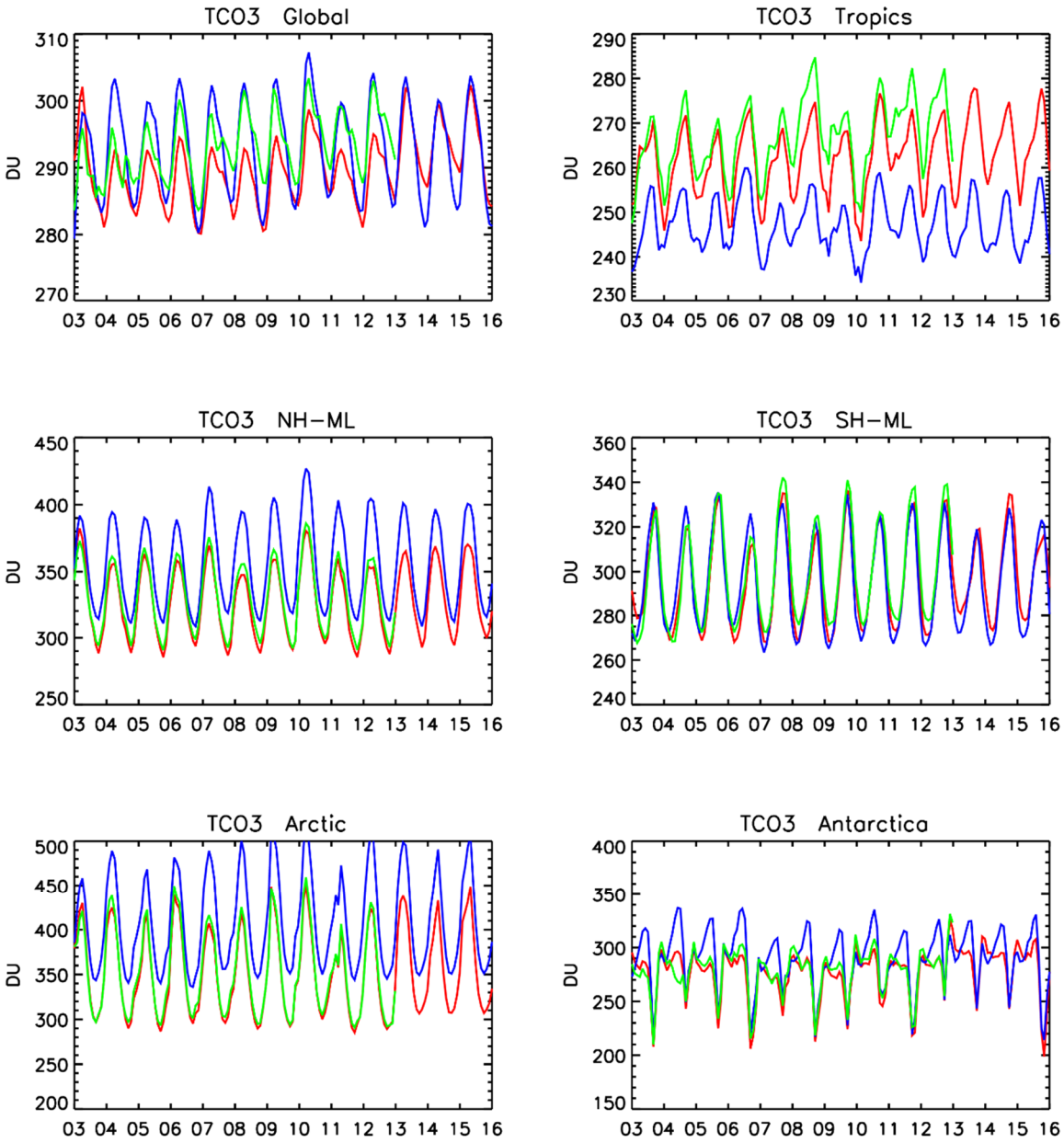

Figure 15 Monthly ozone TC (DU) area averaged over different regions (see Table 3) from CAMSiRA (black), CR (blue) and MACCRA (green) for 2003–2015.

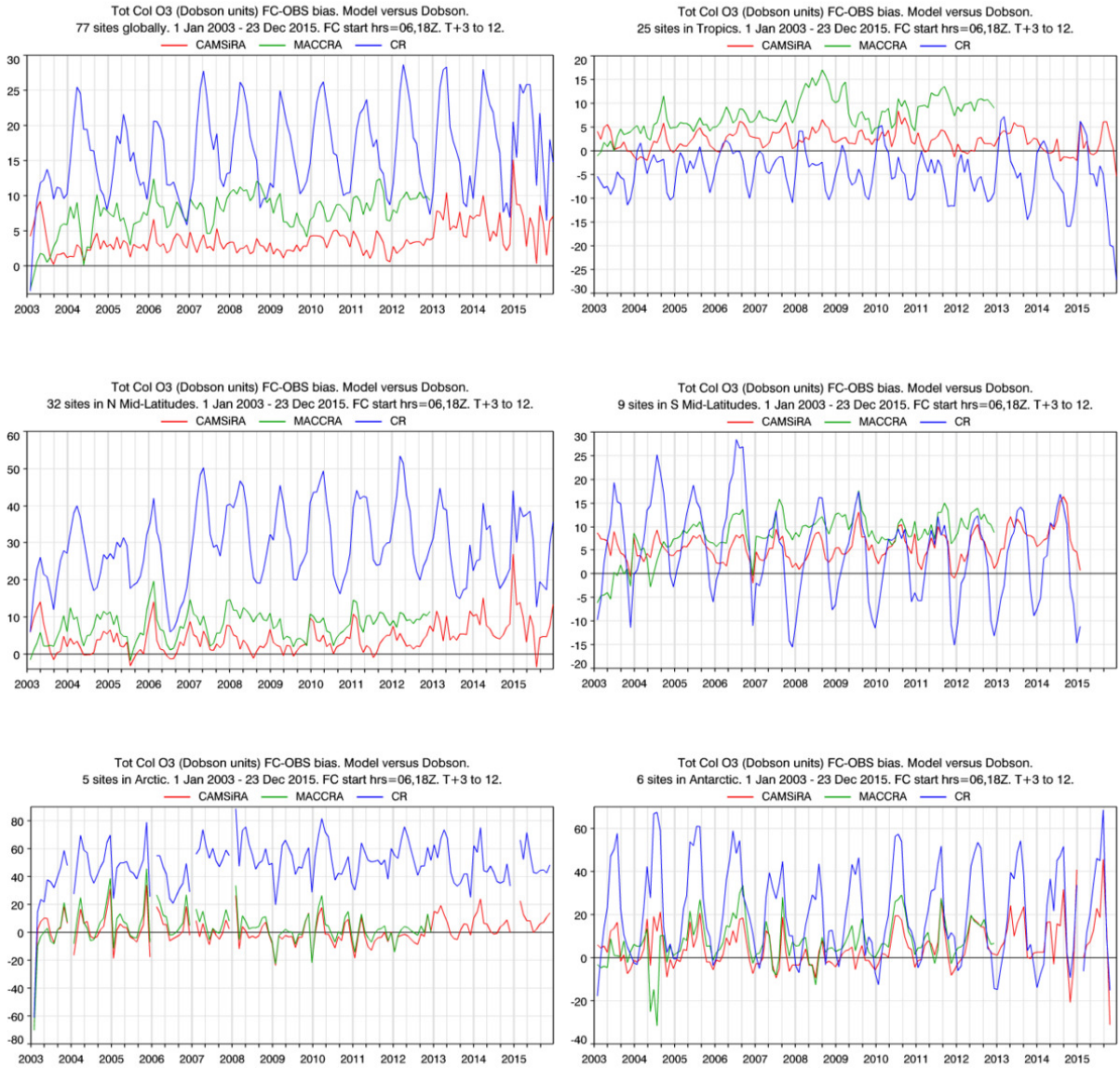

Figure 16 Time series of monthly mean bias in DU against WOUDC Dobson sun photometers for the globe (top left), the tropics (top right), NH mid-latitudes (middle left), SH mid-latitudes (middle right), the Arctic (bottom left) and Antarctica (bottom right) for CAMSiRA (red), CR(blue) and MACCRA (green).

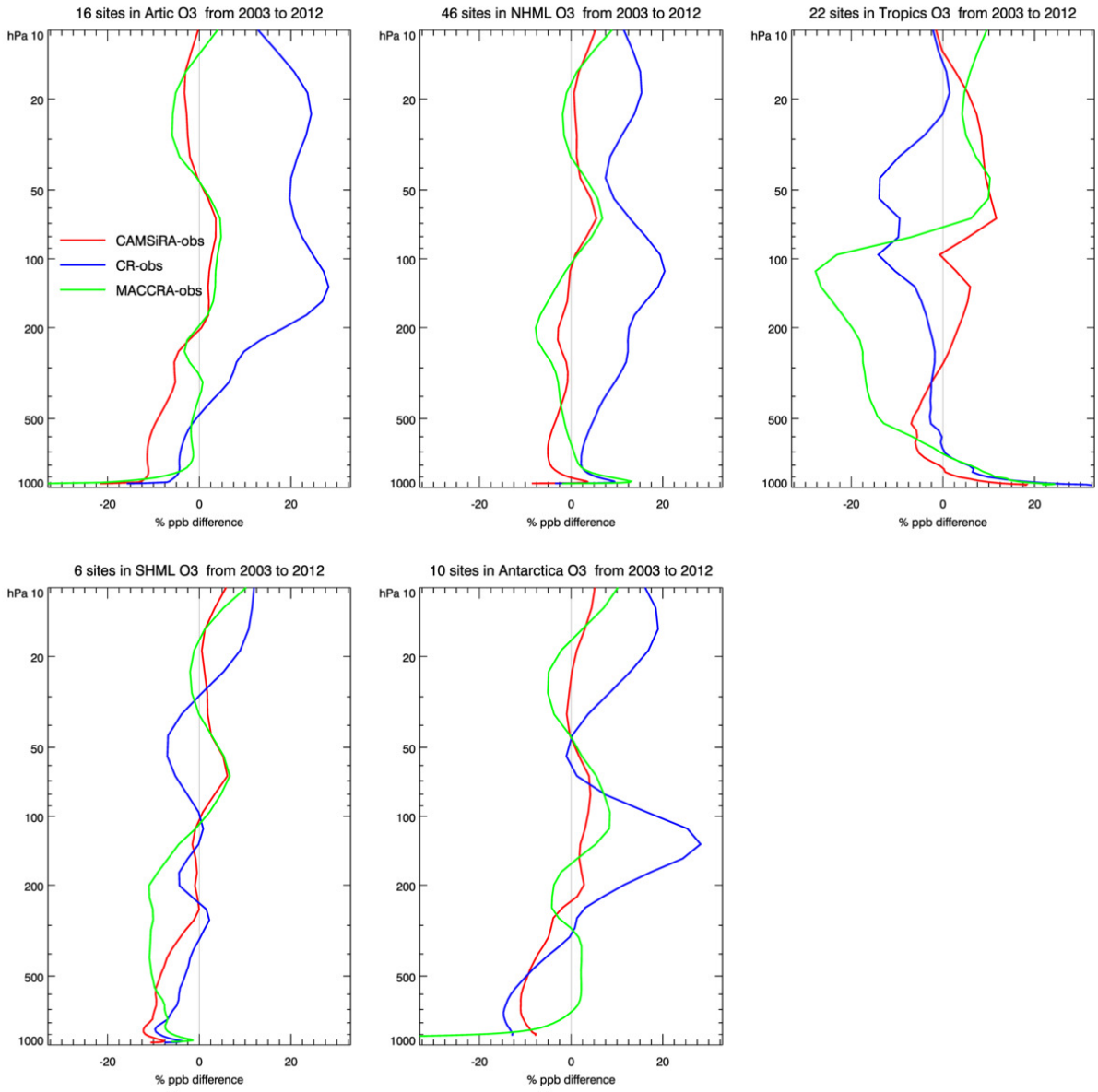

Figure 17 Mean relative bias of CAMSiRA (red), MACCRA (green) and CR (blue) against ozone sondes in the Arctic (top left), NH mid-latitudes (top middle), Tropics (top right), SH-mod-latitudes (bottom left) and Antarctica (bottom middle) for the period 2003–2012.

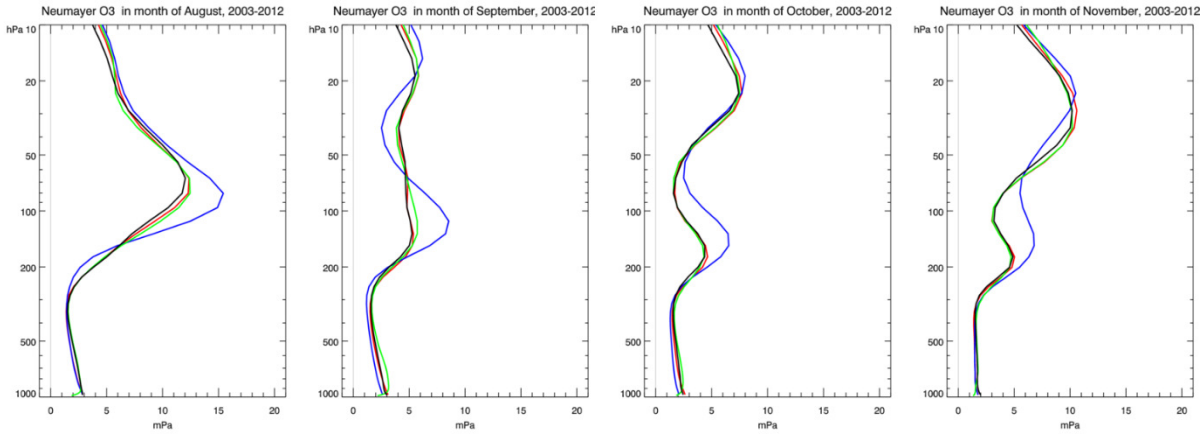

1783

1784 *Figure 18 Monthly mean ozone profiles (mPa) at Neumayer Station from ozone sondes, of*
1785 *CAMSiRA (red), MACCRA (green) and CR (blue) for August to November (2003–20012).*

1786

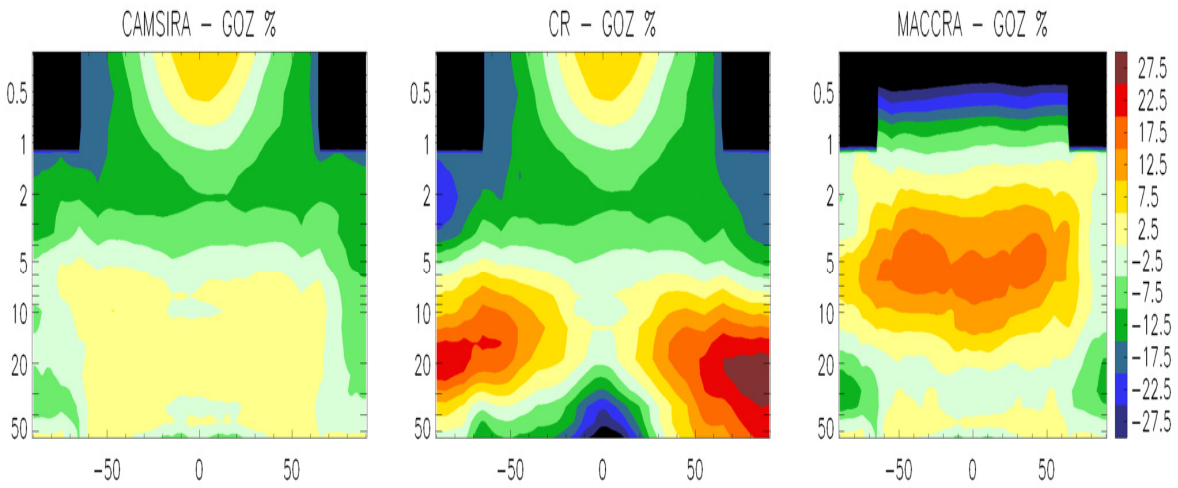

1787

1788 *Figure 19 Cross sections (50–0.3 hPa) of the relative biases of zonally averaged ozone*
1789 *(%) of CAMSiRA (left), CR (middle) and MACCRA (right) against the GOZCARDS*
1790 *product (GOZ) for the period 2005–2012.*

1791

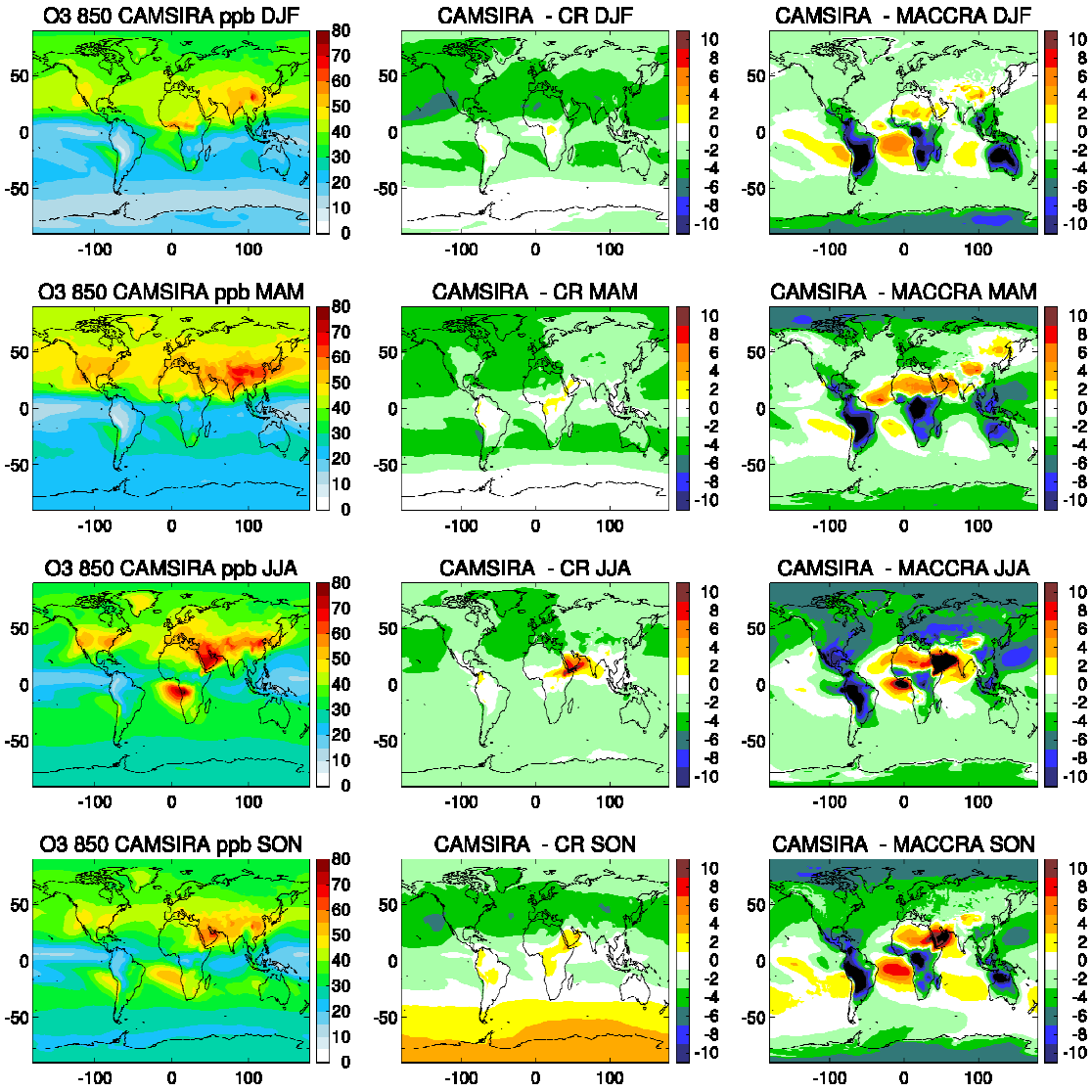

1792

1793 *Figure 20 Seasonal averaged ozone at 850 hPa (ppb) from CAMSiRA (left), difference*
1794 *between CAMSIRA and CR (middle) and CAMSiRA and MACCRA (right, 2003–2012) for*
1795 *the season DJF (row 1), MAM (row 2), JJA (row 3) and SON (row 4).*

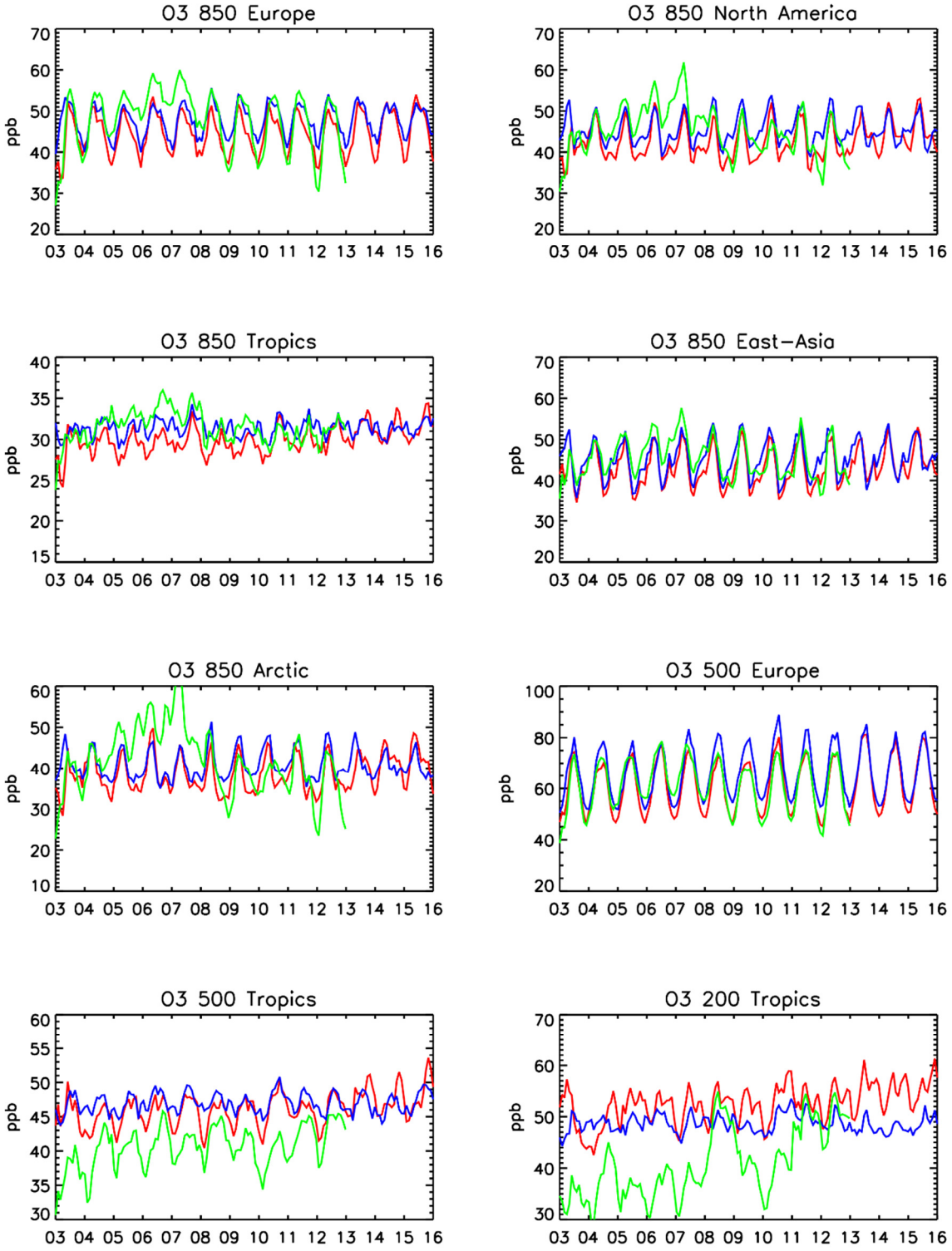

Figure 21 Monthly ozone volume mixing ratio at 850, 500 and 200 hPa over different regions (see Table 3) from CAMSiRA (red), CR (blue) and MACCRA (green) for 2003–2015.

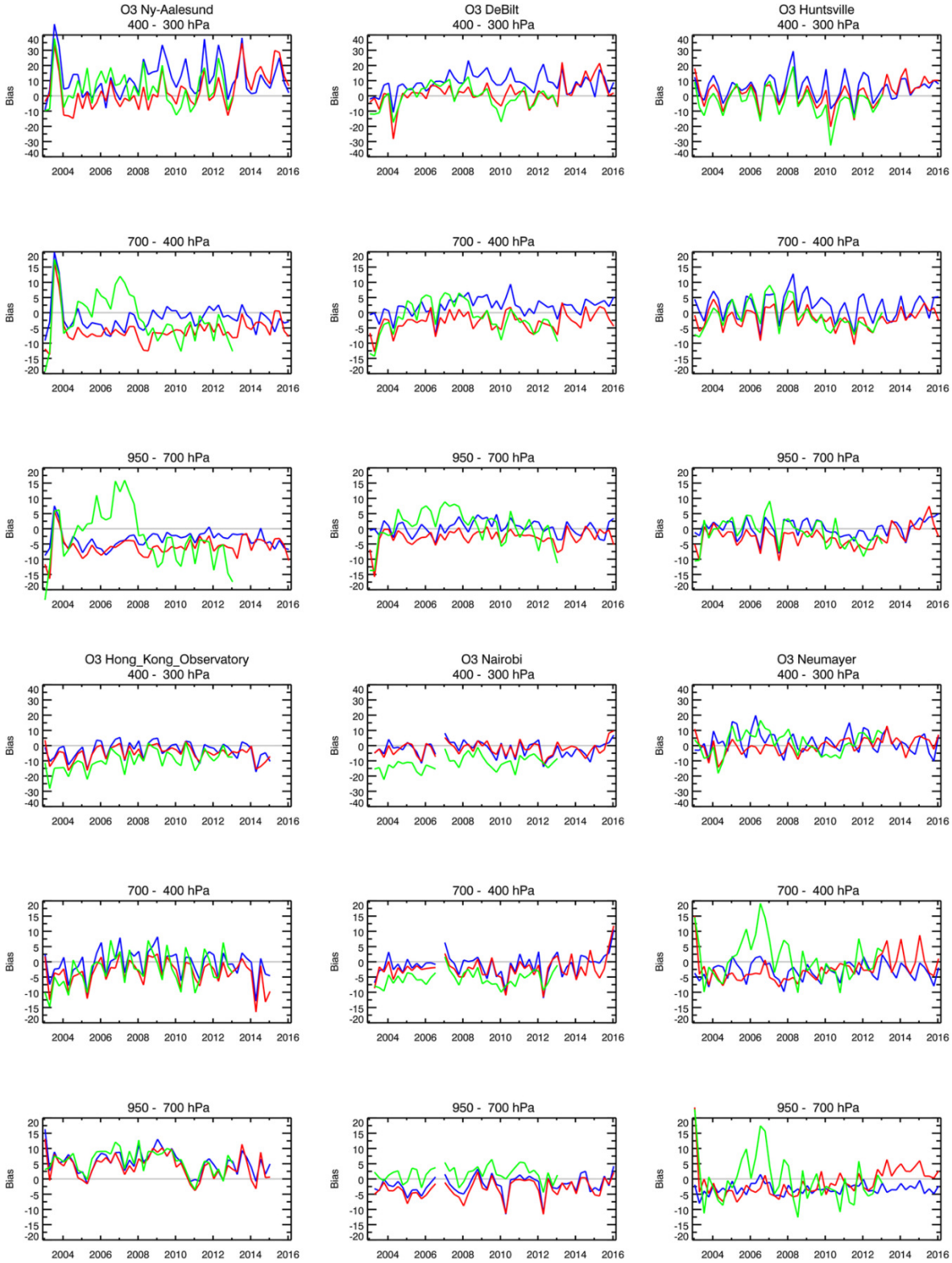

Figure 22 Time series of seasonal mean ozone bias in ppb in the pressure ranges 950-700, 700-400 and 400-300 hPa against ozone sondes at Ny-Ålesund, DeBilt, Huntsville, Hong Kong Observatory, Nairobi and Neymayer station for CAMSiRA (red), CR (blue) and MACCRA (green).

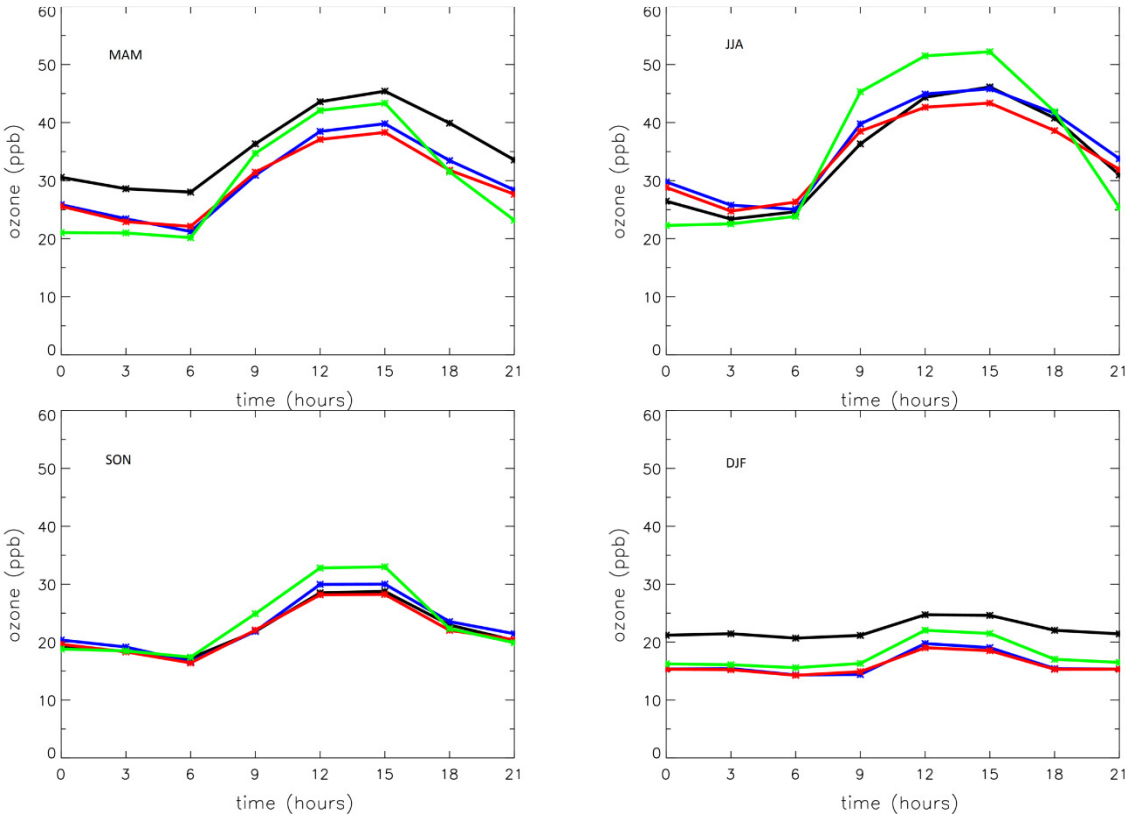

Figure 23 Average diurnal cycle of ozone at EMEP-AirBase stations in Europe (black) for the seasons MAM (top left), JJA (top right), SON (bottom left) and DJF (bottom right) for CAMSiRA (red), CR (blue) and MACCRA (green).

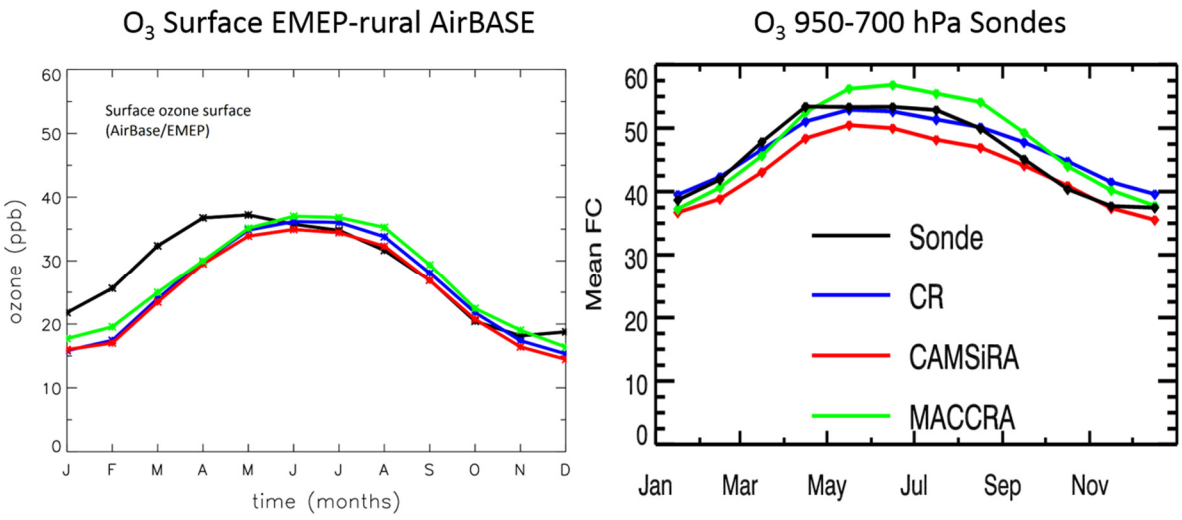

1811

1812 *Figure 24 Average seasonal cycle of surface ozone at EMEP-AirBase stations (left) and*
1813 *at European ozone sonde sites in the pressure range (950–700 hPa) for CAMSiRA (red),*
1814 *CR (blue) and MACCRA (green).*